


## RESEARCH ARTICLE

# Domestic cat embryos reveal unique transcriptomes of developing incisor, canine, and premolar teeth

Emily D. Woodruff<sup>1,2</sup>  | Bonnie K. Kircher<sup>1</sup> | Brooke A. Armfield<sup>3</sup> | Julie K. Levy<sup>4</sup> | Jonathan I. Bloch<sup>1,2</sup> | Martin J. Cohn<sup>1,3</sup>

<sup>1</sup>Department of Biology, University of Florida, Gainesville, Florida, USA

<sup>2</sup>Department of Natural History, Florida Museum of Natural History, University of Florida, Gainesville, Florida, USA

<sup>3</sup>Department of Molecular Genetics and Microbiology, University of Florida, Gainesville, Florida, USA

<sup>4</sup>Department of Small Animal Clinical Sciences, College of Veterinary Medicine, University of Florida, Gainesville, Florida, USA

## Correspondence

Emily D. Woodruff and Martin J. Cohn, Department of Biology, University of Florida, Gainesville, FL, USA.

Email: [ewoodruff@genetics.utah.edu](mailto:ewoodruff@genetics.utah.edu) and [mjcohn@ufl.edu](mailto:mjcohn@ufl.edu)

## Present address

Emily D. Woodruff, Department of Human Genetics, University of Utah, Salt Lake City, Utah, USA.

Bonnie K. Kircher, Department of Genetics, University of Texas MD Anderson Cancer Center, Houston, Texas, USA.

## Funding information

National Science Foundation, Grant/Award Number: 1455572

## Abstract

Division of the dentition into morphologically distinct classes of teeth (incisors, canines, premolars, and molars) and the acquisition of tribosphenic molars facilitated precise occlusion between the teeth early in mammal evolution. Despite the evolutionary and ecological importance of distinct classes of teeth with unique cusp, crest, and basin morphologies, relatively little is known about the genetic basis for the development of different tooth classes within the embryo. Here we investigated genetic differences between developing deciduous incisor, canine, and premolar teeth in the domestic cat (*Felis catus*), which we propose to be a new model for tooth development. We examined differences in both developmental timing and crown morphology between the three tooth classes. Using RNA sequencing of early bell stage tooth germs, we showed that each of the three deciduous tooth classes possess a unique transcriptional profile. Three notable groups of genes emerged from our differential expression analysis; genes involved in the extracellular matrix (ECM), Wnt pathway signaling, and members of multiple homeobox gene families (*Lhx*, *Dlx*, *Alx*, and *Nkx*). Our results suggest that ECM genes may play a previously under-appreciated role in shaping the surface of the tooth crown during development. Differential regulation of these genes likely underlies differences in tooth crown shape and size, although subtle temporal differences in development between the tooth germs could also be responsible. This study provides foundational data for future experiments to examine the function of these candidate genes in tooth development to directly test their potential effects on crown morphology.

## KEYWORDS

canine, cat, heterodonty, incisor, premolar, transcriptome

## 1 | INTRODUCTION

Mammal dentitions are morphologically complex structures that reflect a range of dietary specializations, feeding behaviors, and life history strategies (Evans et al., 2007; Gingerich, 1977; Rose, 2006; Strait, 1993). In mammals, teeth can differ dramatically between species in the occlusal cusp pattern, as well as the number and shape of teeth in the dentition (Kielan-Jaworowska et al., 2004; Rose, 2006;

Ungar, 2010). Many mammals are heterodont, possessing multiple classes of differently shaped teeth which typically include incisors, canines, premolars, and molars. Precise occlusion, the complementary fitting of upper and lower tribosphenic (tri-cuspid) molars during chewing, is considered a major advance in mammalian evolution close to the origin of boreosphenidan mammals (eutherians, metatherians, and relatives with tribosphenic molars), that distinguished mammals from other vertebrates (Luo et al., 2001). Evidence from the fossil

record shows that acquisition of precisely occluding tribosphenic molars in early mammals spurred dramatic diversification of tooth morphologies within and across mammalian lineages (Luo et al., 2001). Functionally, precisely occluding tribosphenic molars enabled improved shearing and grinding capabilities (Davis, 2011).

Proper molecular patterning of tooth surfaces within the dentition during embryonic development is essential to facilitate precise occlusion, and in heterodont dentitions achieving these complementary, interlocking crown morphologies is a complex developmental process. While the genetic underpinnings of tooth development have been studied extensively in laboratory mice (*Mus musculus domesticus*) and have been reviewed previously (Jernvall & Thesleff, 2000; Thesleff & Sharpe, 1997; Tucker & Sharpe, 2004), because mice lack canines and premolars, the development of these two tooth classes is understudied. Homeobox genes play critical roles in patterning the dentition into distinct regions in which different tooth classes form, known as the homeobox code (McCollum & Sharpe, 2001; Sharpe, 1995). Initially studied in incisors and molars of mice, the homeobox code has been extended to canine and premolar teeth in shrews (*Suncus murinus*, *Cryptotis parva*) and ferrets (*Mustela furo*) (Miletich et al., 2011; Wakamatsu et al., 2019; Yamanaka et al., 2015).

The domestic cat, *Felis catus*, is a well-suited model for studying the development of different tooth classes because the deciduous incisor, canine, and premolar teeth differ in overall crown shape, cusp number,

and relative position along the dental arch. The deciduous dentition of juvenile *F. catus* consists of 26 teeth; within each half of the upper and lower dentitions are three incisors ( $DI^{1-3}$  and  $DI_{1-3}$ ), one canine ( $DC^1$  and  $DC_1$ ), three upper premolars ( $DP^{2-4}$ ), and 2 lower premolars ( $DP_{3-4}$ ) (Aiello & Moses, 2016) (Figure 1a-c). *F. catus* has lost the first upper deciduous premolar ( $DP^1$ ) as well as the first and second lower deciduous premolars ( $DP_{1-2}$ ) (Van Valkenburgh, 2007). In *F. catus*, the crowns of incisors and canines have a single main cusp, but the canines are larger than the incisors in both crown height and medial-lateral width (Figure 1a). The anterior-most upper premolar ( $DP^2$ ) crown is considerably smaller than that of the posterior premolars and has one main cusp.  $DP^3$  and  $DP_4$  make up the deciduous carnassial pair, a specialized blade-like tooth complex that evolved in felids and other carnivorans (Slaughter et al., 1974). In contrast to the incisors and canine, the  $DP^3$  crown is longer anterior-posteriorly and multicusped, including a protocone, parastyle, paracone, and metacone (Figure 1a,a'). The tritubercular crown of  $DP^4$  is smaller than that of  $DP^3$  and includes a protocone, a paracone, and a metacone.

In this study we investigated gene expression differences associated with dental developmental stage and tooth crown morphology. We identified temporal differences in development within the upper deciduous dentition of the domestic cat, and used comparative transcriptomics to determine the genetic differences between three tooth classes (incisor, canine, and premolar) during

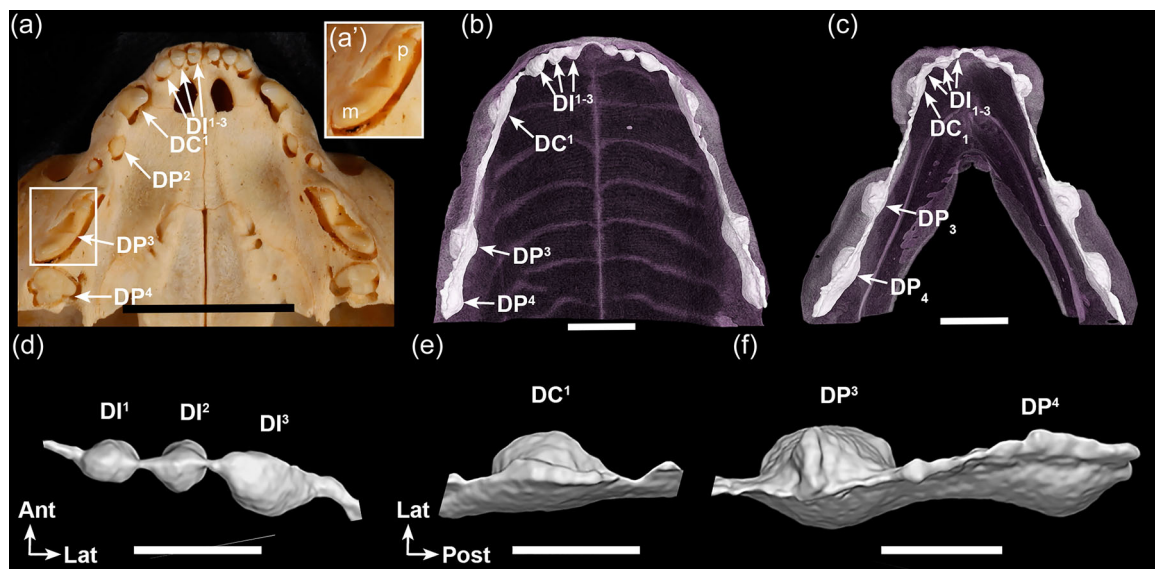


**FIGURE 1** Domestic cat (*Felis catus*) deciduous dentition in a juvenile (a) and an embryo at stage 18 (~5 weeks postconception) (b–f) in occlusal view. Juvenile domestic cats have three upper deciduous incisors in the premaxilla ( $DI^{1-3}$ ), and one deciduous canine ( $DC^1$ ) and three deciduous premolars ( $DP^{2-4}$ ) in the maxilla (a). A three-dimensional (3-D) rendering of an embryonic cat dentition at stage 18 showing the upper (b, d–f) and lower (c) dental epithelia in gray and the palate and soft tissue in the oral cavity in light purple. The upper dentition (a, b, d–f) is viewed from the ventral aspect and the lower dentition (c) is viewed from the dorsal aspect; both show the occlusal surfaces of the teeth before eruption has occurred (gum tissue has been made transparent in b, c). Magnified views of the upper right tooth germs (d–f) show differences in size and morphology among the tooth classes. Six upper and six lower tooth germs are visible,  $DI^{1-3}$ ,  $DI_{1-3}$ ,  $DC^1$ ,  $DC_1$ ,  $DP^{2-4}$ , and  $DP_{3-4}$  connected by an interdental lamina.  $DI^{1-3}$ ,  $DI_{1-3}$ ,  $DC^1$ ,  $DC_1$ ,  $DP^{3-4}$ , and  $DP_{3-4}$  are at the early bell stage, but the incisors and  $DP_4$  are slightly delayed in development compared to the canine and premolars.  $DP^2$  is at the bud stage, but it is not apparent in the 3-D rendering other than as a slight thickening of the dental lamina.  $DP^3$  is larger than  $DP^4$  in the embryo (b, f) and in the juvenile (a) but only the paracone (p) and metacone (m) are clearly visible (a') because the tooth is not fully erupted. Scale bars: 1 cm in (a) 1 mm in (b and c), 0.5 mm in (d–f). Photo in (a) taken by EDW, Florida Museum of Natural History Mammalogy Collection, UF-M 12845. DI, deciduous incisor; DC, deciduous canine; DP, deciduous premolar; p, paracone; m, metacone.

embryonic development. Our differential expression analyses revealed that each tooth class possessed a relatively unique transcriptome and three groups of differentially expressed genes emerged from this analysis, genes involved in the extracellular matrix (ECM), Wnt pathway signaling, and homeobox genes. Subsequent spatial expression analyses of ECM and Wnt pathway candidate genes revealed differences in expression domains. Collectively these results show that there are subtle differences in developmental stage between incisors and cheek teeth (canine and premolar), and suggest that differential gene expression patterns likely arise from both temporal and morphological differences between tooth classes.

## 2 | METHODS

### 2.1 | Acquisition and preparation of embryonic cat tissue

Embryonic cat tissue was collected from gravid uteri removed during spay/neuter clinics for humane community cat population management at the University of Florida College of Veterinary Medicine (UF IACUC protocol 201508818). Because the date of conception was unknown, the developmental stage of each embryo was determined based on previously published descriptions and photographs (Knospe, 2002). Cat embryos for microcomputed tomography ( $\mu$ CT) scanning were fixed in 4% paraformaldehyde (PFA) upon collection (see Supporting Information: Methods 5.1 for  $\mu$ CT methods). Embryos used for histology or immunofluorescence were fixed in 4% PFA at 4°C overnight for small embryos or for 3–4 days for larger embryos, and then dehydrated in ethanol (25% EtOH, 50% EtOH, and 70% EtOH). Heads or whole embryos intended for RNA-seq were frozen in Optimal Cutting Temperature medium (OCT, Tissue Tek) on dry ice immediately after dissection.

### 2.2 | Histology and immunofluorescence

For frozen sections used in histology and immunofluorescence, embryonic heads were rehydrated from 70% EtOH, rinsed in phosphate buffered saline (PBS), dehydrated in 30% sucrose at 4°C for 12–48 h, and incubated in equal amounts of OCT and sucrose (30% sucrose in PBS) at 4°C overnight. Samples were embedded in OCT, frozen on dry ice, and stored at  $-80^{\circ}\text{C}$ . 10  $\mu\text{m}$  cryosections were cut in the coronal plane on a Leica cryostat, mounted on Superfrost Plus glass slides (Thermo Fisher Scientific), and stained with hematoxylin and eosin or used for immunofluorescence (see Supporting Information: Methods 5.2 for immunofluorescence).

For paraffin sections, heads were rehydrated, rinsed in PBS, fixed overnight in 4% PFA at 4°C, rinsed in PBS, and placed in 70% ethanol. Paraffin processing was performed at the Molecular Pathology Core in the University of Florida School of Dental Medicine. Paraffin-embedded cat heads were sectioned on a microtome at 8  $\mu\text{m}$  and stained with Masson trichrome. Histological descriptions are based

on two embryos at the bud stage and three embryos each at the cap and bell stages.

### 2.3 | RNA sequencing and differential expression analysis

Dental epithelial and mesenchymal tissues from early bell stage (stage 18) deciduous incisor ( $\text{DI}^3$ ), canine ( $\text{DC}^1$ ), and premolar ( $\text{DP}^3$ ) were collected using laser capture microdissection, and RNA was extracted for each tooth class from three individual cat embryos from the same litter (Supporting Information: Figure 1, Supporting Information: Table 1). A total of nine RNA-seq libraries were prepared and sequenced at the University of Florida Interdisciplinary Center for Biotechnology Research (Supporting Information: Methods 5.3). Sequence data are available on the National Center for Biotechnology Information (NCBI) sequence read archive (<https://www.ncbi.nlm.nih.gov/sra>) in BioProject PRJNA643853.

Bioinformatics analysis of the RNA-seq data is described in Supporting Information: 5.4. Briefly, reads were trimmed and filtered using Trimmomatic v0.33 (Bolger et al., 2014) and aligned to the *F. catus* genome (version 9; obtained from NCBI) in Hisat2 (Pertea et al., 2016). Transcripts were assembled in Stringtie (Pertea et al., 2016), and differential expression was estimated using Cuffdiff (Trapnell et al., 2012). Predicted protein sequences for differentially expressed genes were obtained using TransDecoder version 5.0.2 (Haas et al., 2013) and these genes were identified using NCBI BLAST.

Statistical overrepresentation tests were performed on the set of differentially expressed genes identified in the BLAST search (Supporting Information: Tables 2–5) using the PANTHER database (<http://pantherdb.org>) *F. catus* gene set ( $N = 19,435$  entries) and Fisher's exact test with a false discovery rate calculation ( $\text{FDR } p < 0.05$ ) (GO Ontology database DOI: 10.5281/zenodo.3727280, released March 23, 2020). We compared our data set against three different annotation sets: "GO molecular function complete," "GO biological process complete," and "GO cellular component complete."

## 3 | RESULTS

### 3.1 | Canine and third premolar are developmentally advanced compared to other upper teeth

Due to the paucity of studies on dental development in *F. catus* (Gaunt, 1959a, 1959b; Moss-Salentijn, 1982), we first documented the developmental sequence of the feline deciduous dentition. We observed the same stages of tooth development in *F. catus* as have been observed for other mammals (bud, cap, and bell), but our histological analysis revealed that the upper deciduous teeth form at different times during embryonic development (Figure 2, Supporting Information:



Figures 3 and 4). At the late bud stage (stage 16, approximately 25–28 days postconception [DPC] [Knospe, 2002]),  $DI^{1-3}$  were in sync, but  $DC^1$  and  $DP^3$  appeared to be slightly more advanced in development and were considerably larger than the upper incisors (Supporting Information: Figure 3a–c). Neither  $DP^2$  nor  $DP^4$  were observed at this stage. At stage 17 (approximately 28–32 DPC [Knospe, 2002])  $DI^{1-3}$  were in the early cap stage,  $DC^1$  and  $DP^3$  were slightly more advanced in the mid cap stage (Supporting Information: Figure 4A–C, and E) but,  $DP^2$  and  $DP^4$  were at the bud stage, a full developmental stage behind the other upper teeth

(Supporting Information: Figure 4d, f). Consistent with the earlier stages, by stage 18 (approximately 32–38 DPC [Knospe, 2002])  $DI^{1-3}$  appeared slightly delayed due to the less-developed inner enamel epithelia compared to that of  $DC^1$  and  $DP^3$  which were at the early bell stage (Figure 2g–i). By stage 19.5 (approximately 40–44 DPC [Knospe, 2002]),  $DP^4$  along with  $DI^{1-3}$ ,  $DC^1$ , and  $DP^3$  were at the mid bell stage (Figure 2a–c, e, f) and we observed ameloblasts and odontoblasts within these teeth (Figure 2b,b'). By contrast,  $DP^2$  was at the late cap stage (Figure 2d). Successional laminae that give rise to the permanent teeth

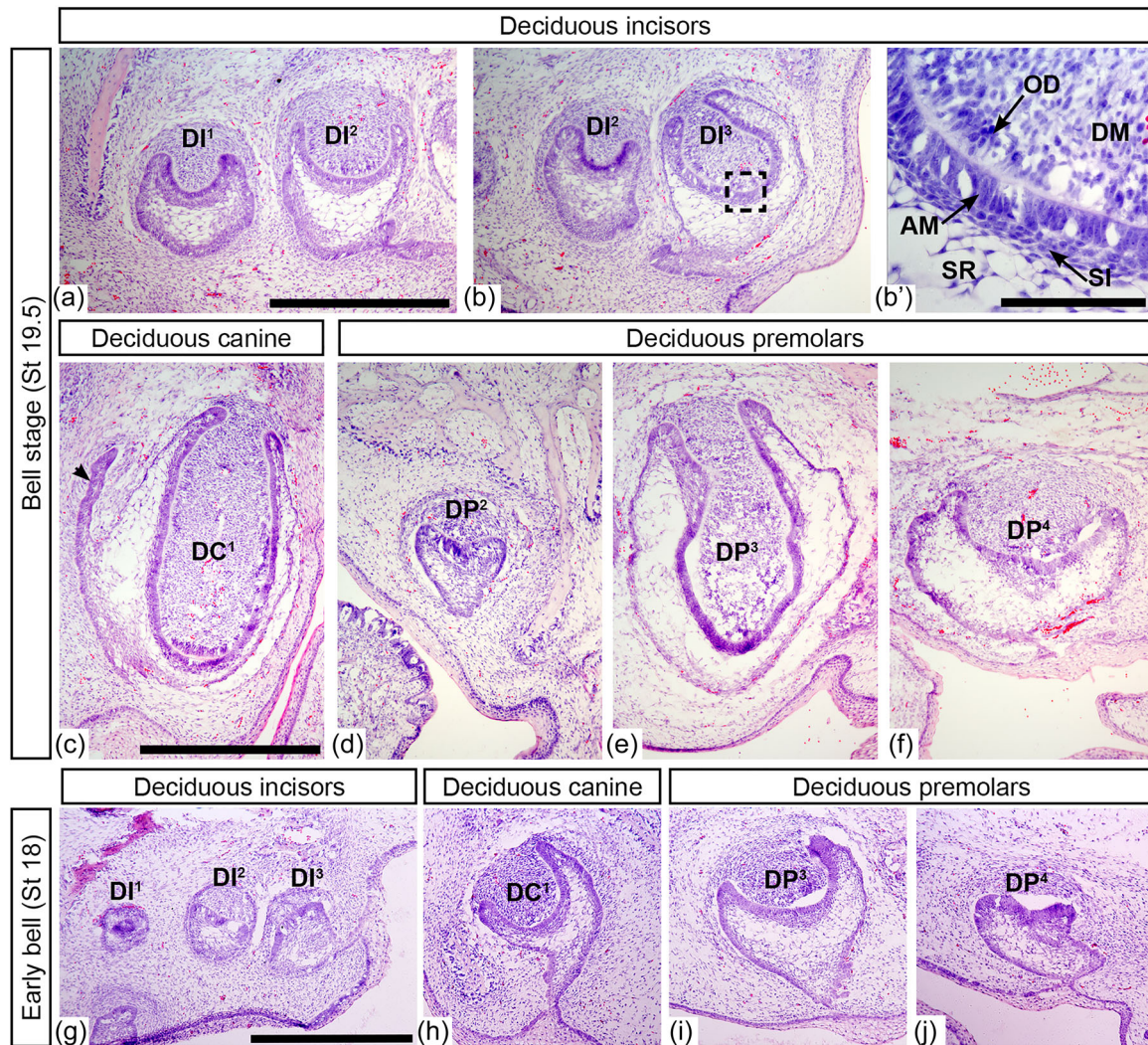


**FIGURE 2** Deciduous teeth at the bell stage from the upper dentition of *Felis catus* showing differentiated ameloblasts and odontoblasts (a–f). Frontal cryosections (10  $\mu$ m) from a stage 19.5 cat embryo stained with hematoxylin and eosin. Note that in the incisors, ameloblasts and odontoblasts are present (b'). The stellate reticulum (SR) comprised the majority of the enamel organ at this stage and the stratum intermedium (SI), the layers of epithelial cells positioned between the inner enamel epithelium and the SR, was also visible (b'). First and second upper incisors (a), second and third upper incisors (b), upper canine with the successional lamina on the lingual side (c, arrowhead), second upper premolar at the cap stage (d), third upper premolar (e), fourth upper premolar (f). Successional laminae were also observed for the premolars in other histological sections (data not shown). Early bell stage upper deciduous tooth germs including those used in RNA-sequencing (g–j). Frontal cryosections (10  $\mu$ m) stained with hematoxylin and eosin show teeth at stage 18. The canine and premolars appear slightly more advanced than the incisors. The upper third incisor (g), canine (h), and third premolar (i) were used in RNA-sequencing. Note that because these teeth are just entering the bell stage, ameloblasts and odontoblasts are not yet visible, in contrast to mid-bell stage teeth (stage 19.5; a–f). Tooth germs from the embryos' right side are shown, except (b and h) which are mirrored for ease of comparison. Scale bars: 500  $\mu$ m (a, c, g); 150  $\mu$ m (b'). Images (a–b); (c–f) are at the same scale. Images (g–j) are at the same scale. AM, ameloblasts; DM, dental mesenchyme; OD, odontoblasts.



were visible in the upper and lower dentitions, though no successional tooth germs had formed (Figure 2c, Supporting Information: Figure 5C–E). Consistent with our observations for the upper teeth, in the lower dentition the incisors were slightly less advanced than the canine and premolar (Supporting Information: Results 6.1).

### 3.2 | Tooth classes differ in epithelial volume at the bell stage

Comparison of relative volumetric measurements of the deciduous dental epithelium from three-dimensional reconstructions of  $\mu$ CT data indicated that at stage 18 the incisors were much smaller than the canine and premolar tooth germs (Figure 1B–F; Supporting Information: Table 6;  $N = 2$  teeth (right and left) per tooth position from one cat embryo). The DC<sup>1</sup> epithelium was approximately three times larger than the DI<sup>3</sup> epithelium, while the DP<sup>3</sup> epithelium was approximately five times larger (Supporting Information: Figure 6). The DP<sup>4</sup> epithelium was similar in size to that of the DC<sup>1</sup>. Due to the challenge of obtaining replicate  $\mu$ CT data sets (acquiring same-stage *F. catus* embryos), we were unable to evaluate the statistical significance of these observed differences in tooth size.

### 3.3 | Unique transcriptomes of early bell stage incisor, canine, and premolar teeth

To identify genes that are differentially expressed between incisor, canine, and premolar teeth and thus are potential candidates for regulating tooth class, we performed RNA-sequencing of dental epithelium and mesenchyme isolated from three deciduous teeth (DI<sup>3</sup>, DC<sup>1</sup>, and DP<sup>3</sup>) at stage 18 (Figure 2g–i, Supporting Information: Figure 1) and compared the transcriptional profiles of each tooth type. As our histological and  $\mu$ CT analyses revealed, at stage 18 these teeth appeared to be at the early bell stage, however, DC<sup>1</sup> and DP<sup>3</sup> were slightly more developmentally advanced than DI<sup>3</sup>.

Our sequence data showed that each tooth class possessed a predominantly unique transcriptome (Figure 3d,e). Differential expression analysis revealed sets of genes that were uniquely expressed in each tooth type, as well as genes that were expressed in multiple teeth but were upregulated in one tooth and downregulated in another (Figure 3, Tables 1–3, Supporting Information: Tables 2–5). A total of 749 differentially expressed genes were detected by Cufflinks using fragments per kilobase per million reads (FPKM) that met our filtering criteria ( $q < 0.05$ , FPKM  $\geq 1$ ,  $\log_2$  fold change  $\geq 1.5$  or  $\leq -1.5$ ; Supporting Information: Methods 5.4) and of these, 111 genes had a  $\log_2$  fold change  $\geq 1.5$  or  $\leq -1.5$  and FPKM  $\geq 1$ , while 639 genes were expressed in one tooth (FPKM  $\geq 1$ ) but were not detected in another (FPKM = 0). In addition, we identified nine genes that met our  $\log_2$  fold change criterion but had an FPKM  $< 1$  for one of the teeth being compared. A subsequent BLAST search using predicted protein sequences identified 262 of these differentially expressed genes (Supporting Information: Tables 2–5, Supporting Information: Methods 5.4).

The canine and premolar shared more genes than the canine and incisor; these relative similarities were apparent in a heatmap and dendrogram (Figure 3d, Supporting Information: Table 9). Scatterplots comparing differentially expressed genes between tooth types showed that the magnitude of differential expression, as measured by FPKM, was lower for the canine and premolar teeth than the other comparisons between tooth classes (Figure 3a–c), indicating greater similarity between these teeth relative to the incisor. The canine and premolar transcriptomes, however, differed considerably from one another and we identified numerous genes that were differentially expressed between these teeth (Figure 3e, Tables 1–3).

Statistical overrepresentation tests using Fisher's exact test and FDR calculation were used to compare the set of 262 differentially expressed genes to *F. catus* genes in the PANTHER database for three gene ontology (GO) annotation sets. In total, 68 differentially expressed genes mapped to the *F. catus* PANTHER reference database and 194 genes were unmapped. Statistically significant (FDR  $p < 0.05$ ) over-represented genes were detected for the "GO cellular component" annotation set for the following categories: gap junction, bicellular tight junction, plasma membrane, and integral component of membrane.

The GO analysis indicated that numerous genes involved in cell junctions as well as the ECM were significantly differentially expressed among the three tooth classes. Next, to discern the tissue(s) (epithelium or mesenchyme) in which differentially expressed genes associated with the ECM were expressed, we performed immunofluorescence to detect these proteins in incisor, canine, and premolar teeth at the bell stage.

### 3.4 | Genes associated with the ECM are differentially expressed among tooth classes

Structural components of the ECM, including multiple collagens, a glycoprotein family member (tenascin), and an intermediate filament family member (keratin), were differentially expressed among tooth classes at stage 18 (Table 1, Supporting Information: Tables 2–5). Transcripts of *Col1a1* (Collagen type 1 alpha 1) were more abundant in the premolar than the incisor ( $\log_2$  fold change 2.42) and likewise, *Col2a1* (Collagen type 2 alpha 1) was highly expressed in the canine relative to the incisor ( $\log_2$  fold change 2.18) (Figure 4a). We detected COL1 protein by immunofluorescence in the ECM at the interface between the dental epithelium and mesenchyme in all three teeth, though the expression was broader in the premolar and canine compared with that of the incisor (Figure 4b–d). In the incisors, *Col7a1* (Collagen type 7 alpha 1) transcripts were more abundant than for either the canine or premolar. Transcripts of *Tgfb1* (Transforming growth factor  $\beta$ -induced, formerly  $\beta$ ig-h3), which encodes an ECM protein capable of binding to collagen types 1, 2, and 4, were more abundant in both the canine and premolar compared with those of the incisor ( $\log_2$  fold change 1.99, 1.34) (Hashimoto et al., 1997).

Two genes encoding cytoskeletal proteins, *Krt16* (Keratin type 1 cytoskeletal 16) and *Tub $\beta$ 2a* (Tubulin beta 2A chain) were

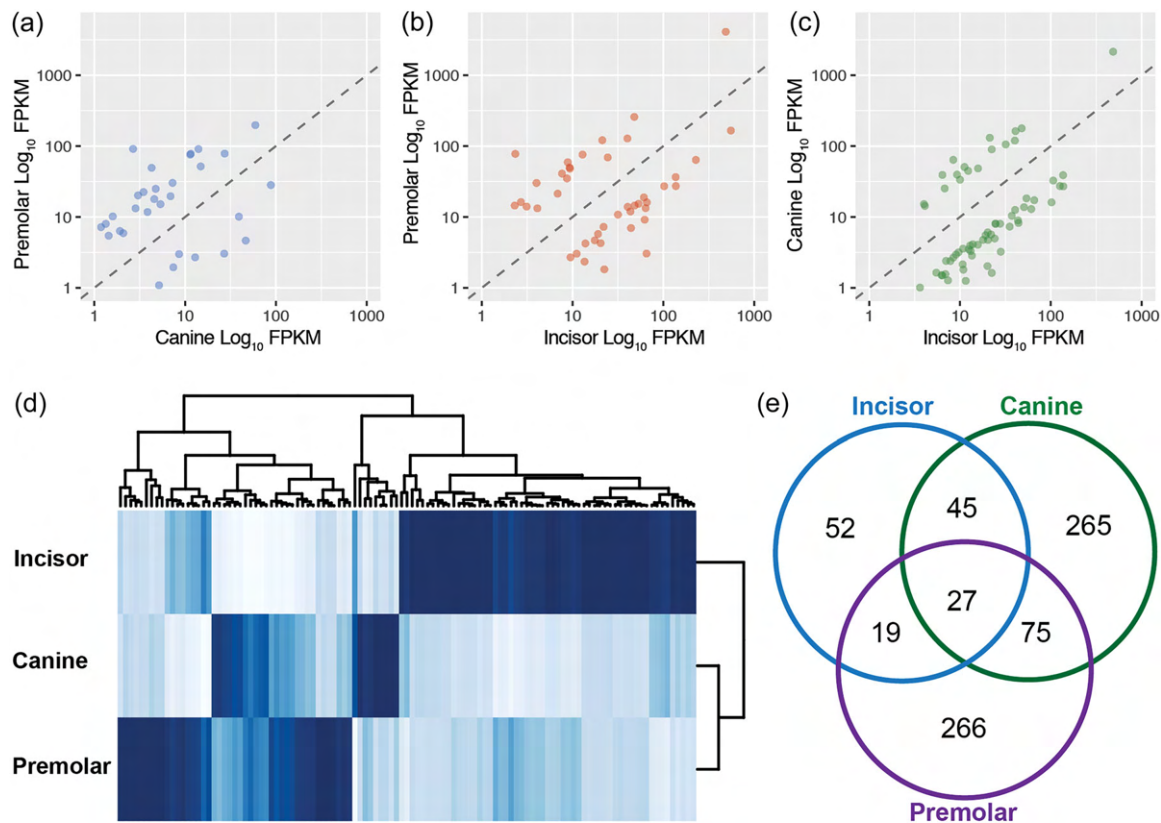


**FIGURE 3** Differential expression patterns between incisor, canine, and premolar tooth germs. Scatterplots (a–c) comparing relative gene expression ( $\log_{10}$  fragments per kilobase per million reads [FPKM]) between teeth for a subset of differentially expressed genes ( $N = 111$  genes excluding presence/absence genes) with a  $\log_2$  fold change  $\geq 1.5$  or  $\leq -1.5$  and FPKM  $\geq 1$ : canine versus premolar  $N = 31$  genes (a), incisor versus premolar  $N = 43$  genes (b), incisor versus canine  $N = 64$  genes (c). Dashed lines are reference lines which indicate a 1:1 relationship between the samples. Note in (a) that the magnitude of differential expression between premolar and canine transcriptomes is lower overall, as these points lie closer to the reference line than those in (b) or (c). Heatmap with dendrograms (d) showing the deciduous canine and premolar samples are most similar to each other based on Jensen–Shannon distance matrix of incisor, canine, and premolar FPKM ( $N = 111$  genes) (see Supporting Information: Table 9). Dark blue values represent higher FPKM values, lighter blue values represent lower FPKM values. Venn Diagram (e) showing the numbers of unique and shared genes between incisor, canine, and premolar samples for the entire data set ( $N = 749$  genes) with a cutoff of  $\log_2$  fold change  $\geq 1.5$  or  $\leq -1.5$  and FPKM  $\geq 1$ .

upregulated in the incisor relative to the canine or premolar (*Krt16*:  $\log_2$  fold change 1.68, 1.54; *Tub $\beta$ 2a*:  $\log_2$  fold change 2.28, 1.85) (Figure 4e). We detected KRT16 prominently in the inner enamel epithelium for all three tooth types, and in the incisor it was also present in the stellate reticulum (Figure 4f–h).

*Tenc* (Tenascin) was slightly upregulated in the incisor relative to that of the canine ( $\log_2$  fold change 1.15) (Figure 4i). TENC was detected prominently in the SR and more weakly detected in the dental mesenchyme of all three teeth (Figure 4j–l). *Nid1* (Nidogen 1), a component of the basement membrane, was upregulated in the canine relative to that of the premolar ( $\log_2$  fold change 1.57). A matrix metalloprotease, *Mmp9*, was upregulated in the premolar ( $\log_2$  fold change 4.60) but effectively absent from the canine (FPKM = 0.27, below the cutoff).

Multiple claudin genes involved in tight junctions were also differentially expressed between all tooth classes. *Cld19* (Claudin 19) was expressed in the premolar but was not detected in the incisor.

Transcripts of *Cldn7* (Claudin 7) were more abundant in the canine ( $\log_2$  fold change 2.09) and the premolar ( $\log_2$  fold change 2.43) than those in the incisor. *Cld6* (Claudin 6) was also more highly expressed in the premolar than the incisor ( $\log_2$  fold change 2.01). In contrast, *Cld3* and *Cld10* (Claudin 3, 10) were upregulated in the incisor relative to the canine (*Cld3*:  $\log_2$  fold change 3.30, *Cld10*:  $\log_2$  fold change 1.41), and *Cld1* (Claudin 1) was upregulated in the incisor compared to the premolar ( $\log_2$  fold change 1.39).

Genes involved in gap junctions were also differentially expressed. *Gja1* (Gap junction alpha 1) was highly expressed in all three teeth and was slightly upregulated in the canine and premolar teeth relative to the incisor ( $\log_2$  fold change 1.26 and 1.18 respectively) but *Gjb5* (Gap junction beta 5) was upregulated in the incisor compared with that of the canine ( $\log_2$  fold change 1.916). Additionally, transcripts of *Panx3* (Pannexin-3), a structural component of gap junctions, were present in the canine but were not detected in the incisor (FPKM = 1.57, FPKM = 0, respectively).

**TABLE 1** Differentially expressed genes associated with the extracellular matrix and cell junctions

Tooth 1	Tooth 2	Tooth 1 FPKM	Tooth 2 FPKM	Log <sub>2</sub> fold change	q Value	Gene name
Incisor	Premolar	254.923	97.2538	-1.39024	0.0049878	Claudin 1
Incisor	Canine	167.51	62.7605	-1.41632	0.0049878	Claudin 10
Incisor	Premolar	0	1.82096	Inf	0.0049878	Claudin 19
Incisor	Canine	20.0667	2.02906	-3.30592	0.0049878	Claudin 3
Incisor	Premolar	8.68125	35.0198	2.0122	0.0237354	Claudin 6
Incisor	Canine	9.27094	39.6268	2.09569	0.00985073	Claudin 7
Incisor	Premolar	9.27094	50.0827	2.43353	0.0049878	Claudin 7
Incisor	Premolar	7.64238	40.9069	2.42025	0.019239	Collagen 1 alpha 1 chain-like
Incisor	Premolar	209.847	478.314	1.18862	0.0237354	Gap junction alpha 1
Incisor	Canine	209.847	505.317	1.26785	0.0049878	Gap junction alpha 1
Incisor	Canine	17.9735	4.76231	-1.91614	0.0049878	Gap junction beta 5
Incisor	Canine	11.1975	50.7678	2.18074	0.0049878	Collagen 2 alpha 1 chain-like
Incisor	Canine	16.9066	7.44416	-1.18341	0.00985073	Collagen 7 alpha 1
Incisor	Canine	40.4652	12.5699	-1.68671	0.0049878	Keratin, type I cytoskeletal 16
Incisor	Premolar	40.4652	13.8901	-1.54262	0.0049878	Keratin, type I cytoskeletal 16
Canine	Premolar	0.271684	6.61275	4.60525	0.0049878	Matrix metalloproteinase 9
Canine	Premolar	8.59186	2.99635	-1.51977	0.0325694	Nidogen 1
Incisor	Canine	0	1.57629	Inf	0.0049878	Pannexin 3
Incisor	Canine	330.223	148.682	-1.15121	0.0049878	Tenascin
Incisor	Canine	43.4768	8.94996	-2.28029	0.0049878	Tubulin beta-2A chain
Incisor	Premolar	43.4768	11.9835	-1.8592	0.0049878	Tubulin beta-2A chain

Note: The sign of the log<sub>2</sub> fold change may differ from those reported in the main text; the comparisons of transcript abundance in the main text were written in terms of upregulation (all positive signs). The values reported here are the same as those generated from Cuffdiff.

### 3.5 | Differential expression of Wnt pathway genes among tooth classes

Wingless/integrase-1 (Wnt) pathway signaling is important at multiple stages of tooth development, including regulating cusp patterning on the tooth crown (Dassule & McMahon, 1998; Zhu et al., 2013). We identified numerous Wnt signaling genes, especially inhibitors of Wnt signaling, that were differentially expressed among the three tooth classes (Table 2, Supporting Information: Tables 2–4). Transcripts of *Wif1* (Wnt inhibitory factor 1) were more abundant in the incisor compared to those in the canine and the premolar (log<sub>2</sub> fold change 1.810) (Figure 4m). We detected WIF1 by immunofluorescence in the stellate reticulum and faintly in the dental epithelium and mesenchyme (Figure 4n–p). *Fst* (Follistatin) was upregulated in incisors relative to canine and premolar (log<sub>2</sub> fold change 2.34 and 2.32, respectively) (Figure 4q). FST was detected by immunofluorescence in the dental epithelium and stellate reticulum, albeit weakly in DP<sup>3</sup> (Figure 4r–t). Another inhibitor of Wnt signaling, *Sfrp2* (Secreted frizzled related protein 2), was more highly expressed in the incisor and canine compared to that of the premolar (log<sub>2</sub> fold change 1.81 and

2.26, respectively). Similarly, transcripts of *Sfrp1* were more abundant in the incisor compared to those of the canine (log<sub>2</sub> fold change 1.22). *Wnt5a* (Wnt family member 5a) was upregulated in the canine relative to the incisor (log<sub>2</sub> fold change 1.61) and it was also upregulated in the premolar (log<sub>2</sub> fold change 1.40), though this fold change fell short of the cutoff. Additionally, *Dkk1* was upregulated in the canine and premolar relative to the incisor (log<sub>2</sub> fold change 1.43 and 1.49, respectively), while *Dkk4* was upregulated in the incisor compared to the canine (log<sub>2</sub> fold change 1.18), although both genes were under our fold change cutoff. *Wisp2* (Wnt1 inducible signaling pathway 2) was detected in the premolar but was absent from the canine (FPKM = 2.04 and FPKM = 0, respectively) and had very low expression, well below our cutoff, in the incisor (FPKM = 0.06).

### 3.6 | Differential expression of homeobox genes at a late stage in dental development

Homeobox genes play critical roles in early patterning of the dentition, however, we detected multiple homeobox genes at the



**TABLE 2** Differentially expressed genes involved in the Wnt signaling pathway

Tooth 1	Tooth 2	Tooth 1 FPKM	Tooth 2 FPKM	Log <sub>2</sub> Fold change	q Value	Gene name
Incisor	Canine	21.1192	57.2352	1.43835	0.0325694	Dickkopf-related 1
Incisor	Premolar	21.1192	59.5508	1.49557	0.019239	Dickkopf-related 1
Incisor	Canine	1015.49	446.643	-1.18499	0.0049878	Dickkopf-related 4
Incisor	Canine	137.252	27.0275	-2.34432	0.0049878	Follistatin
Incisor	Premolar	137.252	27.3122	-2.32921	0.0049878	Follistatin
Incisor	Canine	18.3669	7.87823	-1.22116	0.0049878	Secreted frizzled-related 1
Canine	Premolar	12.9231	2.6932	-2.26257	0.0049878	Secreted frizzled-related 2
Incisor	Premolar	9.48209	2.6932	-1.81589	0.0457699	Secreted frizzled-related 2
Incisor	Canine	40.858	162.68	1.99335	0.0049878	Transforming growth factor-beta-induced
Incisor	Canine	136.401	38.8779	-1.81083	0.0049878	Wnt inhibitory factor 1
Incisor	Premolar	136.401	36.5649	-1.89932	0.0049878	Wnt inhibitory factor 1
Canine	Premolar	0	2.04784	Inf	0.0049878	Wnt1-inducible signaling pathway 2
Incisor	Premolar	15.7944	41.8877	1.40711	0.0049878	Wnt5a
Incisor	Canine	15.7944	48.4182	1.61614	0.0049878	Wnt5a

Note: The sign of the log<sub>2</sub> fold change may differ from those reported in the main text; the comparisons of transcript abundance in the main text were written in terms of upregulation (all positive signs). The values reported here are the same as those generated from Cuffdiff.

**TABLE 3** Differentially expressed homeobox genes

Tooth 1	Tooth 2	Tooth 1 FPKM	Tooth 2 FPKM	Log <sub>2</sub> fold change	q Value	Gene name
Incisor	Canine	65.2938	27.0174	-1.27305	0.0049878	Alx1
Incisor	Premolar	65.2938	3.04268	-4.42353	0.0049878	Alx1
Canine	Premolar	27.0174	3.04268	-3.15048	0.0049878	Alx1
Incisor	Premolar	2.99779	0	-Inf	0.0049878	Alx4
Incisor	Canine	56.5441	133.827	1.24292	0.019239	Dlx3
Incisor	Canine	26.7717	74.2304	1.4713	0.0049878	Dlx4
Incisor	Canine	82.5208	226.688	1.45788	0.0145862	Dlx6
Incisor	Premolar	82.5208	211.865	1.36031	0.0414242	Dlx6
Incisor	Canine	0	4.93425	Inf	0.0049878	Lhx9
Canine	Premolar	4.93425	0	-Inf	0.0049878	Lhx9
Incisor	Premolar	20.3335	4.27492	-2.24989	0.0049878	Nkx3.1
Incisor	Canine	20.3335	4.74313	-2.09995	0.0049878	Nkx3.1

Note: The sign of the log<sub>2</sub> fold change may differ from those reported in the main text; the comparisons of transcript abundance in the main text were written in terms of upregulation (all positive signs). The values reported here are the same as those generated from Cuffdiff.

bell stage that were significantly differentially expressed among incisor, canine, and premolar teeth including members of *Dlx*, *Alx*, *Lhx*, and *Nkx3-1* gene families (Chen et al., 1996; Denaxa et al., 2009; Grigoriou et al., 1998; Jowett et al., 1993; Qiu et al., 1997; Thomas et al., 1997; Tureckova et al., 2002; Zhao et al., 2000) (Table 3, Supporting Information: Tables 2–4). *Dlx6* (Distal-less homeobox 6) was more highly expressed in the canine and premolar than in the

incisor (log<sub>2</sub> fold change 1.45, 1.36, respectively). Additionally, transcripts of *Dlx3* and *Dlx4* were upregulated in the canine relative to those in the incisor. The LIM homeobox genes *Lhx6* and *Lhx9* were both differentially expressed among teeth; *Lhx6* was expressed in the premolar (FPKM = 5.55) but it was not detected in the incisor (FPKM = 0) and it was nearly absent from the canine (FPKM = 0.86). Similarly, *Lhx9* transcripts were detected in the canine (FPKM = 4.93)

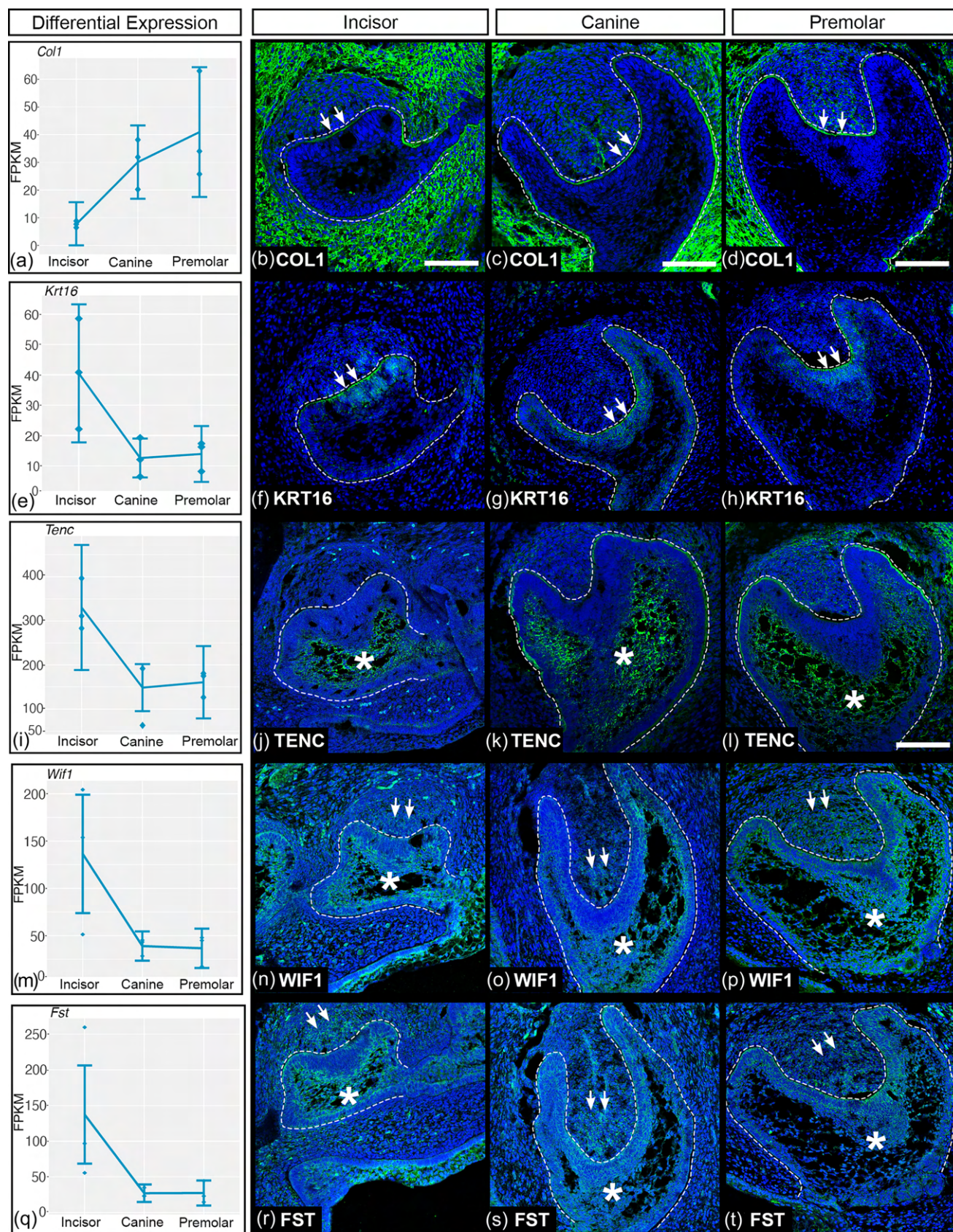


FIGURE 4 (See caption on next page)



but not in the incisor or premolar (FPKM = 0 for both). Transcripts of ALX homeobox genes were also differentially expressed; *Alx1* was significantly upregulated in the incisor compared with those of the canine and premolar ( $\log_2$  fold change 1.27 and 4.42, respectively) while *Alx4* was upregulated in the incisor (FPKM = 2.99) but was not detected in the premolar (FPKM = 0). Additionally, *Nkx3.1* (Nk3 homeobox 1) was upregulated in the incisor relative to that of the canine and premolar ( $\log_2$  fold change 2.09 and 2.24, respectively).

## 4 | DISCUSSION

### 4.1 | Asynchronous tooth development within the upper deciduous dentition

Our histological analysis showed that in *F. catus*, DC<sup>1</sup> and DP<sup>3</sup> develop in sync with one another and are the most developmentally advanced at the stages we examined, while DI<sup>1-3</sup> appeared slightly delayed relative to DC<sup>1</sup> and DP<sup>3</sup>. We observed a much greater temporal delay in the development of DP<sup>2</sup>, consistent with a previous report, as well as DP<sup>4</sup> (Gaunt, 1959a). DP<sup>2</sup> is present in juvenile and adult *F. catus* dentitions but, due to its diminutive crown and lack of occlusion with a lower tooth, it is essentially nonfunctional (Aiello & Moses, 2016) (Figure 1a). We propose that the asynchronous developmental sequence observed for DP<sup>2</sup> and DP<sup>4</sup> and, to a lesser extent, DI<sup>1-3</sup> may allow the larger teeth (i.e., DC<sup>1</sup>, DP<sup>3</sup>) sufficient time to undergo morphogenesis and subsequently produce mineralized tissues (enamel and dentin) so that each tooth is fully formed before eruption. It is possible that DC<sup>1</sup> and DP<sup>3</sup> are initiated slightly earlier in development than DI<sup>3</sup> but younger embryos, earlier than stage 16, would be required to address this. Additionally, it is conceivable that the marked developmental delay of DP<sup>2</sup> reflects relaxed constraint on developmental timing, given that it lacks a functional role in chewing, this tooth position could be subject to less selective pressure than teeth at other positions in the dentition. In support of the latter hypothesis, DP<sup>2</sup> in another felid, *Lynx lynx*, is considered a supernumerary tooth because it is present infrequently in juveniles and is not typically replaced by a permanent tooth, both of which are characteristic of evolutionary tooth loss (Werdelin, 1987).

Our results are consistent with previous reports of temporal differences in development between tooth classes in other mammals.

In the house shrew (*S. murinus*) permanent dentition, the developing canine was delayed relative to the incisors and premolar, whereas in the pig (*Sus scrofa*), temporal heterogeneity was observed at numerous tooth positions in the lower deciduous dentition (Štembír-ek et al., 2010; Yamanaka et al., 2010).

### 4.2 | Differential expression of ECM genes suggest a potential role in modulating tooth crown morphogenesis

We identified numerous genes involved in the ECM, basement membrane, and cell junctions that are differentially expressed between tooth classes at the early bell stage. The early bell stage is an important stage during morphogenesis of the tooth crown, just after the initial cusp pattern has been established molecularly but before cellular differentiation and subsequent deposition of mineralized tissues. Differentially expressed genes associated with ECM and cell junctions detected here are known to play important roles in odontogenesis. Previous studies showed that mutations in four of these genes (*Col1a1*, *Col1a2*, *Col7a1*, and *Krt16*) are associated with aberrant tooth development, including enamel and dentin defects (Andersson et al., 2017; Duverger et al., 2019; Umemoto et al., 2012). Our transcriptomic and spatial expression results are congruent with previous findings that collagen proteins are produced throughout the bell stage, initially in dental mesenchyme, and subsequently in predentin and dentin (He et al., 2010; Landin et al., 2012; Thesleff et al., 1981; Zvackova et al., 2017). Likewise, our results are consistent with previous work showing *Tenc* expression in the basement membrane just before odontoblast differentiation (Thesleff et al., 1987).

Genes encoding proteins present in gap junctions and tight junctions were also differentially expressed among all three tooth classes. Previous work showed that gap junctions between newly differentiated odontoblasts increase in abundance as the cells become more tightly packed (Larsson & Bloom, 1973; Sasaki & Garant, 1996). *Pnx3*, which is expressed in dental pulp and preodontoblasts, has been shown to regulate preodontoblast proliferation and odontoblast differentiation (Fu et al., 2015; Iwamoto et al., 2017; Panchin et al., 2000). *Claudin 10*, which was upregulated in the incisors, has been documented in odontoblasts (Ohazama & Sharpe, 2007).

One possible explanation for the patterns of differential expression observed in genes associated with the ECM, basement

**FIGURE 4** Quantitative comparisons and spatial localization of differentially expressed extracellular matrix and Wnt pathway proteins. Gene expression plots show fragments per kilobase per million reads per tooth (three replicates) with confidence intervals (a, e, i, m). Note the different Y axes. Immunofluorescence on early bell stage teeth shows the spatial expression patterns of differentially expressed ECM genes (b–d, f–h, j–l) and Wnt pathway genes (n–p, r–t). Collagen 1 (COL1) expression was detected in the basement membrane of the inner enamel epithelium (arrows), in the dental follicle and outside the tooth germ throughout the facial mesenchyme (b–d). Keratin 16 (KRT16) expression was detected in the inner enamel epithelium and the basement membrane surrounding the entire enamel organ (arrows) (f–h). Tenascin (TENC) expression was detected within the stellate reticulum (SR) (asterisk) (j–l). Wnt inhibitory factor 1 (WIF1) was detected in the SR (asterisk), dental mesenchyme, especially in the premolar (arrows), and faintly in the dental epithelium (n–p). Follistatin (FST) was detected in the dental mesenchyme, particularly in the incisor (arrows), the dental epithelium and SR (asterisk) (r–t). Images are representative of sections from at least three embryos. Scale bars: 100  $\mu$ m; all images are at the same scale except (l).



membrane, and cell junctions, is a subtle temporal difference in which the canine and premolar were slightly more advanced in development than the incisor (Figure 1d–f, Figure 2g–i, and Supporting Information: Table 6). Another possibility is that differential expression patterns we observed are due to morphogenetic differences among tooth classes. In the incisor and canine, one large cusp forms whereas on the premolar, multiple cusps form guided by secondary enamel knots, signaling centers in the dental epithelium (Jernvall et al., 1994, 1995; Keränen et al., 1998; Matalova et al., 2005; Vaahtokari et al., 1996). To form the cusps on the tooth crown, the dental epithelium undergoes folding and differential growth, primarily due to proliferation within the cervical loops at the juncture of the inner and outer epithelia (Nanci, 2013). ECM (epithelial and mesenchymal) as well as epithelial cell junctions and basement membrane components help facilitate folding of the inner enamel epithelium (Marin-Riera et al., 2018).

One caveat to our analysis is that differences in cell proportions between samples used for RNA-sequencing have been shown to influence differential gene expression analyses (Hallikas et al., 2021; Pantalacci et al., 2017). Incisors in *F. catus* are considerably smaller than the canine and premolars, and it is conceivable that our differential expression analysis may be affected by having fewer cells collected for the incisor tooth germs than for the canine and premolar teeth. Additional study of *F. catus* embryonic teeth will be required to address this potential bias.

Altogether, our results suggest that DC<sup>1</sup> and DP<sup>3</sup> likely require more time to achieve their larger sizes, respectively, and undergo greater morphogenetic changes than DI<sup>3</sup>. Modulation of genes associated with the ECM and cell junctions may be associated with tissue growth and rearrangement within the tooth, particularly folding of the inner enamel epithelium. Whether the expression differences in particular genes between the three tooth classes are due to differences in developmental timing or crown morphology remains to be determined.

#### 4.3 | Upregulation of Wnt antagonists in incisor compared to canine and premolar

Modulation of Wnt signaling is important for the formation and maintenance of the primary and secondary enamel knots and, in turn, for the proper patterning of cusps on the occlusal surface (Dassule & McMahon, 1998; Zhu et al., 2013). Overexpression of *Wnt3* leads to the loss of ameloblasts and stabilization of  $\beta$ -catenin in the epithelium leads to the development of malformed supernumerary teeth (Järvinen et al., 2006; Liu et al., 2008; Millar et al., 2003). Multiple secreted inhibitors of Wnt signaling (*Wif1*, *Sfrp2*, and *Dkk4*) were upregulated in the incisors and downregulated in both the canine and premolar. *Fst*, a target of Wnt signaling, was upregulated in incisors and plays a role in the asymmetric deposition of enamel in *M. musculus* incisors by inhibiting ameloblast differentiation (Jones et al., 2015; Wang et al., 2004; Willert et al., 2002). *Dkk1* is upregulated in preodontoblasts and odontoblasts (Fjeld et al., 2005)

and was detected in all three tooth germs. It is possible that some mesenchyme cells within these early bell stage teeth were preodontoblasts. In contrast to the incisors, the canine and premolar showed upregulation of *Wnt5a*, a Wnt ligand. In the premolar, *Wisp2*, which encodes an activator of Wnt/ $\beta$ -catenin signaling, was also upregulated (Grünberg et al., 2014; Pennica et al., 1998). Altogether, canine and premolar-specific expression of Wnt ligands and activators coupled with incisor-specific upregulation of Wnt antagonists, indicate that canonical Wnt signaling appears to be downregulated in the incisors relative to the canine and premolar.

#### 4.4 | Differential expression of homeobox genes suggest positional effects on bell stage teeth

Homeobox genes are essential to proper patterning of the dentition early in development, including *Dlx* (Distal-less homeobox), *Msx* (Msh homeobox), and *Lhx* (LIM homeobox) gene families (Chen et al., 1996; Denaxa et al., 2009; Grigoriou et al., 1998; Jowett et al., 1993; Qiu et al., 1997; Thomas et al., 1997; Tureckova et al., 2002; Zhao et al., 2000). The dental homeobox code is a proposed mechanism for regionalization of the heterodont dentition in which the developing jaw is subdivided into regions that are capable of forming different types of teeth as a result of overlapping homeobox gene expression patterns (McCollum & Sharpe, 2001; Sharpe, 1995).

Previous studies of heterodont mammals including the house shrew (*S. murinus*) and the ferret (*M. furo*), as well as a marsupial, the short-tailed opossum (*Monodelphis domestica*), demonstrated conservation of the homeobox code among placental mammals and marsupials and extended the homeobox code to include canine and premolar teeth. These studies showed that distinct combinatorial expression domains of *Barx1*, *Msx1*, and *Alx3* distinguish the incisor, canine, and premolar regions from one another (Miletich et al., 2011; Wakamatsu et al., 2019; Yamanaka et al., 2015). In addition to specifying regions within the dentition, expression of *Barx1* in the least shrew (*C. parva*) has been shown to correlate positively with the number of cusps on premolar and molar teeth; teeth with more cusps have higher *Barx1* expression (Miletich et al., 2011).

Our differential expression analysis revealed a role for homeobox genes much later in dental development, at the early bell stage. In *F. catus*, *Dlx3*, *Dlx4*, and *Dlx6* were upregulated in the canine relative to the incisor and *Dlx6* was also upregulated in the premolar. These results are congruent with previous findings in *M. musculus* in which *Dlx2* and *Dlx3* were expressed in ameloblasts and *Dlx6* was expressed in the dental papilla (Lézet et al., 2008; Zhao et al., 2000). Previous transcriptomic profiling of *M. musculus* incisors and molars found that *Dlx6* was upregulated in the first molar relative to the incisor (Laugel-Haushalter et al., 2013). In *F. catus* we detected upregulation of *Lhx6* in the premolar and *Lhx9* in the canine. Though *M. musculus* does not have canines or premolars, *Lhx6* and *Lhx7* are required for the development of molars, but not incisors (Denaxa et al., 2009; Grigoriou et al., 1998). These results suggest that LIM homeobox genes are important for the development of canines, premolars, and

molars but not incisors. Interestingly, *Nkx3.1*, a negative regulator of epithelial growth in the prostate, was highly upregulated in the incisor, which is smaller than the canine or premolar teeth, suggesting that *Nkx3.1* may perform a similar function in the dental epithelium to help limit tooth size (Lei et al., 2006). Functional experiments to test whether *Nkx3.1* affects tooth size would be needed to address this hypothesis.

#### 4.5 | Insight from the mammalian fossil record on incisor and canine crown morphology

Recent work on dental development in mammal species with incisor, canine, premolar, and molar teeth have significantly enhanced our understanding of dental patterning and the molecular regulation of tooth class identity but, how different crown morphologies form in distinct tooth classes remains to be determined. The fossil record provides some insight into this question because crown morphologies have varied extensively within individual tooth classes throughout mammalian evolution in different lineages. Tooth crown morphology is tightly associated with a mammal's dietary ecology and teeth at different positions in the tooth row perform distinct functions during chewing; incisors are used primarily to procure food, canines pierce and hold, premolars hold and prepare food for the molars, which usually shear, crush, or grind (Rose, 2006). The appearance of functionally analogous tribosphenic molars in multiple lineages, including early mammaliaformes (e.g., tribosphenidians and docodonts) and in Therian mammals, is generally thought to have given rise to the diversity of crown morphologies observed in both fossil and extant placental (Eutherian) mammals (Davis, 2011; Kielan-Jaworowska et al., 2004; Luo et al., 2001; Rose, 2006).

Examination of extant and extinct mammals brings to light numerous examples of cusp patterns that diverge from the "typical" cusp pattern of a particular tooth class. Though the majority of mammal species, including *F. catus*, have incisors with one main cusp that is either conical or spatulate, multi-cusped incisors with complex crown morphologies have evolved independently in different groups of mammals including extinct plesiadapiform primates (e.g., plesiadapoids, paromomyids, micromomyids, and saxonellids), common shrews (e.g., *Sorex*), and nyctitheriids (Bloch et al., 2002, 2007; Gingerich, 1975, 1976; Manz & Bloch, 2015; Rose et al., 1993; Rose, 1973; Silcox & Gunnell, 2008) (Figure 5 and Supporting Information: Results 6.2).

The morphological diversity in incisor crowns raises the question of how the typical (ancestral) single-cusped incisor crown could be modified developmentally to form a complex crown as seen in species such as *Ignacius graybullianus* and *Plesiadapis churchilli* (Figure 5). We found that in *F. catus* each tooth class exhibits a predominantly unique transcriptional profile at the early bell stage. If differences in gene expression regulate tooth class identity, we predict that a multi-cusped incisor would possess a gene expression profile distinct from that of a multi-cusped premolar or molar. Specifically, we predict that for an incisor to develop multiple cusps, a

shift in gene expression that led to the formation of a secondary enamel knot(s), could give rise to an additional cusp (or cusps) on the incisor crown, without affecting the other tooth classes (Jernvall et al., 1994; Keränen et al., 1998; Kettunen & Thesleff, 1998). In molars of house mice (*M. musculus*), and sibling voles (*Microtus rossiaemeridionalis* and *Microtus epiroticus*) the addition of multiple cusps on the molar crown results from repeated expression of the same molecular cascade associated with cusp formation (Jernvall et al., 1994; Keränen et al., 1998). Cusp number has been shown to correlate with primary enamel knot size and ectodysplasin signaling specifically has been shown to regulate cusp number and pattern in *M. musculus* molars (Harjunmaa et al., 2012, 2014).

From an evolutionary perspective, subtle shifts in the expression of specific genes (i.e., those associated with secondary enamel knots)

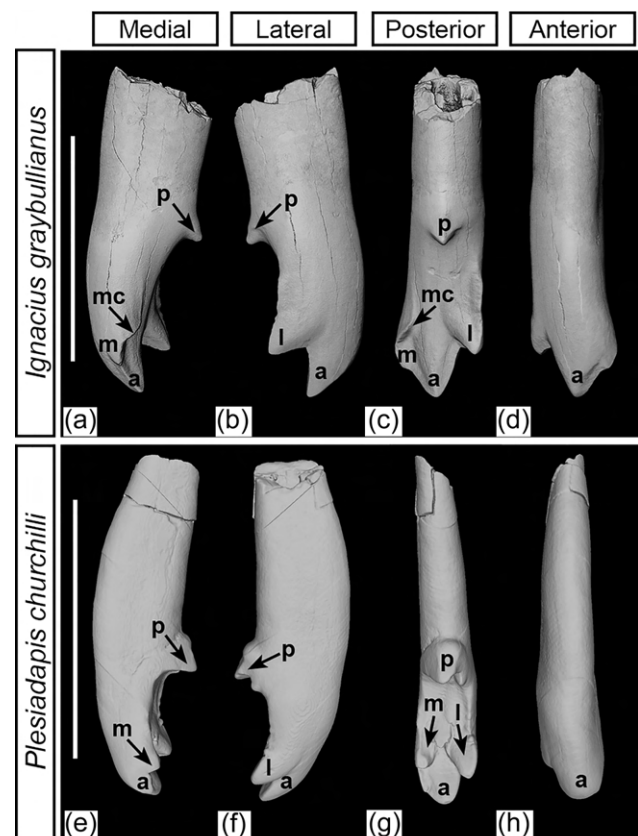


**FIGURE 5** Upper central incisors ( $I^1$ ) of two species of fossil Plesiadapiform Primates, Eocene *Ignacius graybullianus* (a–d) and Paleocene *Plesiadapis churchilli* (e–h), each with multiple, prominent cusps on the occlusal surface. three-dimensional renderings from microcomputed tomography scans of fossil incisors of *I. graybullianus* (Florida Museum of Natural History Vertebrate Paleontology Collection; UF-VP 331494) and *P. churchilli* (University of Alberta Laboratory for Vertebrate Paleontology; UALVP 9470; Morphosource ID: M24106) (see Acknowledgments for specimen details). The upper  $I^1$  of *I. graybullianus* is described here for the first time (see Supporting Information: Results 6.2). The upper  $I^1$  of *P. churchilli* was previously described (Gingerich, 1976). Scale bars: 5 mm. a, anterocone; l, laterocone; m, mediocone; mc, mediocrista; p, postercone.

during tooth development among individuals could result in morphological variation of a heritable trait (e.g., cusp number, size, or arrangement on the tooth crown) within a population on which natural selection could act, thereby altering tooth crown morphology within a particular region in the dentition, such as the central incisors.

In contrast to incisors, canine morphology appears limited to single-cusped teeth in fossil and in extant mammals with rare exceptions in flying lemurs (Dermoptera) (Kielan-Jaworowska et al., 2004; Rose, 2006). In one extant flying lemur, *Galeopterus*, the canine possesses small cuspules similar to the incisors, however, in the other extant genus, *Cynocephalus*, the canine is single-cusped (Stafford & Szalay, 2000). Within fossil members of Plagiomenidae, *Plagiomene* also has a canine with a small cusp at the base of the tooth crown (Rose, 1973). Despite the lack of morphological diversity within canine crowns, there are some variations on canine shape. Canines are incisiform in some species, including humans, while in other species they are dramatically enlarged (e.g., sabertooth cat [*Smilodon*]). The difference between incisor and canine teeth in terms of their observable morphologies implies that the incisors may be more malleable developmentally than the canines. Alternatively, there may be developmental and/or functional (e.g., occlusion) constraints that, in the majority of mammals, inhibit cusps from forming on the canine.

Taking morphological evidence from extant and fossil mammals into consideration along with the transcriptomic data presented here, it appears that a tooth's regional position and crown morphology (namely, the number, and arrangement of cusps) may be developmentally decoupled from one another. The degree to which tooth position along the anterior-posterior axis influences crown morphology is likely determined by both developmental and functional constraints. The occurrence of multi-cusped incisors in distinct mammal lineages and the conspicuous lack of multi-cusped incisors in the majority of mammal species suggests that the incisors may be more developmentally labile than the canines.

## AUTHOR CONTRIBUTIONS

Emily D. Woodruff, Martin J. Cohn, and Brooke A. Armfield designed the experiments. Emily D. Woodruff, Brooke A. Armfield, and Bonnie K. Kircher collected feline tissue provided by Julie K. Levy, and Emily D. Woodruff and Brooke A. Armfield performed the laser-capture microdissection. Emily D. Woodruff performed the histological assays, RNA-extractions, genotyping, and bioinformatics analyses of the RNA-seq data. Emily D. Woodruff and Bonnie K. Kircher CT-scanned the embryos and Bonnie K. Kircher generated the 3-D reconstructions. Emily D. Woodruff conducted the immunofluorescence. Emily D. Woodruff, Martin J. Cohn, and Jonathan I. Bloch wrote the manuscript. All authors read and approved the final manuscript.

## ACKNOWLEDGMENTS

We thank Operation Catnip for sharing the uteri removed during routine spay/neuter surgery, Dr. Thom Sanger for assistance collecting embryos, Galaxy Gutierrez and Blake Hauer for help with

sectioning embryos, and Emily Merton for technical support. We thank Dr. Verity Mathis and Dr. David Reed for access to the UF Mammalogy collections, staff at the University of Florida High Performance Computing Center, especially Dr. Matt Gitzendanner and Dr. Oleksandr Moskalenko, and Dr. Gary Scheiffle and Dr. Edward Stanley at the University of Florida Nanoscale Research Facility.  $\mu$ CT reconstructions of the upper incisor of *Ignacius graybullianus* (Florida Museum of Natural History Vertebrate Paleontology Collection: UF-VP 331494) were graciously provided by Dr. Paul Morse (Duke University) and Margarita Hernandez (Pennsylvania State University). Dr. Douglas Boyer (Duke University) kindly made  $\mu$ CT reconstructions of *Plesiadapis* incisors available, the collection of which was funded by NSF BCS 1317525 (to DM Boyer and ER Seiffert), 1552848 (to DM Boyer) and Duke University Trinity College of Arts and Sciences. The following file was downloaded from [www.MorphoSource.org](http://www.MorphoSource.org), Duke University: upper incisor of *Plesiadapis churchilli* (University of Alberta Laboratory for Vertebrate Paleontology: UALVP 9470; Morphosource ID: M24106). Finally, we thank members of the Cohn laboratory and Dr. Gareth Fraser for insightful discussion of this study. This study was supported by an NSF DDRIG 1455572 to EDW and MJC, and a University of Florida Michael L. May grant to EDW.

## CONFLICTS OF INTEREST

The authors declare no conflict of interest.

## DATA AVAILABILITY STATEMENT

Sequence data from this study will be freely available to the public on the NCBI sequence read archive (<https://www.ncbi.nlm.nih.gov/sra>) BioProject PRJNA643853.

## ORCID

Emily D. Woodruff  <http://orcid.org/0000-0001-5267-6094>

## PEER REVIEW

The peer review history for this article is available at <https://publons.com/publon/10.1002/jez.b.23168>

## REFERENCES

- Aiello, S., & Moses, M. (2016). *The merck veterinary manual* (11th ed.). Merck.
- Andersson, K., Dahllöf, G., Lindahl, K., Kindmark, A., Grigelioniene, G., Åström, E., & Malmgren, B. (2017). Mutations in COL1A1 and COL1A2 and dental aberrations in children and adolescents with osteogenesis imperfecta—A retrospective cohort study. *PLoS One*, 12(5), e0176466. <https://doi.org/10.1371/journal.pone.0176466>
- Bloch, J. I., Boyer, D. M., Gingerich, P. D., & Gunnell, G. F. (2002). New primitive paromomyid from the Clarkforkian of Wyoming and dental eruption in Plesiadapiformes. *Journal of Vertebrate Paleontology*, 22(2), 366–379. [https://doi.org/10.1671/0272-4634\(2002\)022\[0366:NPPFTC\]2.0.CO;2](https://doi.org/10.1671/0272-4634(2002)022[0366:NPPFTC]2.0.CO;2)
- Bloch, J. I., Silcox, M. T., Boyer, D. M., & Sargis, E. J. (2007). New paleocene skeletons and the relationship of plesiadapiforms to crown-clade primates. *Proceedings of the National Academy of Sciences*, 104(4), 1159–1164. <https://doi.org/10.1073/pnas.0610579104>



- Bolger, A. M., Lohse, M., & Usadel, B. (2014). Trimmomatic: A flexible trimmer for illumina sequence data. *Bioinformatics (Oxford, England)*, 30(15), 2114–2120. <https://doi.org/10.1093/bioinformatics/btu170>
- Chen, Y., Bei, M., Woo, I., Satokata, I., & Maas, R. (1996). Msx1 controls inductive signaling in mammalian tooth morphogenesis. *Development*, 122(10), 3035–3044.
- Dassule, H. R., & McMahon, A. P. (1998). Analysis of epithelial–mesenchymal interactions in the initial morphogenesis of the mammalian tooth. *Developmental Biology*, 202(2), 215–227. <https://doi.org/10.1006/dbio.1998.8992>
- Davis, B. M. (2011). Evolution of the tribosphenic molar pattern in early mammals, with comments on the “Dual-Origin” hypothesis. *Journal of Mammalian Evolution*, 18(4), 227–244. <https://doi.org/10.1007/s10914-011-9168-8>
- Denaxa, M., Sharpe, P. T., & Pachnis, V. (2009). The LIM homeodomain transcription factors Lhx6 and Lhx7 are key regulators of mammalian dentition. *Developmental Biology*, 333(2), 324–336. <https://doi.org/10.1016/j.ydbio.2009.07.001>
- Duverger, O., Cross, M. A., Smith, F. J. D., & Morasso, M. I. (2019). Enamel anomalies in a pachyonychia congenita patient with a mutation in KRT16. *Journal of Investigative Dermatology*, 139(1), 238–241. <https://doi.org/10.1016/j.jid.2018.07.005>
- Evans, A. R., Wilson, G. P., Fortelius, M., & Jernvall, J. (2007). High-level similarity of dentitions in carnivorans and rodents. *Nature*, 445(7123), 78–81. <https://doi.org/10.1038/nature05433>
- Fjeld, K., Kettunen, P., Furmanek, T., Kvinnsland, I. H., & Luukko, K. (2005). Dynamic expression of Wnt signaling-related Dickkopf1, -2, and -3 mRNAs in the developing mouse tooth. *Developmental Dynamics*, 233(1), 161–166. <https://doi.org/10.1002/dvdy.20285>
- Fu, D., Song, F., Sun, H., Pei, D., Wang, Y., Lei, J., & Huang, C. (2015). Expression of Pannexin3 in human odontoblast-like cells and its hemichannel function in mediating ATP release. *Archives of Oral Biology*, 60(10), 1510–1516. <https://doi.org/10.1016/j.archoralbio.2015.07.005>
- Gaunt, W. A. (1959a). The development of the deciduous cheek teeth of the cat. *Acta Anatomica*, 38, 187–212.
- Gaunt, W. A. (1959b). The vascular supply to the dental lamina during early development. *Acta Anatomica*, 37, 232–252.
- Gingerich, P. D. (1975). New North American Plesiadapidae (Mammalia, Primates) and a biostratigraphic zonation of the Middle and Upper Paleocene, *Contributions from the Museum of Paleontology* (Vol. 24, issue 13). University of Michigan. <http://deepblue.lib.umich.edu/handle/2027.42/48480>
- Gingerich, P. D. (1976). Cranial anatomy and evolution of Early Tertiary Plesiadapidae (Mammalia, Primates), *Contributions from the Museum of Paleontology* (Vol. 15). University of Michigan. <http://deepblue.lib.umich.edu/handle/2027.42/48615>
- Gingerich, P. D. (1977). Patterns of Evolution in the Mammalian Fossil Record. In A. Hallam (Ed.), *Patterns of Evolution as Illustrated by the Fossil Record* (Vol. 5, p. 591). Elsevier.
- Grigoriou, M., Tucker, A. S., Sharpe, P. T., & Pachnis, V. (1998). Expression and regulation of Lhx6 and Lhx7, a novel subfamily of LIM homeodomain encoding genes, suggests a role in mammalian head development. *Development (Cambridge, England)*, 125(11), 2063–2074.
- Grünberg, J. R., Hammarstedt, A., Hedjazifaz, S., & Smith, U. (2014). The novel secreted adipokine WNT1-inducible signaling pathway protein 2 (WISP2) is a mesenchymal cell activator of Canonical WNT. *Journal of Biological Chemistry*, 289(10), 6899–6907. <https://doi.org/10.1074/jbc.M113.511964>
- Haas, B. J., Papanicolaou, A., Yassour, M., Grabherr, M., Blood, P. D., Bowden, J., Couger, M. B., Eccles, D., Li, B., Lieber, M., MacManes, M. D., Ott, M., Orvis, J., Pochet, N., Strozzi, F., Weeks, N., Westerman, R., William, T., Dewey, C. N., ... Regav, A. (2013). De novo transcript sequence reconstruction from RNA-seq using the Trinity platform for reference generation and analysis. *Nature Protocols*, 8(8), 1494–1512. <https://doi.org/10.1038/nprot.2013.084>
- Hallikas, O., Das Roy, R., Christensen, M. M., Renvoisé, E., Sulic, A.-M., & Jernvall, J. (2021). System-level analyses of keystone genes required for mammalian tooth development. *Journal of Experimental Zoology Part B: Molecular and Developmental Evolution*, 336(1), 7–17. <https://doi.org/10.1002/jez.b.23009>
- Harjunmaa, E., Kallonen, A., Voutilainen, M., Hämäläinen, K., Mikkola, M. L., & Jernvall, J. (2012). On the difficulty of increasing dental complexity. *Nature*, 483(7389), 324–327. <https://doi.org/10.1038/nature10876>
- Harjunmaa, E., Seidel, K., Häkkinen, T., Renvoisé, E., Corfe, I. J., Kallonen, A., Zhang, Z. Q., Evans, A. R., Mikkola, M. L., Salazar-Ciudad, I., Klein, O. D., & Jernvall, J. (2014). Replaying evolutionary transitions from the dental fossil record. *Nature*, 512(7512), 44–48. <https://doi.org/10.1038/nature13613>
- Hashimoto, K., Noshiro, M., Ohno, S., Kawamoto, T., Satakeda, H., Akagawa, Y., Nakashima, K., Okimura, A., Ishida, H., Okamoto, T., Pan, H., Shen, M., Yan, W., & Kato, Y. (1997). Characterization of a cartilage-derived 66-kDa protein (RGD-CAP/βig-h3) that binds to collagen1. *Biochimica et Biophysica Acta (BBA) - Molecular Cell Research*, 1355(3), 303–314. [https://doi.org/10.1016/S0167-4889\(96\)00147-4](https://doi.org/10.1016/S0167-4889(96)00147-4)
- He, P., Zhang, Y., Kim, S. O., Radlanski, R. J., Butcher, K., Schneider, R. A., & DenBesten, P. K. (2010). Ameloblast differentiation in the human developing tooth: Effects of extracellular matrices. *Matrix Biology*, 29(5), 411–419. <https://doi.org/10.1016/j.matbio.2010.03.001>
- Iwamoto, T., Nakamura, T., Ishikawa, M., Yoshizaki, K., Sugimoto, A., Ida-Yonemochi, H., Ohshima, H., Saito, M., Yamada, Y., & Fukumoto, S. (2017). Pannexin 3 regulates proliferation and differentiation of odontoblasts via its hemichannel activities. *PLoS One*, 12(5), e0177557. <https://doi.org/10.1371/journal.pone.0177557>
- Järvinen, E., Salazar-Ciudad, I., Birchmeier, W., Taketo, M. M., Jernvall, J., & Thesleff, I. (2006). Continuous tooth generation in mouse is induced by activated epithelial Wnt/beta-catenin signaling. *Proceedings of the National Academy of Sciences of the United States of America*, 103(49), 18627–18632. <https://doi.org/10.1073/pnas.0607289103>
- Jernvall, J. (1995). *Mammalian Molar Cusp Patterns: Developmental Mechanisms of Diversity* (Vol. 198). Acta Zoologica Fennica.
- Jernvall, J., Kettunen, P., Karavanova, I., Martin, L. B., & Thesleff, I. (1994). Evidence for the role of the enamel knot as a control center in mammalian tooth cusp formation: Non-dividing cells express growth stimulating Fgf-4 gene. *International Journal of Developmental Biology*, 38(3), 463–469.
- Jernvall, J. & Thesleff, I. (2000). Reiterative signaling and patterning during mammalian tooth morphogenesis. *Mechanisms of Development*, 92(1), 19–29. [https://doi.org/10.1016/S0925-4773\(99\)00322-6](https://doi.org/10.1016/S0925-4773(99)00322-6)
- Jones, A. E., Price, F. D., Le Grand, F., Soleimani, V. D., Dick, S. A., Megeney, L. A., & Rudnicki, M. A. (2015). Wnt/β-catenin controls follistatin signalling to regulate satellite cell myogenic potential. *Skeletal Muscle*, 5, 14. <https://doi.org/10.1186/s13395-015-0038-6>
- Jowett, A. K., Vainio, S., Ferguson, M. W., Sharpe, P. T., & Thesleff, I. (1993). Epithelial–mesenchymal interactions are required for Msx 1 and Msx 2 gene expression in the developing murine molar tooth. *Development*, 117(2), 461–470.
- Keränen, S. V., Aberg, T., Kettunen, P., Thesleff, I., & Jernvall, J. (1998). Association of developmental regulatory genes with the development of different molar tooth shapes in two species of rodents. *Development Genes and Evolution*, 208(9), 477–486. <https://doi.org/10.1007/s004270050206>
- Kettunen, P., & Thesleff, I. (1998). Expression and function of FGFs-4, -8, and -9 suggest functional redundancy and repetitive use as epithelial signals during tooth morphogenesis. *Developmental*

- Dynamics*, 211(3), 256–268. [https://doi.org/10.1002/\(SICI\)1097-0177\(199803\)211:3%3C256::AID-AJA7%3E3.0.CO;2-G](https://doi.org/10.1002/(SICI)1097-0177(199803)211:3%3C256::AID-AJA7%3E3.0.CO;2-G)
- Kielan-Jaworowska, Z., Cifelli, R. L., & Luo, Z.-X. (2004). *Mammals from the Age of Dinosaurs: Origins, Evolution, and Structure*. Columbia University Press.
- Knospe, C. (2002). Periods and stages of the prenatal development of the domestic cat. *Anatomia, Histologia, Embryologia*, 31(1), 37–51. <https://doi.org/10.1046/j.1439-0264.2002.00360.x>
- Landin, M. A., dos, S. S., Shabestari, M., Babaie, E., Reseland, J. E., & Osmundsen, H. (2012). Gene expression profiling during murine tooth development. *Frontiers in Genetics*, 3, 139. <https://doi.org/10.3389/fgene.2012.00139>
- Larsson, Å. & Bloom, G. D. (1973). Studies on dentinogenesis in the rat. *Zeitschrift für Anatomie und Entwicklungsgeschichte*, 139(3), 227–246. <https://doi.org/10.1007/BF00519966>
- Laugel-Haushalter, V., Paschaki, M., Thibault-Carpentier, C., Dembelé, D., Dollé, P., & Bloch-Zupan, A. (2013). Molars and incisors: Show your microarray IDs. *BMC Research Notes*, 6, 113. <https://doi.org/10.1186/1756-0500-6-113>
- Lei, Q., Jiao, J., Xin, L., Chang, C.-J., Wang, S., Gao, J., Gleave, M. E., Witte, O. N., Liu, X., & Wu, H. (2006). NKX3.1 stabilizes p53, inhibits AKT activation, and blocks prostate cancer initiation caused by PTEN loss. *Cancer Cell*, 9(5), 367–378. <https://doi.org/10.1016/j.ccr.2006.03.031>
- Lézot, F., Thomas, B., Greene, S. R., Hotton, D., Yuan, Z.-A., Castaneda, B., Bolaños, A., Depew, M., Sharpe, P., Gibson, C. W., & Berdal, A. (2008). Physiological implications of DLX homeoproteins in enamel formation. *Journal of Cellular Physiology*, 216(3), 688–697. <https://doi.org/10.1002/jcp.21448>
- Liu, F., Chu, E. Y., Watt, B., Zhang, Y., Gallant, N. M., Andl, T., Yang, S. H., Lu, M. M., Piccolo, S., Schmidt-Ullrich, R., Taketo, M. M., Morrissey, E. E., Atit, R., Dlugosz, A. A., & Millar, S. E. (2008). Wnt/ $\beta$ -catenin signaling directs multiple stages of tooth morphogenesis. *Developmental Biology*, 313(1), 210–224. <https://doi.org/10.1016/j.ydbio.2007.10.016>
- Luo, Z.-X., Cifelli, R. L., & Kielan-Jaworowska, Z. (2001). Dual origin of tribosphenic mammals. *Nature*, 409(6816), 53–57. <https://doi.org/10.1038/35051023>
- Manz, C. L., & Bloch, J. I. (2015). Systematics and Phylogeny of Paleocene-Eocene Nyctitheriidae (Mammalia, Eulipotyphla?) with description of a new species from the late Paleocene of the Clarks Fork Basin, Wyoming, USA. *Journal of Mammalian Evolution*, 22(3), 307–342. <https://doi.org/10.1007/s10914-014-9284-3>
- Marin-Riera, M., Moustakas-Verho, J., Savriama, Y., Jernvall, J., & Salazar-Ciudad, I. (2018). Differential tissue growth and cell adhesion alone drive early tooth morphogenesis: An ex vivo and in silico study. *PLoS Computational Biology*, 14(2), e1005981. <https://doi.org/10.1371/journal.pcbi.1005981>
- Matalova, E., Tucker, A. S., & Misek, I. (2005). Apoptosis-related factors (Fas receptor, Fas ligand, FADD) in early tooth development of the field vole (*Microtus agrestis*). *Archives of Oral Biology*, 50(2), 165–169. <https://doi.org/10.1016/j.archoralbio.2004.10.012>
- McCollum, M., & Sharpe, P. T. (2001). Evolution and development of teeth. *Journal of Anatomy*, 199(1–2), 153–159. <https://doi.org/10.1046/j.1469-7580.2001.19910153.x>
- Miletich, I., Yu, W.-Y., Zhang, R., Yang, K., Caixeta de Andrade, S., Pereira, S. F., Ohazama, A., Mock, O. B., Buchner, G., Sealby, J., Webster, Z., Zhao, M., Bei, M., & Sharpe, P. T. (2011). Developmental stalling and organ-autonomous regulation of morphogenesis. *Proceedings of the National Academy of Sciences*, 108(48), 19270–19275. <https://doi.org/10.1073/pnas.1112801108>
- Millar, S. E., Koyama, E., Reddy, S. T., Andl, T., Gaddapara, T., Piddington, R., & Gibson, C. W. (2003). Over- and ectopic expression of Wnt3 causes progressive loss of ameloblasts in postnatal mouse incisor teeth. *Connective Tissue Research*, 44(Suppl 1), 124–129.
- Moss-Salentijn, L. (1982). Morphological aspects of the growth behavior of the early dental lamina in the cat and rat, *Teeth: Form function and evolution* (pp. 7–20). Columbia University Press. <https://ci.nii.ac.jp/naid/10023893480/>
- Nanci, A. (2013). *Ten Cate's Oral Histology* (8th ed.). Elsevier.
- Ohazama, A., & Sharpe, P. T. (2007). Expression of claudins in murine tooth development. *Developmental Dynamics*, 236(1), 290–294. <https://doi.org/10.1002/dvdy.21001>
- Panchin, Y., Kelmanson, I., Matz, M., Lukyanov, K., Usman, N., & Lukyanov, S. (2000). A ubiquitous family of putative gap junction molecules. *Current Biology*, 10(13), R473–R474. [https://doi.org/10.1016/S0960-9822\(00\)00576-5](https://doi.org/10.1016/S0960-9822(00)00576-5)
- Pantalacci, S., Guéguen, L., Petit, C., Lambert, A., Peterková, R., & Sémon, M. (2017). Transcriptomic signatures shaped by cell proportions shed light on comparative developmental biology. *Genome Biology*, 18(1), 29. <https://doi.org/10.1186/s13059-017-1157-7>
- Pennica, D., Swanson, T. A., Welsh, J. W., Roy, M. A., Lawrence, D. A., Lee, J., Brush, J., Taneyhill, L. A., Deuel, B., Lew, M., Watanabe, C., Cohen, R. L., Melhem, M. F., Finley, G. G., Quirke, P., Goddard, A. D., Hillan, K. J., Gurney, A. L., Botstein, D., & Levine, A. J. (1998). WISP genes are members of the connective tissue growth factor family that are up-regulated in Wnt-1-transformed cells and aberrantly expressed in human colon tumors. *Proceedings of the National Academy of Sciences*, 95(25), 14717–14722.
- Perteau, M., Kim, D., Perteau, G., Leek, J. T., & Salzberg, S. L. (2016). Transcript-level expression analysis of RNA-seq experiments with HISAT, StringTie and Ballgown. *Nature Protocols*, 11(9), 1650–1667. <https://doi.org/10.1038/nprot.2016.095>
- Qiu, M., Bulfone, A., Ghattas, I., Meneses, J. J., Christensen, L., Sharpe, P. T., Presley, R., Pedersen, R. A., & Rubenstein, J. L. (1997). Role of the Dlx homeobox genes in proximodistal patterning of the branchial arches: Mutations of Dlx-1, Dlx-2, and Dlx-1 and -2 alter morphogenesis of proximal skeletal and soft tissue structures derived from the first and second arches. *Developmental Biology*, 185(2), 165–184. <https://doi.org/10.1006/dbio.1997.8556>
- Rose, K. D. (1973). The mandibular dentition of Plagiomenes (Dermoptera, Plagiomenidae), *Breviora*. Museum of Comparative Zoology (Vol. 1973, issue. 411 pp. 410–436). Harvard University.
- Rose, K. D. (2006). *The Beginning of the Age of Mammals*. Johns Hopkins University Press.
- Rose, K. D., Beard, K. C., & Houde, P. (1993). Exceptional new dentitions of the diminutive plesiadapiforms *Tinimomys* and *Niptomomys* (Mammalia), with comments on the upper incisors of Plesiadapiformes. *Annals of Carnegie Museum*, 62(4), 23.
- Sasaki, T., & Garant, P. R. (1996). Structure and organization of odontoblasts. *The Anatomical Record*, 245(2), 235–249. [https://doi.org/10.1002/\(SICI\)1097-0185\(199606\)245:2%3C235::AID-AR10%3E3.0.CO;2-Q](https://doi.org/10.1002/(SICI)1097-0185(199606)245:2%3C235::AID-AR10%3E3.0.CO;2-Q)
- Sharpe, P. T. (1995). Homeobox genes and orofacial development. *Connective Tissue Research*, 32(1–4), 17–25. <https://doi.org/10.3109/03008209509013701>
- Silcox, M. T., & Gunnell, G. F. (2008). Plesiadapiformes. In C. M. Janis, G. F. Gunnell, & M. D. Uhen (Eds.), *Evolution of Tertiary Mammals of North America* (pp. 207–238). Cambridge University Press. <https://doi.org/10.1017/CBO9780511541438.015>
- Slaughter, B., Pine, R., & Etoh Pine, N. (1974). Eruption of cheek teeth in Insectivora and Carnivora. *Journal of Mammalogy*, 55, 115–125. <https://doi.org/10.2307/1379261>
- Stafford, B. J., & Szalay, F. S. (2000). Craniodental functional morphology and taxonomy of dermopterans. *Journal of Mammalogy*, 81(2), 26–385.
- Štembírek, J., Buchtová, M., Král, T., Matalová, E., Lozanoff, S., & Mišek, I. (2010). Early morphogenesis of heterodont dentition in minipigs. *European Journal of Oral Sciences*, 118(6), 547–558. <https://doi.org/10.1111/j.1600-0722.2010.00772.x>

- Strait, S. G. (1993). Differences in occlusal morphology and molar size in frugivores and faunivores. *Journal of Human Evolution*, 25(6), 471–484. <https://doi.org/10.1006/jhev.1993.1062>
- Thesleff, I., Barrach, H. J., Foidart, J. M., Vaheri, A., Pratt, R. M., & Martin, G. R. (1981). Changes in the distribution of type IV collagen, laminin, proteoglycan, and fibronectin during mouse tooth development. *Developmental Biology*, 81(1), 182–192. [https://doi.org/10.1016/0012-1606\(81\)90361-4](https://doi.org/10.1016/0012-1606(81)90361-4)
- Thesleff, I., Mackie, E., Vainio, S., & Chiquet-Ehrismann, R. (1987). Changes in the distribution of tenascin during tooth development. *Development*, 20, 25. [https://doi.org/10.1016/0045-6039\(87\)90076-5](https://doi.org/10.1016/0045-6039(87)90076-5)
- Thesleff, I. & Sharpe, P. (1997). Signalling networks regulating dental development. *Mechanisms of Development*, 67(2), 111–123.
- Thomas, B. L., Tucker, A. S., Qui, M., Ferguson, C. A., Hardcastle, Z., Rubenstein, J. L., & Sharpe, P. T. (1997). Role of *Dlx-1* and *Dlx-2* genes in patterning of the murine dentition. *Development*, 124(23), 4811–4818.
- Trapnell, C., Roberts, A., Goff, L., Pertea, G., Kim, D., Kelley, D. R., Pimentel, H., Salzberg, S. L., Rinn, J. L., & Pachter, L. (2012). Differential gene and transcript expression analysis of RNA-seq experiments with TopHat and Cufflinks. *Nature Protocols*, 7(3), 562–578. <https://doi.org/10.1038/nprot.2012.016>
- Tucker, A., & Sharpe, P. (2004). The cutting-edge of mammalian development; how the embryo makes teeth. *Nature Reviews Genetics*, 5(7), 499–508. <https://doi.org/10.1038/nrg1380>
- Tureckova, J., Sahlberg, C., Aberg, T., Ruch, J. V., Thesleff, I., & Peterkova, R. (2002). Comparison of expression of the *Msx-1*, *Msx-2*, *Bmp-2* and *Bmp-4* genes in the mouse upper diastemal and molar tooth primordia. *International Journal of Developmental Biology*, 39(3), 459–468. <https://doi.org/10.1387/ijdb.7577436>
- Umemoto, H., Akiyama, M., Domon, T., Nomura, T., Shinkuma, S., Ito, K., Asaka, T., Sawamura, D., Uitto, J., Uo, M., Kitagawa, Y., & Shimizu, H. (2012). Type VII collagen deficiency causes defective tooth enamel formation due to poor differentiation of ameloblasts. *The American Journal of Pathology*, 181(5), 1659–1671. <https://doi.org/10.1016/j.ajpath.2012.07.018>
- Unger, P. S. (2010). *Mammal Teeth: Origin, Evolution, and Diversity*. Johns Hopkins University Press.
- Vaahokari, A., Aberg, T., Jernvall, J., Keränen, S., & Thesleff, I. (1996). The enamel knot as a signaling center in the developing mouse tooth. *Mechanisms of Development*, 54(1), 39–43. [https://doi.org/10.1016/0925-4773\(95\)00459-9](https://doi.org/10.1016/0925-4773(95)00459-9)
- Van Valkenburgh, B. (2007). Deja vu: The evolution of feeding morphologies in the Carnivora. *Integrative and comparative biology*, 47(1), 147–163. <https://doi.org/10.1093/icb/pcm016>
- Wakamatsu, Y., Egawa, S., Terashita, Y., Kawasaki, H., Tamura, K., & Suzuki, K. (2019). Homeobox code model of heterodont tooth in mammals revised. *Scientific Reports*, 9(1), 1–13. <https://doi.org/10.1038/s41598-019-49116-x>
- Wang, X.-P., Suomalainen, M., Jorgez, C. J., Matzuk, M. M., Werner, S., & Thesleff, I. (2004). Follistatin regulates enamel patterning in mouse incisors by asymmetrically inhibiting BMP signaling and ameloblast differentiation. *Developmental Cell*, 7(5), 719–730. <https://doi.org/10.1016/j.devcel.2004.09.012>
- Werdelin, L. (1987). Supernumerary teeth in *Lynx lynx* and the irreversibility of evolution. *Journal of the Zoological Society of London*, 211, 259–266.
- Willert, J., Epping, M., Pollack, J. R., Brown, P. O., & Nusse, R. (2002). A transcriptional response to Wnt protein in human embryonic carcinoma cells. *BMC Developmental Biology*, 2, 8. <https://doi.org/10.1186/1471-213x-2-8>
- Yamanaka, A., Iwai, H., Uemura, M., & Goto, T. (2015). Patterning of mammalian heterodont dentition within the upper and lower jaws. *Evolution & Development*, 17(2), 127–138. <https://doi.org/10.1111/ede.12116>
- Yamanaka, A., Yasui, K., Sonomura, T., Iwai, H., & Uemura, M. (2010). Development of deciduous and permanent dentitions in the upper jaw of the house shrew (*Suncus murinus*). *Archives of Oral Biology*, 55(4), 279–287. <https://doi.org/10.1016/j.archoralbio.2010.02.006>
- Zhao, Z., Stock, D. W., Buchanan, A. V., & Weiss, K. M. (2000). Expression of *Dlx* genes during the development of the murine dentition. *Development, Genes and Evolution*, 210(5), 270–275. <https://doi.org/10.1007/s004270050314>
- Zhu, X., Zhao, P., Liu, Y., Zhang, X., Fu, J., Ivy Yu, H.-M., Qiu, M., Chen, Y., Hsu, W., & Zhang, Z. (2013). Intra-epithelial requirement of canonical wnt signaling for tooth morphogenesis. *Journal of Biological Chemistry*, 288(17), 12080–12089. <https://doi.org/10.1074/jbc.M113.462473>
- Zvackova, I., Matalova, E., & Lesot, H. (2017). Regulators of collagen fibrillogenesis during molar development in the mouse. *Frontiers in Physiology*, 8, 8. <https://doi.org/10.3389/fphys.2017.00554>

## SUPPORTING INFORMATION

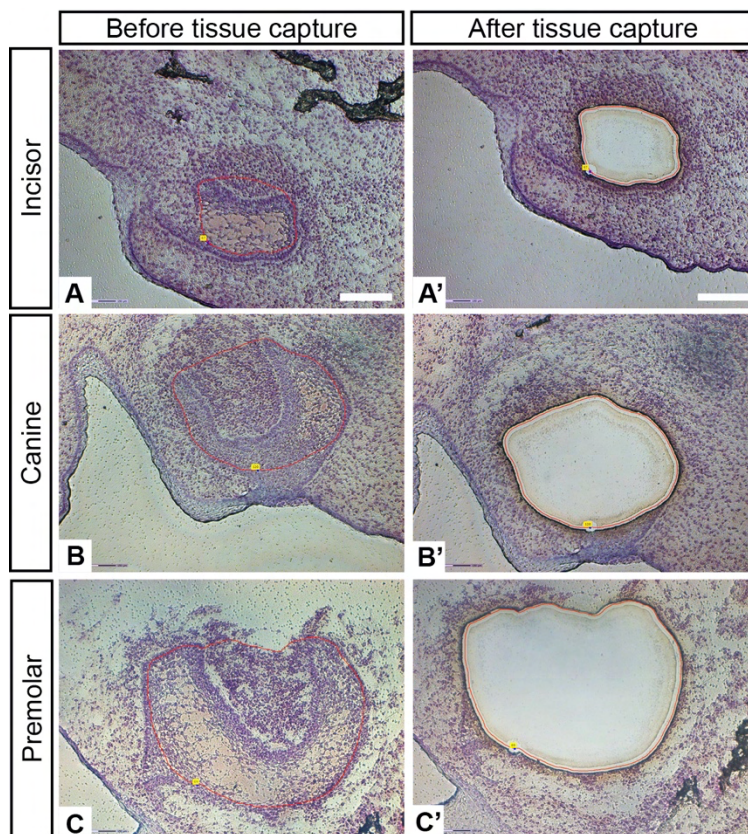
Additional supporting information can be found online in the Supporting Information section at the end of this article.

**How to cite this article:** Woodruff, E. D., Kircher, B. K., Armfield, B. A., Levy, J. K., Bloch, J. I., & Cohn, M. J. (2022). Domestic cat embryos reveal unique transcriptomes of developing incisor, canine, and premolar teeth. *Journal of Experimental Zoology Part B: Molecular and Developmental Evolution*, 1–16. <https://doi.org/10.1002/jez.b.23168>

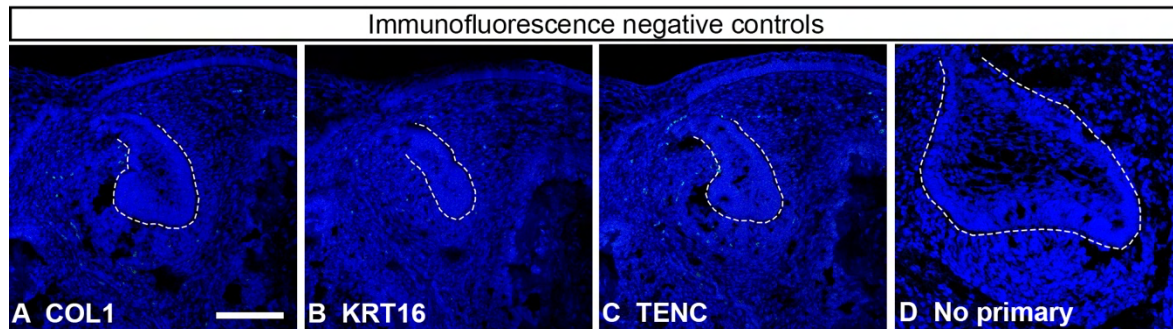


**“Domestic cat embryos reveal unique transcriptomes of developing incisor, canine, and premolar teeth”. (2022). Woodruff, E.D., Kircher, B.K., Armfield, B.A., Levy, J.K., Bloch, J.I., Cohn, M.J. *Journal of Evolutionary Zoology Part B: Molecular and Developmental Evolution*.**

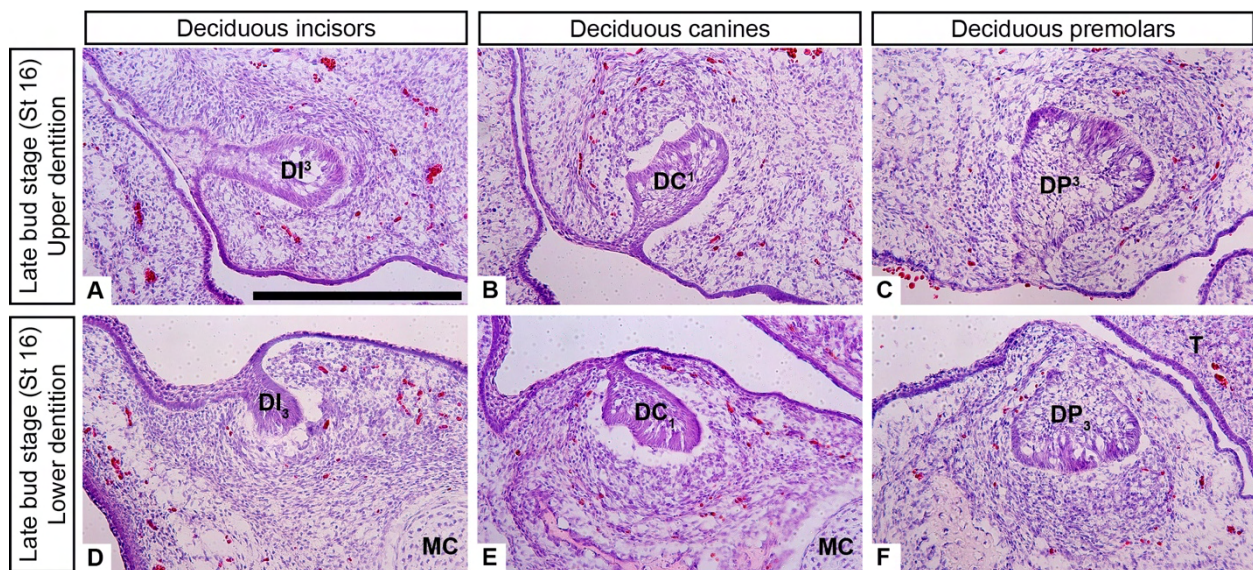
## Supplementary Figures



**Supplementary Figure 1. Laser capture microdissection (LCM) of dental epithelial and mesenchymal tissues used for RNA-sequencing.** Representative frontal cryosections (10 $\mu$ m) stained with cresyl violet showing the tissue that was collected for RNA sequencing from the upper dentition: deciduous third incisors (A, A'), deciduous canines (B, B'), and deciduous third premolars (C, C'). The tissue within the red line was collected, including both dental epithelium and mesenchyme. The dental follicle (the edge of tooth germ) was not captured, to ensure that only dental tissue was collected. To maintain consistency during tissue capture, the dental mesenchyme between the opposing sides of the inner enamel epithelium was collected. Only tooth germs from the embryos' right side are shown. Scale bars: 150 $\mu$ m, images are at the same scale.

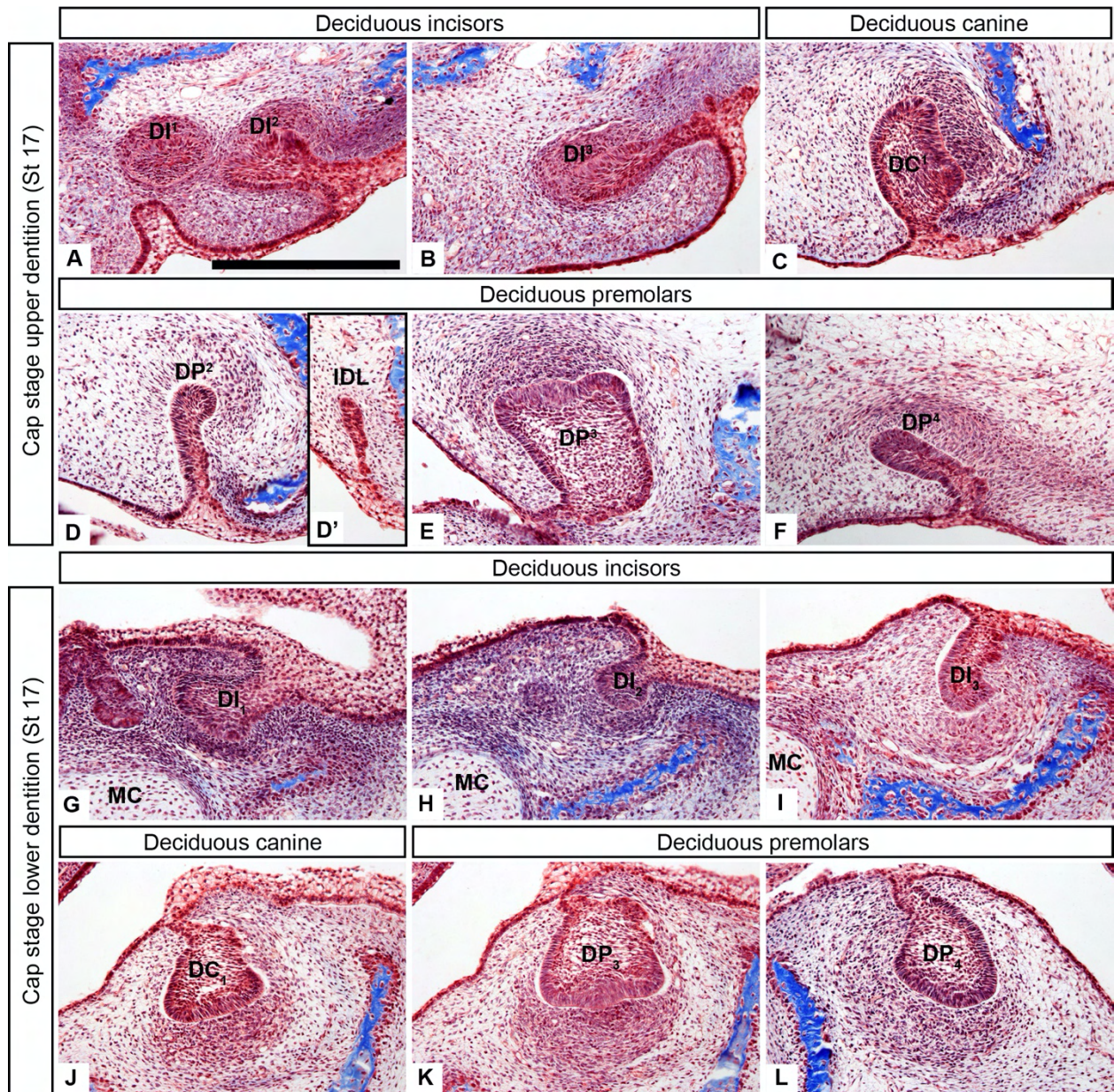


**Supplementary Figure 2. Negative controls for immunofluorescence.** No fluorescent signal was observed on tissue sections of the lower dentition incubated in primary antibody but not secondary antibody except the blue nuclear counterstain (Hoechst) (A-C). Negative controls in which the primary antibodies were omitted and only a secondary antibody was used produced equivalent results (D). The dental epithelium is outlined with a white dotted line. Mild autofluorescence can be observed in red blood cells in some sections. Scale bar is 100µm, images are at the same scale.



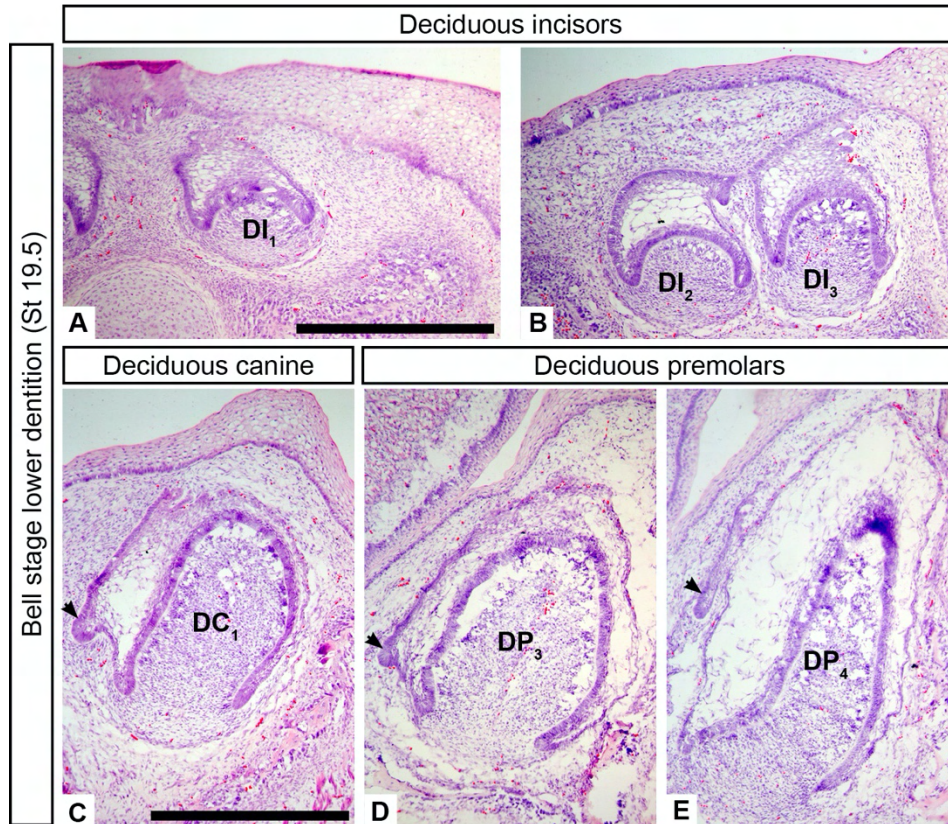
**Supplementary Figure 3. Histological sections of late bud stage deciduous tooth germs in a stage 16 *F. catus* embryo.** Cryosections (10µm) in the frontal plane were stained with hematoxylin and eosin. The dental epithelial buds have grown into the adjacent mesenchyme which has condensed around the epithelial buds. Upper third incisor (A), upper canine (B), upper third premolar bud (C), lower third incisor (D), lower canine (E), lower third premolar (F). Only tooth germs from the embryos' right side are shown. Scale bar: 300µm, all images are at the same scale. MC: Meckel's cartilage, T: tongue.





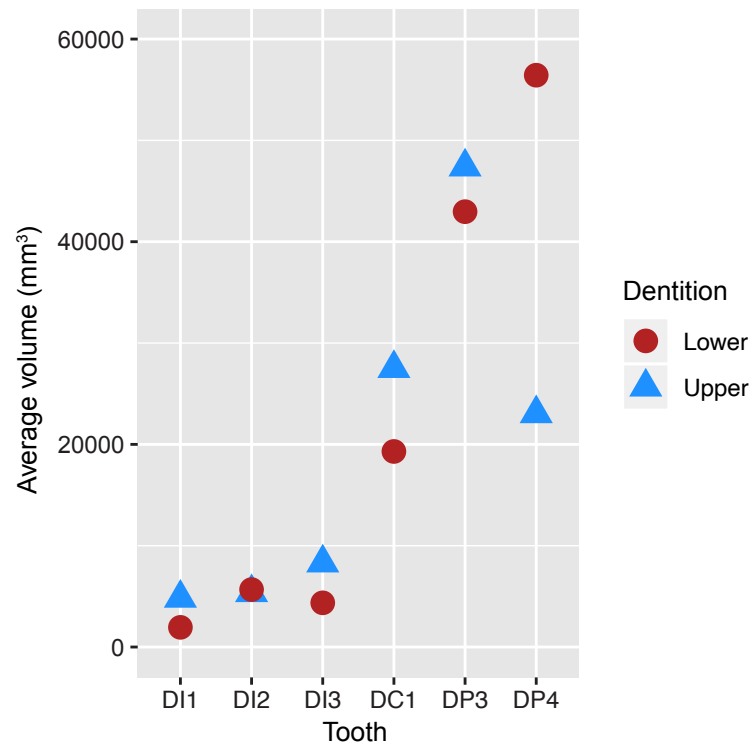
**Supplementary Figure 4. Histological sections showing cap stage deciduous teeth from upper (A-F) and lower (G-L) dentitions of *F. catus* at stage 17.** Paraffin sections (8 $\mu$ m) in the frontal plane were stained with Masson Trichrome. First and second upper incisors (A), third upper incisor (B), upper canine (C), second upper premolar (bud stage) (D), interdental lamina (IDL) between DP<sup>2</sup> and DP<sup>3</sup> (D'), third upper premolar (E), fourth upper premolar (bud stage) (F), first lower incisor (G), second lower incisor (H), third lower incisor (I), lower canine (J), third lower premolar (K), fourth lower premolar (L). Note that in the upper canine the thickened, elongate inner enamel epithelium is oriented buccally. DP<sup>2</sup> and DP<sup>4</sup> are approximately one stage behind the other upper tooth germs in development (DI<sup>1-3</sup>, DC<sup>1</sup>, DP<sup>3</sup>), at the bud stage. Only tooth germs from the embryo's right side are shown. Scale bar: 300 $\mu$ m, all images are at the same scale. MC: Meckel's cartilage, IDL: interdental lamina.





**Supplementary Figure 5. Lower dentition at the bell stage in a stage 19.5 *F. catus* embryo.** Frontal cryosections (10 $\mu$ m) stained with hematoxylin and eosin. First lower incisor (A), Second and third lower incisors (B), lower canine (C), third lower premolar (D), fourth lower premolar (E). The successional lamina on the lingual aspect of the deciduous canine (C), and third and fourth deciduous premolars (D, E) is indicated with arrowheads. Only tooth germs from the embryo's left side are shown. Scale bars: 500 $\mu$ m, images are at the same scale.





**Supplementary Figure 6. Epithelial volume at early bell stage shows differences in size among incisor, canine, and premolar tooth classes.** Epithelial volumes of 3-D reconstructed  $\mu$ CT data were measured in VG Studio Max and averages were taken of the left and right teeth (N=2 per tooth position). Lower teeth are shown here in red circles and upper teeth in blue triangles. Measurement data are presented in Supplementary Table 6.

## SUPPORTING INFORMATION

**“Domestic cat embryos reveal unique transcriptomes of developing incisor, canine, and premolar teeth”. (2022). Woodruff, E.D., Kircher, B.K., Armfield, B.A., Levy, J.K., Bloch, J.I., Cohn, M.J. *Journal of Experimental Zoology Part B: Molecular and Developmental Evolution*.**

### 5 Supplementary Methods

#### 5.1 Micro-computed tomography ( $\mu$ CT) scanning

After fixation in 4% PFA, *F. catus* embryos were stored temporarily in PBS treated with diethyl-pyrocabonate (DEPC PBS) at 4°C. Prior to  $\mu$ CT scanning, embryos were rinsed in DEPC PBS and stained in Lugol’s iodine solution (1.25% I<sub>2</sub>, 2.5% KI in DEPC water), a contrast-enhancing agent, at room temperature with agitation for 2-3 days. Cat embryos were removed from Lugol’s solution, rinsed in PBS, and placed in a clear plastic bag inside a thin, clear plastic tube for CT scanning. The cat embryos were scanned in a GE V|TOME|X M 240 Nano CT scanner (General Electric) at the University of Florida Nanoscale Research Facility. A 180 kV x-ray tube and a diamond target were used with the following settings: voltage: 60kV, current: 200 $\mu$ A, power: 12.0. The following parameters were set in Datos2 software (General Electric): timing: 200ms, averaging: 3, skip: 1, sensitivity: 4, number of images: 2200. The scan resolution was 5.773 $\mu$ m. Initial data processing and generation of tiff image stacks was performed in Datos 2; 3-D reconstructions and volumetric measurements were performed using VG Studio Max v3.3.4 (Volume Graphics).

#### 5.2 Immunofluorescence

Immunofluorescence was performed on at least three stage 18 *F. catus* embryos for each gene of interest. Antigen retrieval was performed prior to embedding tissue by dissecting off the back of head and the brain and incubating tissue overnight in citrate buffer (10mM sodium citrate buffer, 0.05% Tween, pH 6.0) at 4°C. Next, tissue was placed in boiling citrate buffer for 5 minutes and then immersed in cold 30% sucrose and incubated overnight at 4°C. Heads were embedded for cryosectioning and sectioned as described for the histological specimens (see Methods 2.2). Tissue was washed in PBS and then PBS with 0.1% Triton X-100 (PBST) and blocked with 1% goat or donkey serum in PBST. Antibodies were diluted in blocking solution (Supplementary Table 7). Slides were incubated with primary antibodies for 1 hour at room

temperature or overnight at 4°C, and secondary antibodies for 1 hour at room temperature. Slides were rinsed with PBST to remove un-bound primary or secondary antibodies, respectively, counterstained with Hoechst (1:30,000), and mounted with Fluoromount (Southern Biotech). Sections were imaged on an LSM 710 or LSM 880 confocal laser-scanning microscope using Zen software (Zeiss), fluorescent signal from all secondary antibodies was pseudocolored green, and composite images were generated in Fiji (Schindelin et al., 2012). Negative controls were performed without secondary antibody (primary antibody only) or lacking primary antibody (secondary antibody only) (Supplementary Figure 2). All negative controls showed no fluorescent signal in the channels corresponding to the secondary antibodies.

### **5.3 Cat tissue preparation, LCM, and RNA extraction, and sequencing**

**Genotyping.** Cat embryos used for RNA-seq were genotyped for sex via polymerase chain reaction (PCR) to amplify portions of the UTX (NCBI accession EU879981) and UTY (NCBI accession EU879982) genes. Primers specific to *F. catus* were designed in Geneious (version 10.0, Biomatters Ltd) using Primer3 (Rozen & Skaletsky, 2000) (Supplementary Table 8). DNA from known male and female cat embryos were used as positive controls and the PCR products were visualized using gel electrophoresis. Male cats have 2 bands (UTX and UTY) and female cats have 1 band (UTX only). For the embryos used in RNA-seq, cat embryo A was male and embryos B and C were female (Supplementary Table 1).

**Tissue preparation.** Work areas were prepared to reduce exogenous RNase contamination by cleaning work surfaces and instruments with 70% ethanol and then RNaseZap (Ambion). Unfixed *F. catus* heads were stored at -80 °C until sectioning, at which time the heads were removed from their OCT molds while still frozen by warming the block slightly (approximately 5 minutes at room temperature) and carefully peeling the OCT away from the frozen tissue. Heads were placed in a sterile petri dish filled with OCT and the midface region, including the palate and upper dentition, was dissected away from the rest of the head. To ensure adequate dehydration, the dissected tissue was swirled in OCT briefly in 4-5 successive wells in a 12-well plate until no more water could be seen surrounding the tissue. Tissue was then embedded in OCT and flash frozen by placing the mold in an ice bucket containing a mixture of 2-methylbutane (previously chilled for 1 hour at -80°C) and dry ice. Once embedded, tissue was stored in OCT at -80°C until sectioning.

PEN membrane slides (Zeiss) were dipped in RNaseZap (Ambion), rinsed in Nanopure water (Thermo Fisher Scientific) and air-dried on a surface treated with RNaseZap. Tissue samples were sectioned at -18°C in the coronal plane at 10µm, mounted on membrane slides, and immediately placed on dry ice. Slides were stored at -80 for up to 3 days until the staining, LCM, and RNA extractions could be performed. Sections were dehydrated in an ethanol series and stained with 1% cresyl violet acetate (Sigma-Aldrich) dissolved in 50% EtOH. Each slide was dipped into the following ethanol solutions for 30 seconds: 95% EtOH, 75% EtOH, 50% EtOH, 1% cresyl violet, 50% EtOH, 75% EtOH, 95% EtOH, 100% EtOH (twice). Solutions were cooled on ice prior to staining and they were kept in an ice bath during staining. After staining, each slide was air dried until the ethanol evaporated (30 seconds to 1 minute) and immediately frozen on dry ice.

***Laser capture microdissection.*** Laser capture microdissection (LCM) was performed immediately after staining the tissue sections using a Zeiss PALM MicroBeam microscope. Slides were removed from dry ice and warmed briefly (2-3 minutes) in a closed 50ml conical tube to reduce condensation on the slide. Upper tooth germs, including both epithelial and mesenchymal tissues were excised (Supplementary Figure 1) and captured in inverted tube caps of 0.65ml microcentrifuge tubes containing 50µl or 70µl lysis buffer (buffer RLT, Quiagen) and 2-mercaptaethanol (βME). “Robo LPC” mode on the PALM RoboSoftware (Zeiss) was employed to collect the tissue sections from each tooth into the inverted caps. Tissue sections were photographed before and after the tissue capture.

***RNA extraction.*** After collection, samples were vortexed for 30 seconds with the tubes inverted to ensure no tissue was stuck in the cap and for 1 minute with the tubes upright to lyse the cells. RNA was extracted using RNeasy Plus Micro kit (Quiagen) according to the manufacturer’s instructions. An additional on-column DNase digestion was performed using RNase-free DNase (Quiagen) to ensure complete removal of all DNA from the RNA samples. Each RNA sample was eluted in 14µl RNase-free water and the elute was run through the column a second time to maximize the RNA yield. RNA samples were stored at -80°C. RNA concentration and quality were assessed using a high-sensitivity Bioanalyzer microfluidics chip (Eukaryote Total RNA Pico assay) at the University of Florida Interdisciplinary Center for Biotechnology Research (UF ICBR) (Supplementary Table 1). RNA samples were submitted to UF ICBR where indexed, un-stranded cDNA libraries were prepared using the Clontech



SMART-Seq V4 Ultra Low Input RNA kit (Clontech Laboratories, Takara Bio Company) and the Nextera XT Index kit (Illumina), and high-throughput paired-end sequencing was performed using two lanes on a HiSeq 3000 sequencer (Illumina) for 2x150 cycles.

#### **5.4 Bioinformatics analysis of RNA-seq data**

***Read quality assessment and adapter trimming.*** All computational analyses for this study were performed using resources at the University of Florida High Performance Computing facility. Initial quality of raw 150 base pair (bp) Illumina reads from the HiSeq 3000 were assessed using FastQC version 0.11.4 (Babraham Bioinformatics:

<http://www.bioinformatics.babraham.ac.uk/projects/fastqc/>). Synthetic DNA sequences used in the Nextera and Clontech kits were detected by FastQC and removed. Reads were trimmed and filtered based on quality, and adapter sequences were removed using Trimmomatic version 0.33 (Bolger, Lohse, & Usadel, 2014) as follows: adapter sequences were removed, the first 10 bases were removed from all reads, a sliding window trimmer (10 bases) was used to exclude low-quality reads with an average Phred quality score cutoff of 20, and finally, reads less than 40 bases in length were excluded from each sample. For the paired reads, the average quality per base was greater than 32, and this high quality was maintained for approximately 100 of 140 bases of the longest trimmed reads. After trimming and filtering, paired-end read counts for individual tooth samples ranged from ~35.2 million to 59.5 million. Altogether, over 100 million reads were retained per tooth class (sum of read pairs across 3 replicates/tooth), yielding total read pair counts of 154,533,473 (incisor), 150,432,534 (canine), and 131,396,055 (premolar).

***Genome-guided transcriptome alignment and assembly.*** The most recent release of the *F. catus* genome, version 9 (“felCat9.0”, GenBank accession: GCF\_000181335.3, RefSeq accession: GCA\_000181335.4) and the associated annotations (release 104) were downloaded from NCBI in January 2018 (genome: [ftp://ftp.ncbi.nlm.nih.gov/genomes/Felis\\_catus/](ftp://ftp.ncbi.nlm.nih.gov/genomes/Felis_catus/); annotations: [https://www.ncbi.nlm.nih.gov/genome/annotation\\_euk/Felis\\_catus/104/](https://www.ncbi.nlm.nih.gov/genome/annotation_euk/Felis_catus/104/)). Annotations from RefSeq and BestRefSeq were used to aid in transcript assembly in Cufflinks (Trapnell et al., 2012). Genome-guided transcriptome alignments were performed using Hisat2 (Pertea, Kim, Pertea, Leek, & Salzberg, 2016); soft-clipping of reads was not permitted. Repetitive regions in the cat genome were masked using the masking coordinates provided with the genome in BEDTools v2.27.0 (Quinlan & Hall, 2010) prior to aligning the reads. Transcripts

were assembled and a master assembly was created by merging all nine individual transcript assemblies in Stringtie (Pertea et al., 2016).

**Differential expression analyses.** Differential expression analyses were performed using Cuffdiff in Cufflinks version 2.2.1 (Trapnell et al. 2012) and the results were visualized in the R package CummeRbund version 2.26.0 (Goff, Trapnell, & Kelley, 2013) in R version 3.6.0 (R Core Team, 2019). The per-condition dispersion model in Cuffdiff was determined to be the best fit for our data, as we did not necessarily expect that each replicate would have similar variance in fragment counts; this was confirmed by a principal components analysis of our data (not shown). Lists of significantly differentially expressed loci ( $\alpha = 0.05$ ; FDR-adjusted  $p$ -value ( $q$ -value)  $< 0.05$ ) were obtained from CummeRbund. Only genes with  $q$ -values less than 0.05, FPKM (fragments per kilobase per million reads) greater than or equal to 1, and a  $\log_2$  fold change  $\geq 1.5$  or  $\leq -1.5$  were considered for further analysis (Figure 2A-E; Supplementary Tables 2-5). Bed files were generated and sequences were obtained for these significantly differentially expressed genes using “getfasta” in BEDTools (Quinlan & Hall, 2010).

Open reading frames were determined for the nucleotide sequences of the differentially expressed genes and these sequences were translated from DNA to amino acids using TransDecoder version 5.0.2 (Haas et al., 2013). The predicted protein coding sequences (amino acids) for differentially expressed genes from TransDecoder were used to conduct a NCBI BLAST search (blastx, BLAST version 2.6.0, (<https://blast.ncbi.nlm.nih.gov/>) against the cat genome (*Felis catus*, taxid: 9685). Accession numbers or GenInfo identifiers (GI) from the BLAST output and the GenBank summary records were obtained for each protein sequence using Batch Entrez (<https://www.ncbi.nlm.nih.gov/sites/batchentrez>). GI numbers and gene names were extracted from the Genbank records and linked to the corresponding “XLOCs” (Cufflinks gene identifiers) and the associated differential expression data (Supplementary Tables 2-5).

## 6 Supplementary Results

### 6.1 Slight delay in development of lower incisors compared with canine and premolars

In contrast to the asynchronous developmental pattern observed in the upper dentition (see Results 3.1), the lower canine (DC<sub>1</sub>) and both lower premolars (DP<sub>3-4</sub>) appeared to develop

synchronously (Supplementary Figure 3D-F; Supplementary Figure 4G-L). Similar to the upper dentition, the lower incisors (DI<sub>1-3</sub>) seemed slightly less advanced than the DC<sub>1</sub> and DP<sub>3-4</sub>. DP<sub>4</sub> was not observed when the other lower teeth were at the bud stage, however, by the time the other teeth were at the cap stage, it had also reached the cap stage (Supplementary Figure 4L). This suggests that the initiation of DP<sub>4</sub> may be slightly delayed but that it proceeds rapidly into the cap stage. Examination of additional *F. catus* embryos between stages 16 and 17 would be necessary to address this.

At all documented developmental stages, we observed a continuous interdental lamina connecting each tooth germ that was oriented towards the palate (Figure 1B-C, Supplementary Figure 4D') consistent with a previous report (Moss-Salentijn, 1982). Despite the presence of a continuous dental lamina, no vestigial tooth germs (*e.g.*, DP<sup>1</sup>/<sub>1</sub> or DP<sub>2</sub>) were observed in the diastema region at the late bud stage, however, it is possible that vestigial diastema teeth are present in *F. catus* embryos at earlier developmental stages and that they had regressed by the late bud stage, which was the earliest stage examined in this study. In mice, vestigial tooth buds have been reported in the upper and lower diastemata which undergo programmed cell death (Peterková, Peterka, Viriot, & Lesot, 2002). Therefore, it would not be surprising if in younger *F. catus* embryos at the initiation/early bud stages vestigial buds were present for the anterior-most premolars (DP<sup>1</sup> and DP<sub>1-2</sub>) which have been lost during felid evolution (Van Valkenburgh, 2007).

## **6.2 Description of a multi-cusped upper central incisor of *Ignacius graybullianus***

We examined dentitions of extant and extinct mammals to investigate the diversity of crown morphologies, especially for incisor and canine teeth which typically possess a single cusp in many mammal species, including *F. catus*. Here we describe an upper central incisor (I<sup>1</sup>) of a species of fossil Plesiadapiform Primate, *Ignacius graybullianus* (UF-VP 331494) for the first time. Although the dentition of *I. graybullianus* has been previously described, the upper incisors were frequently missing (Bown, 1979; Bown & Rose, 1976; Kay, Thewissen, & Yoder, 1992; Rose & Gingerich, 1976; Silcox, Rose, & Bown, 2008). The newly described specimen is an isolated right upper central incisor from the Early Eocene epoch (Wasatchian 2 faunal zone) found in the Willwood formation of the Bighorn Basin, Wyoming, USA, and it is housed in the University of Florida Vertebrate Paleontology Collection (UF-VP 331494).

The I<sup>1</sup> crown of *Ignacius graybullianus* exhibits a multi-cusped "mitten-shaped" crown with cusp morphology characteristic of paromomyids, including other species of *Ignacius* (Bloch, Silcox, Boyer, & Sargis, 2007; Rose, Beard, & Houde, 1993). The anterocone and laterocone are comparatively larger than the mediocone and posterocone, and a mediocrista is present (Figure 5A-D). We compared the I<sup>1</sup> of *I. graybullianus* to that of *Phenacolemur simonsi*, *Phenacolemur pagei*, *Acidomomys hebeticus* and *Arcius lapparenti*.

Similar to *Phenacolemur simonsi*, a small mediocrista runs proximolaterally from the mediocone, however, the mediocone itself appears less distinct than that of *P. simonsi*, dwarfed by the comparatively large anterocone and laterocone (Rose et al., 1993). Instead, the mediocone of *I. graybullianus* is more similar to that of *Phenacolemur pagei* (Rose et al., 1993). The crown of *I. graybullianus* lacks the double posterocone found in *Acidomomys hebeticus* and has a smaller mediocone (Bloch, Boyer, Gingerich, & Gunnell, 2002). Additionally, although the mediocrista appears similar between *A. hebeticus* and *I. graybullianus*, *A. hebeticus* has a small cuspule on the base of the mediocrista that is not present in *I. graybullianus* (Bloch et al., 2002). The crown morphology of *I. graybullianus* differs considerably from that of a European paromomyid, *Arcius lapparenti*. In *A. lapparenti*, the anterocone, laterocone, and mediocone are more similar in size to one another and the posterocone is much larger, relative to the other cusps, than in *I. graybullianus* (Rose et al., 1993).



## References

- Bloch, J. I., Boyer, D. M., Gingerich, P. D., & Gunnell, G. F. (2002). New primitive paromomyid from the Clarkforkian of Wyoming and dental eruption in Plesiadapiformes. *Journal of Vertebrate Paleontology*, 22(2), 366–379. [https://doi.org/10.1671/0272-4634\(2002\)022\[0366:NPPFTC\]2.0.CO;2](https://doi.org/10.1671/0272-4634(2002)022[0366:NPPFTC]2.0.CO;2)
- Bloch, J. I., Silcox, M. T., Boyer, D. M., & Sargis, E. J. (2007). New Paleocene skeletons and the relationship of plesiadapiforms to crown-clade primates. *Proceedings of the National Academy of Sciences*, 104(4), 1159–1164. <https://doi.org/10.1073/pnas.0610579104>
- Bolger, A. M., Lohse, M., & Usadel, B. (2014). Trimmomatic: A flexible trimmer for Illumina sequence data. *Bioinformatics (Oxford, England)*, 30(15), 2114–2120. <https://doi.org/10.1093/bioinformatics/btu170>
- Bown, T. M. (1979). Geology and mammalian paleontology of the Sand Creek facies, Lower Willwood Formation (Lower Eocene), Washakie County, Wyoming. *The Geological Survey of Wyoming*, 2.
- Bown, T. M., & Rose, K. D. (1976). New early tertiary primates and a reappraisal of some plesiadapiformes. *Folia Primatologica*, 26(2), 109–138. Scopus. <https://doi.org/10.1159/000155734>
- Goff, L., Trapnell, C., & Kelley, D. (2013). *cummeRbund: Analysis, exploration, manipulation, and visualization of Cufflinks high-throughput sequencing data*. R package version 2.14.0.
- Haas, B. J., Papanicolaou, A., Yassour, M., Grabherr, M., Blood, P. D., Bowden, J., ... Regev, A. (2013). De novo transcript sequence reconstruction from RNA-seq using the Trinity platform for reference generation and analysis. *Nature Protocols*, 8(8), 1494–1512. <https://doi.org/10.1038/nprot.2013.084>

- Kay, R. F., Thewissen, J. G. M., & Yoder, A. D. (1992). Cranial anatomy of *Ignacius graybullianus* and the affinities of the Plesiadapiformes. *American Journal of Physical Anthropology*, 89(4), 477–498. <https://doi.org/10.1002/ajpa.1330890409>
- Moss-Salentijn, L. (1982). Morphological aspects of the growth behavior of the early dental lamina in the cat and rat. In *Teeth: Form function and evolution* (pp. 7–20). Columbia University Press. Retrieved from <https://ci.nii.ac.jp/naid/10023893480/>
- Pertea, M., Kim, D., Pertea, G., Leek, J. T., & Salzberg, S. L. (2016). Transcript-level expression analysis of RNA-seq experiments with HISAT, StringTie and Ballgown. *Nature Protocols*, 11(9), 1650–1667. <https://doi.org/10.1038/nprot.2016.095>
- Peterková, R., Peterka, M., Viriot, L., & Lesot, H. (2002). Development of the vestigial tooth primordia as part of mouse odontogenesis. *Connective Tissue Research*, 43(2–3), 120–128.
- Quinlan, A. R., & Hall, I. M. (2010). BEDTools: A flexible suite of utilities for comparing genomic features. *Bioinformatics*, 26(6), 841–842. <https://doi.org/10.1093/bioinformatics/btq033>
- R Core Team. (2019). *R: A language and environment for statistical computing*. R Foundation for Statistical Computing, Vienna, Austria. Retrieved from <https://www.R-project.org/>
- Rose, K. D., Beard, K. C., & Houde, P. (1993). Exceptional new dentitions of the diminutive plesiadapiforms *Tinimomys* and *Niptomomys* (Mammalia), with comments on the upper incisors of Plesiadapiformes. *Annals of Carnegie Museum*, 62(4), 23.
- Rose, K. D., & Gingerich, P. D. (1976). Partial skull of the Plesiadapiform Primate *Ignacius* from the Early Eocene of Wyoming. *Contributions from the Museum of Paleontology, University of Michigan*, 24(17), 12.

- Rozen, S., & Skaletsky, H. (2000). Primer3 on the WWW for general users and for biologist programmers. *Methods in Molecular Biology (Clifton, N.J.)*, 132, 365–386.
- Schindelin, J., Arganda-Carreras, I., Frise, E., Kaynig, V., Longair, M., Pietzsch, T., ... Cardona, A. (2012). Fiji: An open-source platform for biological-image analysis. *Nature Methods*, 9(7), 676–682. <https://doi.org/10.1038/nmeth.2019>
- Silcox, M. T., Rose, K. D., & Bown, T. M. (2008). Early Eocene Paromomyidae (Mammalia, Primates) from the Southern Bighorn Basin, Wyoming: Systematics and evolution. *Journal of Paleontology*, 82(6), 40.
- Trapnell, C., Roberts, A., Goff, L., Pertea, G., Kim, D., Kelley, D. R., ... Pachter, L. (2012). Differential gene and transcript expression analysis of RNA-seq experiments with TopHat and Cufflinks. *Nature Protocols*, 7(3), 562–578. <https://doi.org/10.1038/nprot.2012.016>
- Van Valkenburgh, B. (2007). Deja vu: The evolution of feeding morphologies in the Carnivora. *Integrative and Comparative Biology*, 47(1), 147–163. <https://doi.org/10.1093/icb/icm016>

## Supplementary Tables

**Supplementary Table 1. Quality (RIN) of *F. catus* embryonic tooth RNA samples use for RNA-sequencing.**  
Three individual embryos (cats A-C) were used for the RNA-sequencing. RIN: RNA Integrity Number.

Sample name	Sex	Tooth	Left/Right	RIN	Concentration (pg/ $\mu$ l) from Bioanalyzer assay
Cat A-DI	Male	Deciduous Incisor	Left	7.3	155 (undiluted)
Cat A-DC	Male	Deciduous Canine	Left	8.7	276 (undiluted)
Cat A-DP	Male	Deciduous Premolar	Right	8.2	267 (undiluted)
Cat B-DI	Female	Deciduous Incisor	Right	8.0	140 (undiluted)
Cat B-DC	Female	Deciduous Canine	Right	8.0	386 (undiluted)
Cat B-DP	Female	Deciduous Premolar	Right	7.9	215 (undiluted)
Cat C-DI	Female	Deciduous Incisor	Right	8.6	32 (undiluted)
Cat C-DC	Female	Deciduous Canine	Right	7.8	37 (1:2 dilution)
Cat C-DP	Female	Deciduous Premolar	Right	7.8	128 (undiluted)



**Supplementary Table 2. Differentially expressed genes with a log<sub>2</sub> fold change ≥ 1.5 or ≤ -1.5.**

Gene ID	Sample 1	Sample 2	Value 1	Value 2	log <sub>2</sub> fold change	q value	Protein name blastx hit	Cat NCBI accession	Cat GI
XLOC_052219	DI	DP	2.34397	77.7958	5.05266	0.0049878	polyadenylate-binding protein 5 [Felis catus]	XP_023105012.1	GI:1304965893
XLOC_024726	DC	DP	4.29267	49.4206	3.52517	0.0282102	WD repeat-containing protein 46 [Felis catus]	XP_003986058.1	GI:410958914
XLOC_052753	DI	DP	485.399	4104.67	3.08002	0.0049878	hemoglobin subunit beta-1 [Felis catus]	XP_003992931.2	GI:755768930
XLOC_008803	DI	DC	8.41875	63.9273	2.92475	0.0049878	von Willebrand factor D and EGF domain-containing protein isoform X5 [Felis catus]	XP_023106171.1	GI:1304886155
XLOC_041243	DI	DP	4.00352	30.2465	2.91743	0.0049878	noelin-3 isoform X2 [Felis catus]	XP_011283129.1	GI:755755329
XLOC_052219	DC	DP	11.5337	77.7958	2.75383	0.0049878	polyadenylate-binding protein 5 [Felis catus]	XP_023105012.1	GI:1304965893
XLOC_014623	DC	DP	3.03462	20.1772	2.73314	0.0049878	homeobox protein SIX2 isoform X2 [Felis catus]	XP_023107414.1	GI:1304892972
XLOC_035668	DC	DP	14.0268	90.8908	2.69594	0.0049878	tachykinin-3 isoform X2 [Felis catus]	XP_019690663.1	GI:1126438115
XLOC_041714	DC	DP	1.59949	10.1833	2.67052	0.0049878	delta and Notch-like epidermal growth factor-related receptor [Felis catus]	XP_023115540.1	GI:1304924216
XLOC_024840	DI	DC	21.2641	130.75	2.62031	0.0049878	LOW QUALITY PROTEIN: synaptonemal complex protein 2 [Felis catus]	XP_023106817.1	GI:1304890682
XLOC_000313	DC	DP	1.18928	7.19072	2.59605	0.0049878	putative histone-lysine N-methyltransferase PRDM6 [Felis catus]	XP_011281724.2	GI:1304877629
XLOC_056801	DC	DP	1.33335	8.01262	2.58721	0.0237354	rho GTPase-activating protein 20 isoform X2 [Felis catus]	XP_023094847.1	GI:1304930333
XLOC_040197	DI	DP	2.70728	16.2457	2.58514	0.0457699	sphingosine 1-phosphate receptor 1 [Felis catus]	XP_003990423.1	GI:410967843
XLOC_024840	DI	DP	21.2641	121.113	2.50986	0.0049878	LOW QUALITY PROTEIN: synaptonemal complex protein 2 [Felis catus]	XP_023106817.1	GI:1304890682
XLOC_066129	DI	DP	9.27094	50.0827	2.43353	0.0049878	claudin-7 [Felis catus]	XP_011287175.1	GI:755787782

XLOC_018898	DI	DP	7.64238	40.9069	2.42025	0.019239	collagen alpha-1(I) chain-like isoform X2 [Felis catus]	XP_023105130.1	GI:1304966287
XLOC_069074	DC	DP	4.74071	24.927	2.39453	0.0049878	coiled-coil domain-containing glutamate-rich protein 2 [Felis catus]	XP_023100972.1	GI:1304951848
XLOC_035913	DI	DC	11.1975	50.7678	2.18074	0.0049878	collagen alpha-2(I) chain-like [Felis catus]	XP_023107954.1	GI:1304895323
XLOC_052753	DI	DC	485.399	2143.97	2.14304	0.0049878	collagen alpha-1(VII) chain isoform X1 [Felis catus]	XP_003992931.2	GI:755768930
XLOC_066129	DI	DC	9.27094	39.6268	2.09569	0.0098507	claudin-7 [Felis catus]	XP_011287175.1	GI:755787782
XLOC_041243	DC	DP	7.2879	30.2465	2.0532	0.0049878	noelin-3 isoform X2 [Felis catus]	XP_011283129.1	GI:755755329
XLOC_072382	DI	DP	8.68125	35.0198	2.0122	0.0237354	claudin-6 isoform X2 [Felis catus]	XP_003998978.1	GI:410985334
XLOC_000365	DI	DC	40.858	162.68	1.99335	0.0049878	transforming growth factor-beta-induced protein ig-h3 [Felis catus]	XP_003980831.1	GI:410948204
XLOC_059868	DI	DC	4.00746	15.2056	1.92384	0.0049878	EMILIN-2 isoform X2 [Felis catus]	XP_023097560.1	GI:1304940637
XLOC_025649	DI	DC	12.2879	44.6937	1.86283	0.0049878	DBH-like monooxygenase protein 1 [Felis catus]	XP_023110147.1	GI:1304903677
XLOC_075038	DC	DP	59.5268	197.576	1.7308	0.0049878	myeloid cell nuclear differentiation antigen [Felis catus]	XP_023102998.1	GI:1304958673
XLOC_041024	DI	DC	31.817	105.469	1.72895	0.0049878	DC-STAMP domain-containing protein 2 isoform X1 [Felis catus]	XP_023103479.1	GI:1304960227
XLOC_041582	DI	DP	40.1658	127.798	1.66982	0.0049878	solute carrier family 40 member 1 [Felis catus]	XP_003991014.1	GI:410969058
XLOC_008549	DI	DC	15.7944	48.4182	1.61614	0.0049878	protein Wnt-5a isoform X1 [Felis catus]	XP_023105612.1	GI:1304884232
XLOC_041582	DI	DC	40.1658	119.667	1.57498	0.0049878	solute carrier family 40 member 1 [Felis catus]	XP_003991014.1	GI:410969058
XLOC_018913	DC	DP	27.2661	78.3779	1.52334	0.0049878	homeodomain-only protein isoform X2 [Felis catus]	XP_011280169.1	GI:755724138
XLOC_076908	DC	DP	2.08514	5.90899	1.50277	0.019239	potassium-transporting ATPase alpha chain 1 [Felis catus]	XP_023101187.1	GI:1304952623
XLOC_018503	DC	DP	5.36164	15.1713	1.5006	0.019239	zinc finger protein 596 isoform X1 [Felis catus]	XP_011279659.1	GI:755713534

XLOC_056208	DC	DP	8.59186	2.99635	-1.51977	0.0325694	nidogen-1 [Felis catus]	XP_003993948.1	GI:410975046
XLOC_068033	DI	DP	40.4652	13.8901	-1.54262	0.0049878	keratin, type I cytoskeletal 16 [Felis catus]	XP_003996910.3	GI:755790084
XLOC_018818	DI	DP	21.9844	7.24376	-1.60167	0.0049878	DNA damage-inducible transcript 4-like protein [Felis catus]	XP_003985190.1	GI:410957135
XLOC_008233	DI	DC	24.5608	8.06094	-1.60734	0.0049878	angiopoietin-related protein 4 [Felis catus]	XP_003981832.3	GI:1304882085
XLOC_034953	DI	DC	9.02551	2.95298	-1.61184	0.0237354	glutaminase liver isoform, mitochondrial isoform X4 [Felis catus]	XP_019690653.1	GI:1126438079
XLOC_034900	DC	DP	88.1183	28.2305	-1.64218	0.0049878	keratin, type II cuticular Hb1-like [Felis catus]	XP_023112864.1	GI:1304914068
XLOC_068033	DI	DC	40.4652	12.5699	-1.68671	0.0049878	keratin, type I cytoskeletal 16 [Felis catus]	XP_003996910.3	GI:755790084
XLOC_047312	DI	DP	60.9268	18.8716	-1.69086	0.0049878	cholecystokinin [Felis catus]	XP_003992259.1	GI:410971612
XLOC_072081	DI	DC	106.311	32.6417	-1.7035	0.0049878	beta-1,3-N-acetylglucosaminyltransferase lunatic fringe [Felis catus]	XP_023102331.1	GI:1304956561
XLOC_030285	DI	DC	12.9084	3.95391	-1.70696	0.0049878	membrane protein FAM174B [Felis catus]	XP_023110719.1	GI:1304905664
XLOC_047118	DI	DC	7.82525	2.39121	-1.7104	0.0237354	mannan-binding lectin serine protease 1 isoform X8 [Felis catus]	XP_019695561.1	GI:1126452716
XLOC_062809	DI	DP	19.1019	5.76641	-1.72797	0.0145862	FERM domain-containing protein 3 isoform X2 [Felis catus]	XP_019671372.2	GI:1304942070
XLOC_052559	DI	DP	553.712	166.066	-1.73738	0.0049878	heat shock protein beta-2 [Felis catus]	XP_003992394.1	GI:410971889
XLOC_056787	DI	DC	5.48069	1.63664	-1.74362	0.019239	sedoheptulokinase isoform X1 [Felis catus]	XP_003996438.1	GI:410980143
XLOC_019399	DI	DC	27.6354	8.03442	-1.78225	0.0049878	nephronectin isoform X3 [Felis catus]	XP_011280111.2	GI:1304898186
XLOC_062809	DI	DC	19.1019	5.52176	-1.79051	0.0049878	FERM domain-containing protein 3 isoform X2 [Felis catus]	XP_019671372.2	GI:1304942070
XLOC_001475	DI	DP	53.44	15.4146	-1.79362	0.0049878	insulin gene enhancer protein ISL-1 [Felis catus]	XP_003981473.1	GI:410949527
XLOC_035702	DI	DC	136.401	38.8779	-1.81083	0.0049878	wnt inhibitory factor 1 [Felis catus]	XP_003989051.1	GI:410965022

XLOC_018695	DI	DP	9.48209	2.6932	-1.81589	0.0457699	LOW QUALITY PROTEIN: secreted frizzled-related protein 2 [Felis catus]	XP_003984978.2	GI:1304897571
XLOC_025265	DI	DC	37.1804	10.4153	-1.83584	0.0049878	lymphotoxin-beta isoform X2 [Felis catus]	XP_019685908.1	GI:1126423350
XLOC_008451	DI	DC	12.4837	3.48756	-1.83976	0.0049878	chondroitin sulfate proteoglycan 5 isoform X3 [Felis catus]	XP_023104092.1	GI:1304883594
XLOC_014560	DI	DC	3.62364	1.01075	-1.84201	0.0370295	SH3 domain-containing RING finger protein 3 [Felis catus]	XP_011279406.3	GI:1304892510
XLOC_069376	DI	DP	43.4768	11.9835	-1.8592	0.0049878	tubulin beta-2A chain [Felis catus]	XP_023109488.1	GI:1304901122
XLOC_019172	DI	DC	50.6506	13.7643	-1.87965	0.0049878	nucleoplasmin-2 isoform X2 [Felis catus]	XP_023108295.1	GI:1304896747
XLOC_035702	DI	DP	136.401	36.5649	-1.89932	0.0049878	wnt inhibitory factor 1 [Felis catus]	XP_003989051.1	GI:410965022
XLOC_035292	DI	DP	17.5351	4.6919	-1.902	0.0049878	coiled-coil domain-containing protein 3 [Felis catus]	XP_019689499.2	GI:1304911437
XLOC_029580	DI	DP	101.894	27.176	-1.90667	0.0049878	COUP transcription factor 2 isoform X1 [Felis catus]	XP_023110726.1	GI:1304905707
XLOC_039926	DI	DC	17.9735	4.76231	-1.91614	0.0049878	gap junction beta-5 protein [Felis catus]	XP_003989888.1	GI:410966741
XLOC_025059	DC	DP	7.43153	1.95098	-1.92946	0.0049878	LOW QUALITY PROTEIN: A-kinase anchor protein 12 [Felis catus]	XP_011280872.2	GI:1304904137
XLOC_018818	DI	DC	21.9844	5.65806	-1.9581	0.0049878	DNA damage-inducible transcript 4-like protein [Felis catus]	XP_003985190.1	GI:410957135
XLOC_062965	DI	DC	13.0805	3.31665	-1.97962	0.0282102	insulin-like growth factor-binding protein-like 1 [Felis catus]	XP_003995732.2	GI:1304943084
XLOC_047371	DI	DC	6.38847	1.49607	-2.09429	0.0370295	transient receptor potential cation channel subfamily M member 2 isoform X4 [Felis catus]	XP_019694862.2	GI:1304928778
XLOC_018589	DI	DC	20.3335	4.74313	-2.09995	0.0049878	homeobox protein Nkx-3	XP_023108242.1	GI:1304896577
XLOC_018913	DI	DC	126.006	27.2661	-2.20831	0.0049878	homeodomain-only protein isoform X2 [Felis catus]	XP_011280169.1	GI:755724138



XLOC_047312	DI	DC	60.9268	12.933	-2.23602	0.0049878	cholecystokinin [Felis catus]	XP_003992259.1	GI:410971612
XLOC_040484	DC	DP	5.15223	1.08782	-2.24375	0.0098507	LOW QUALITY PROTEIN: integrin alpha-4 [Felis catus]	XP_003990960.2	GI:755759602
XLOC_018589	DI	DP	20.3335	4.27492	-2.24989	0.0049878	homeobox protein Nkx-3	XP_023108242.1	GI:1304896577
XLOC_018695	DC	DP	12.9231	2.6932	-2.26257	0.0049878	LOW QUALITY PROTEIN: secreted frizzled-related protein 2 [Felis catus]	XP_003984978.2	GI:1304897571
XLOC_069376	DI	DC	43.4768	8.94996	-2.28029	0.0049878	tubulin beta-2A chain [Felis catus]	XP_023109488.1	GI:1304901122
XLOC_001470	DI	DP	137.252	27.3122	-2.32921	0.0049878	follistatin isoform X3 [Felis catus]	XP_023116552.1	GI:1304880054
XLOC_001470	DI	DC	137.252	27.0275	-2.34432	0.0049878	follistatin isoform X3 [Felis catus]	XP_023116552.1	GI:1304880054
XLOC_065793	DI	DC	44.0558	8.21587	-2.42284	0.0049878	lysosomal-trafficking regulator [Felis catus]	NP_001277171.1	GI:589811485
XLOC_008030	DI	DC	7.37618	1.27322	-2.53439	0.0049878	rho guanine nucleotide exchange factor 5 isoform X1 [Felis catus]	XP_023106447.1	GI:1304889372
XLOC_065793	DI	DP	44.0558	6.98771	-2.65644	0.0145862	lysosomal-trafficking regulator [Felis catus]	NP_001277171.1	GI:589811485
XLOC_029580	DI	DC	101.894	16.1002	-2.66192	0.0049878	COUP transcription factor 2 isoform X1 [Felis catus]	XP_023110726.1	GI:1304905707
XLOC_000669	DI	DP	62.2157	9.16867	-2.76249	0.0049878	HLA class II histocompatibility antigen gamma chain isoform X1 [Felis catus]	XP_003981534.3	GI:1304879928
XLOC_035054	DC	DP	27.0174	3.04268	-3.15048	0.0049878	ALX homeobox protein 1 [Felis catus]	XP_003989139.1	GI:410965202
XLOC_002368	DI	DC	11.5532	1.25756	-3.19959	0.0049878	BTB/POZ domain-containing protein KCTD4 [Felis catus]	XP_003980454.1	GI:410947439
XLOC_072180	DI	DC	20.0667	2.02906	-3.30592	0.0049878	claudin-3 [Felis catus]	XP_011288653.1	GI:755800735
XLOC_082342	DC	DP	46.4792	4.64596	-3.32254	0.0098507	integrin-linked protein kinase [Felis catus]	XP_023095290.1	GI:1304932138
XLOC_007812	DI	DP	22.3684	1.82351	-3.61668	0.0049878	metabotropic glutamate receptor 3 isoform X1 [Felis catus]	XP_006929208.1	GI:586978917
XLOC_007812	DI	DC	22.3684	1.62583	-3.78222	0.0049878	metabotropic glutamate receptor 3 isoform X1 [Felis catus]	XP_006929208.1	GI:586978917
XLOC_035054	DI	DP	65.2938	3.04268	-4.42353	0.0049878	ALX homeobox protein 1 [Felis catus]	XP_003989139.1	GI:410965202

**Supplementary Table 3. Differentially expressed genes with log<sub>2</sub> fold change between 1 and 1.5 or -1 and -1.5.**

Gene ID	Sample 1	Sample 2	Value 1	Value 2	log <sub>2</sub> fold change	q value	Protein name blastx hit	Cat NCBI accession	Cat GI
XLOC_056585	DI	DP	21.1192	59.5508	1.49557	0.019239	dickkopf-related protein 1 [Felis catus]	XP_023096086.1	GI:1304935051
XLOC_066390	DI	DC	26.7717	74.2304	1.4713	0.0049878	homeobox protein DLX-4 [Felis catus]	XP_019673274.1	GI:1126475815
XLOC_025649	DI	DP	12.2879	33.7917	1.45943	0.0049878	DBH-like monooxygenase protein 1 [Felis catus]	XP_023110147.1	GI:1304903677
XLOC_008791	DI	DC	82.5208	226.688	1.45788	0.0145862	homeobox protein DLX-6 [Felis catus]	XP_011278697.2	GI:1304886048
XLOC_056585	DI	DC	21.1192	57.2352	1.43835	0.0325694	dickkopf-related protein 1 [Felis catus]	XP_023096086.1	GI:1304935051
XLOC_008850	DC	DP	128.808	346.505	1.42765	0.0049878	late secretory pathway protein AVL9 homolog isoform X1 [Felis catus]	XP_023106245.1	GI:1304886548
XLOC_034900	DI	DC	33.091	88.1183	1.413	0.019239	keratin, type II cuticular Hb1-like [Felis catus]	XP_023112864.1	GI:1304914068
XLOC_008549	DI	DP	15.7944	41.8877	1.40711	0.0049878	protein Wnt-5a isoform X1 [Felis catus]	XP_023105612.1	GI:1304884232
XLOC_059712	DI	DC	27.2611	70.7802	1.3765	0.0145862	transmembrane protein 119 [Felis catus]	XP_023097272.1	GI:1304939435
XLOC_008791	DI	DP	82.5208	211.865	1.36031	0.0414242	homeobox protein DLX-6 [Felis catus]	XP_011278697.2	GI:1304886048
XLOC_000365	DI	DP	40.858	103.832	1.34556	0.0049878	transforming growth factor-beta-induced protein ig-h3 [Felis catus]	XP_003980831.1	GI:410948204
XLOC_007932	DC	DP	3.35718	8.46251	1.33383	0.0237354	caveolin-2 [Felis catus]	NP_001162165.1	GI:274315920
XLOC_001373	DI	DC	88.707	223.483	1.33304	0.0049878	homeobox protein MSX-2 [Felis catus]	XP_006927971.2	GI:755692582
XLOC_019360	DC	DP	49.3573	123.755	1.32615	0.0325694	neurotrypsin isoform X2 [Felis catus]	XP_023108616.1	GI:1304898002
XLOC_069757	DC	DP	19.8101	49.0286	1.30739	0.0145862	zinc finger protein 260 [Felis catus]	XP_006941431.1	GI:587014381
XLOC_030661	DC	DP	4504.56	11130.4	1.30505	0.0049878	40S ribosomal protein S29 [Felis catus]	XP_003987659.1	GI:410962194
XLOC_024990	DI	DC	24.7768	60.7726	1.29443	0.0237354	hairy/enhancer-of-split related with YRPW motif protein 2 isoform X3 [Felis catus]	XP_019686729.1	GI:1126425918

XLOC_056850	DC	DP	176.172	429.716	1.28639	0.0049878	protein RRP5 homolog isoform X1 [Felis catus]	XP_023096649.1	GI:1304937317
XLOC_018643	DI	DC	32.5875	79.1068	1.27949	0.0049878	scavenger receptor class A member 3 [Felis catus]	XP_011279843.1	GI:755715511
XLOC_024981	DI	DC	209.847	505.317	1.26785	0.0049878	gap junction alpha-1 protein [Felis catus]	XP_003986563.3	GI:1126425850
XLOC_065776	DI	DC	56.5441	133.827	1.24292	0.019239	homeobox protein DLX-3 [Felis catus]	XP_023099992.1	GI:1304948590
XLOC_069757	DI	DP	20.8944	49.0286	1.2305	0.0414242	zinc finger protein 260 [Felis catus]	XP_006941431.1	GI:587014381
XLOC_024981	DI	DP	209.847	478.314	1.18862	0.0237354	gap junction alpha-1 protein [Felis catus]	XP_003986563.3	GI:1126425850
XLOC_008850	DI	DP	155.85	346.505	1.15271	0.0237354	late secretory pathway protein AVL9 homolog isoform X1 [Felis catus]	XP_023106245.1	GI:1304886548
XLOC_014859	DI	DP	323.901	686.8	1.08434	0.0237354	39S ribosomal protein L33, mitochondrial isoform X3 [Felis catus]	XP_023107769.1	GI:1304894575
XLOC_013606	DC	DP	29.068	61.5345	1.08197	0.0145862	potassium voltage-gated channel subfamily KQT member 2 isoform X14 [Felis catus]	XP_023106751.1	GI:1304890508
XLOC_000330	DC	DP	9.80775	20.6434	1.07368	0.0325694	solute carrier family 12 member 2 isoform X2 [Felis catus]	XP_023110531.1	GI:1304877711
XLOC_019057	DC	DP	709.118	1478.24	1.05978	0.0282102	ATP synthase subunit e, mitochondrial [Felis catus]	XP_006931364.1	GI:586985338
XLOC_066162	DC	DP	917.286	1901.09	1.05138	0.019239	60S ribosomal protein L26-like 1 [Felis catus]	XP_019694422.1	GI:1126401337
XLOC_041440	DI	DC	367.414	183.673	-1.00027	0.0049878	C-X-C chemokine receptor type 4 [Felis catus]	NP_001009826.1	GI:57770319
XLOC_056777	DI	DC	52.3033	25.8003	-1.01951	0.0325694	PDZ and LIM domain protein 1 [Felis catus]	XP_023096528.1	GI:1304936793
XLOC_056381	DI	DC	216.727	103.506	-1.06616	0.0049878	cytochrome P450 26C1 [Felis catus]	XP_023096515.1	GI:1304936730
XLOC_000165	DI	DP	64.8809	30.8647	-1.07183	0.0145862	Krüppel-like factor 5 isoform X1 [Felis catus]	XP_023107987.1	GI:1304876730
XLOC_014781	DI	DC	100.074	46.7814	-1.09706	0.00985073	LOW QUALITY PROTEIN: forkhead box protein I3 [Felis catus]	XP_011279547.3	GI:1304893970
XLOC_008406	DI	DC	297.771	138.758	-1.10163	0.0282102	transmembrane protein 59-like [Felis catus]	XP_003982132.1	GI:410950884

XLOC_056887	DI	DP	28.0717	12.7422	-1.13951	0.0049878	GDNF family receptor alpha-1 isoform X2 [Felis catus]	XP_023096746.1	GI:1304937659
XLOC_063033	DI	DC	330.223	148.682	-1.15121	0.0049878	tenascin [Felis catus]	XP_011286776.2	GI:1304943578
XLOC_008462	DI	DC	16.9066	7.44416	-1.18341	0.00985073	collagen alpha-1(VII) chain isoform X1 [Felis catus]	XP_003982214.1	GI:410951049
XLOC_018615	DI	DC	1015.49	446.643	-1.18499	0.0049878	dickkopf-related protein 4 [Felis catus]	XP_023108335.1	GI:1304896887
XLOC_066465	DI	DC	1481.78	642.984	-1.20447	0.0049878	keratin, type I cytoskeletal 14 [Felis catus]	XP_003996909.2	GI:1304947266
XLOC_018621	DI	DC	18.3669	7.87823	-1.22116	0.0049878	secreted frizzled-related protein 1 isoform X2 [Felis catus]	XP_019684080.1	GI:1126417773
XLOC_056887	DI	DC	28.0717	11.949	-1.23222	0.0049878	GDNF family receptor alpha-1 isoform X2 [Felis catus]	XP_023096746.1	GI:1304937659
XLOC_073954	DI	DC	52.4092	21.7988	-1.26557	0.0237354	suppressor of cytokine signaling 1 [Felis catus]	XP_023102353.1	GI:1304956607
XLOC_034712	DI	DC	20.6459	8.56985	-1.26851	0.0457699	tapasin-related protein isoform X1 [Felis catus]	XP_023112473.1	GI:1304912654
XLOC_035054	DI	DC	65.2938	27.0174	-1.27305	0.0049878	ALX homeobox protein 1 [Felis catus]	XP_003989139.1	GI:410965202
XLOC_024645	DI	DC	28.4545	11.7643	-1.27424	0.0145862	leukocyte elastase inhibitor [Felis catus]	XP_003985901.1	GI:410958594
XLOC_018643	DC	DP	79.1068	32.4913	-1.28375	0.0049878	scavenger receptor class A member 3 [Felis catus]	XP_011279843.1	GI:755715511
XLOC_035292	DI	DC	17.5351	7.16319	-1.29157	0.00985073	coiled-coil domain-containing protein 3 [Felis catus]	XP_019689499.2	GI:1304911437
XLOC_008594	DI	DC	12.1669	4.85522	-1.32535	0.0237354	eukaryotic translation initiation factor 4E type 3 isoform X1 [Felis catus]	XP_023105726.1	GI:1304884646
XLOC_030831	DI	DC	19.4298	7.74963	-1.32607	0.00985073	ribosomal protein S3a, partial [Felis catus]	AAT76631.1	GI:50402817
XLOC_052019	DI	DC	23.3953	9.12661	-1.35807	0.0049878	suppressor of tumorigenicity 14 protein isoform X1 [Felis catus]	XP_003992636.2	GI:755768027
XLOC_056381	DI	DP	216.727	82.8106	-1.38799	0.0049878	cytochrome P450 26C1 [Felis catus]	XP_023096515.1	GI:1304936730
XLOC_047110	DI	DP	254.923	97.2538	-1.39024	0.0049878	claudin-1 [Felis catus]	XP_003991843.1	GI:410970757



XLOC_029618	DI	DC	3.64743	1.38422	-1.39781	0.00985073	chondroitin sulfate proteoglycan 4 [Felis catus]	XP_003986971.2	GI:586988418
XLOC_069515	DI	DC	22.493	8.5296	-1.39893	0.0325694	C-type lectin domain family 11 member A [Felis catus]	XP_003997518.2	GI:1304950868
XLOC_072081	DI	DP	106.311	40.1197	-1.40591	0.0049878	beta-1,3-N-acetylglucosaminyltransferase lunatic fringe [Felis catus]	XP_023102331.1	GI:1304956561
XLOC_000669	DI	DC	62.2157	23.4552	-1.40737	0.0049878	HLA class II histocompatibility antigen gamma chain isoform X1 [Felis catus]	XP_003981534.3	GI:1304879928
XLOC_013606	DI	DC	77.3498	29.068	-1.41197	0.0049878	potassium voltage-gated channel subfamily KQT member 2 isoform X14 [Felis catus]	XP_023106751.1	GI:1304890508
XLOC_008464	DI	DP	54.3102	20.3977	-1.41281	0.019239	collagen alpha-1(VII) chain isoform X3 [Felis catus]	XP_019676735.1	GI:1126405002
XLOC_000193	DI	DC	167.51	62.7605	-1.41632	0.0049878	claudin-10 isoform X4 [Felis catus]	XP_023108436.1	GI:1304876895
XLOC_024610	DI	DP	31.5132	11.4699	-1.4581	0.0049878	enhancer of filamentation 1 isoform X1 [Felis catus]	XP_003985851.1	GI:410958491
XLOC_066465	DI	DP	1481.78	537.697	-1.46246	0.0049878	keratin, type I cytoskeletal 14 [Felis catus]	XP_003996909.2	GI:1304947266
XLOC_007430	DI	DC	16.9739	6.07204	-1.48307	0.0145862	LOW QUALITY PROTEIN: interleukin-27 receptor subunit alpha [Felis catus]	XP_006928550.3	GI:1304882753
XLOC_034833	DI	DC	22.2436	7.88991	-1.49531	0.0049878	PDZ domain-containing RING finger protein 4 isoform X1 [Felis catus]	XP_023112716.1	GI:1304913565

**Supplementary Table 4. Differentially expressed genes that are present in one tooth class and absent in another tooth class.**

Gene ID	Sample 1	Sample 2	Value 1	Value 2	log <sub>2</sub> fold change	q value	Protein name blastx hit	Cat NCBI accession	Cat GI
XLOC_052980	DI	DC	0	16.2703	Inf	0.0049878	HRAS-like suppressor 3 isoform X2 [Felis catus]	XP_011285277.1	GI:755772548
XLOC_052980	DI	DP	0	11.5996	Inf	0.0049878	HRAS-like suppressor 3 isoform X2 [Felis catus]	XP_011285277.1	GI:755772548
XLOC_014355	DC	DP	0.27168	6.61275	4.60525	0.0049878	matrix metalloproteinase-9 [Felis catus]	XP_003983461.2	GI:1304891154
XLOC_074364	DC	DP	0	5.58434	Inf	0.0049878	LOW QUALITY PROTEIN: tenascin-R [Felis catus]	XP_011289215.2	GI:1304958494
XLOC_074364	DI	DP	0	5.58434	Inf	0.0049878	LOW QUALITY PROTEIN: tenascin-R [Felis catus]	XP_011289215.2	GI:1304958494
XLOC_063054	DI	DP	0	5.55021	Inf	0.0049878	LIM/homeobox protein Lhx6 isoform X1 [Felis catus]	XP_023098453.1	GI:1304943720
XLOC_001057	DI	DC	0	5.29889	Inf	0.0049878	pleckstrin homology domain-containing family G member 3 isoform X3 [Felis catus]	XP_011281571.2	GI:1304909056
XLOC_039819	DI	DC	0	5.10322	Inf	0.0049878	complement C1q subcomponent subunit A [Felis catus]	XP_006934451.1	GI:586994524
XLOC_074445	DI	DC	0	4.93425	Inf	0.0049878	LIM/homeobox protein Lhx9 isoform X5 [Felis catus]	XP_023103420.1	GI:1304960035
XLOC_059279	DC	DP	0.95707	4.85345	2.34232	0.0049878	sushi domain-containing protein 2 [Felis catus]	XP_011286069.1	GI:755779082
XLOC_014247	DI	DP	0	4.62184	Inf	0.0049878	uncharacterized protein LOC109498652 [Felis catus]	XP_019683694.1	GI:1126416505
XLOC_003844	DC	DP	0	4.23094	Inf	0.0049878	7-dehydrocholesterol reductase [Felis catus]	XP_003993820.1	GI:410974780
XLOC_019321	DC	DP	0.62704	3.65991	2.54519	0.0049878	protocadherin-10 isoform X1 [Felis catus]	XP_011279986.1	GI:755722194
XLOC_047387	DC	DP	0	3.63883	Inf	0.0049878	tonsoku-like protein isoform X4 [Felis catus]	XP_011289827.1	GI:755811451
XLOC_047387	DI	DP	0	3.63883	Inf	0.0049878	tonsoku-like protein isoform X4 [Felis catus]	XP_011289827.1	GI:755811451
XLOC_052524	DI	DP	0	3.17772	Inf	0.0049878	stromelysin-1 [Felis catus]	XP_003992356.1	GI:410971811
XLOC_062738	DI	DC	0	3.09526	Inf	0.0049878	ubiquitin conjugation factor E4 B isoform X5 [Felis catus]	XP_019691675.1	GI:1126441180

XLOC_008056	DI	DC	0	3.01692	Inf	0.0049878	SCO-spondin, partial [Felis catus]	XP_023098097.1	GI:1304881189
XLOC_035161	DI	DC	0	2.95249	Inf	0.0049878	APOBEC3H [Felis catus]	ABW06962.1	GI:157966950
XLOC_074585	DI	DP	0	2.85653	Inf	0.0049878	V-set and immunoglobulin domain-containing protein 8 isoform X2 [Felis catus]	XP_006943110.1	GI:587018980
XLOC_032358	DI	DP	0	2.72968	Inf	0.0049878	long-chain specific acyl-CoA dehydrogenase, mitochondrial isoform X2 [Felis catus]	XP_006935588.2	GI:755760571
XLOC_066462	DC	DP	0	2.72144	Inf	0.0049878	keratin, type I cuticular Ha2 isoform X1 [Felis catus]	XP_003996905.4	GI:1304946957
XLOC_059220	DI	DP	0	2.66028	Inf	0.0049878	serine dehydratase-like isoform X2 [Felis catus]	XP_003994748.1	GI:410976692
XLOC_002858	DI	DP	0	2.6239	Inf	0.0049878	transmembrane protease serine 6 isoform X3 [Felis catus]	XP_023113232.1	GI:1304915557
XLOC_047675	DI	DP	0	2.60555	Inf	0.0049878	sterile alpha motif domain-containing protein 7 isoform X2 [Felis catus]	XP_003991974.3	GI:1126453171
XLOC_068940	DI	DC	0	2.58867	Inf	0.0049878	ras-interacting protein 1 [Felis catus]	XP_023101674.1	GI:1304954443
XLOC_012918	DI	DP	0	2.57202	Inf	0.0049878	LOW QUALITY PROTEIN: sp110 nuclear body protein [Felis catus]	XP_011283934.3	GI:1304924307
XLOC_024784	DC	DP	0	2.56094	Inf	0.0282102	adenylate cyclase type 10-like isoform X5 [Felis catus]	XP_023109712.1	GI:1304901941
XLOC_062701	DI	DC	0	2.47529	Inf	0.0049878	lipocalin-like 1 protein [Felis catus]	XP_006939733.1	GI:587009727
XLOC_051912	DI	DC	0	2.44738	Inf	0.0049878	layilin isoform X1 [Felis catus]	XP_023094852.1	GI:1304930363
XLOC_003267	DI	DP	0	2.38976	Inf	0.0049878	uncharacterized protein LOC105260444 [Felis catus]	XP_023095181.1	GI:1304875494
XLOC_014247	DI	DC	0	2.3872	Inf	0.0049878	uncharacterized protein LOC109498652 [Felis catus]	XP_019683694.1	GI:1126416505
XLOC_074453	DI	DC	0	2.38648	Inf	0.0049878	probable G-protein coupled receptor 179 isoform X2 [Felis catus]	XP_019673337.1	GI:1126476004
XLOC_065522	DC	DP	0	2.36341	Inf	0.0049878	tumor necrosis factor ligand superfamily member 13 isoform X2 [Felis catus]	XP_019672436.1	GI:1126473133
XLOC_065522	DI	DP	0	2.36341	Inf	0.0049878	tumor necrosis factor ligand superfamily member 13 isoform X2 [Felis catus]	XP_019672436.1	GI:1126473133

XLOC_008839	DI	DC	0	2.30429	Inf	0.0049878	protein LLP homolog isoform X1 [Felis catus]	XP_019690738.1	GI:1126438349
XLOC_056773	DI	DP	0	2.27269	Inf	0.0049878	retinol binding protein 4 precursor [Felis catus]	NP_001277178.1	GI:589811507
XLOC_074561	DI	DC	0	2.22151	Inf	0.0049878	TNF receptor-associated factor 5 isoform X1 [Felis catus]	XP_003999373.1	GI:410986146
XLOC_013604	DI	DC	0	2.19861	Inf	0.0049878	tyrosine-protein kinase Srms [Felis catus]	XP_019683567.2	GI:1304890471
XLOC_056023	DI	DC	0	2.18129	Inf	0.0414242	RNA-binding protein 14 isoform X2 [Felis catus]	XP_019668274.1	GI:1126460276
XLOC_040233	DI	DP	0	2.14747	Inf	0.0049878	protein AF-17 isoform X3 [Felis catus]	XP_023100021.1	GI:1304948674
XLOC_035329	DI	DP	0	2.14423	Inf	0.0049878	uncharacterized protein C10orf67 homolog, mitochondrial isoform X1 [Felis catus]	XP_019689629.1	GI:1126434976
XLOC_062701	DI	DP	0	2.1239	Inf	0.0049878	lipocalin-like 1 protein [Felis catus]	XP_006939733.1	GI:587009727
XLOC_041202	DI	DC	0	2.09852	Inf	0.0049878	collagen alpha-1(XXIV) chain isoform X1 [Felis catus]	XP_019692917.1	GI:1126444797
XLOC_082525	DI	DP	0	2.09109	Inf	0.0049878	uncharacterized protein LOC109495721 isoform X1 [Felis catus]	XP_023105495.1	GI:1304874902
XLOC_066379	DC	DP	0	2.0644	Inf	0.0049878	MYCBP-associated protein [Felis catus]	XP_023099231.1	GI:1304946110
XLOC_014373	DC	DP	0	2.04784	Inf	0.0049878	WNT1-inducible-signaling pathway protein 2 [Felis catus]	XP_003983496.1	GI:410953676
XLOC_001167	DI	DC	0	2.0372	Inf	0.0049878	LOW QUALITY PROTEIN: GDNF family receptor alpha-3 [Felis catus]	XP_003980852.1	GI:410948247
XLOC_008839	DI	DP	0	1.99466	Inf	0.0457699	protein LLP homolog isoform X1 [Felis catus]	XP_019690738.1	GI:1126438349
XLOC_041567	DI	DC	0	1.98278	Inf	0.0049878	zinc finger protein 385B isoform X3 [Felis catus]	XP_023115284.1	GI:1304923180
XLOC_041231	DI	DC	0	1.97284	Inf	0.0049878	tissue factor [Felis catus]	XP_006934991.2	GI:755755479
XLOC_001184	DI	DC	0	1.9653	Inf	0.0049878	anion exchange protein 4 isoform X5 [Felis catus]	XP_023111595.1	GI:1304878132
XLOC_065615	DI	DC	0	1.94514	Inf	0.0049878	ATP-sensitive inward rectifier potassium channel 12 isoform X3 [Felis catus]	XP_023099263.1	GI:1304946183
XLOC_062657	DI	DC	0	1.92286	Inf	0.0049878	serine/threonine-protein kinase MRCK gamma isoform X10 [Felis catus]	XP_023095798.1	GI:1304933954

XLOC_005598	DI	DP	0	1.90641	Inf	0.0049878	wee1-like protein kinase isoform X2 [Felis catus]	XP_023095323.1	GI:1304932262
XLOC_000659	DI	DP	0	1.89727	Inf	0.0049878	proton-coupled amino acid transporter 2 [Felis catus]	XP_003981425.1	GI:410949431
XLOC_000670	DI	DP	0	1.87097	Inf	0.0049878	arylsulfatase I [Felis catus]	XP_003981535.2	GI:1304879933
XLOC_047584	DI	DP	0	1.85933	Inf	0.0049878	LOW QUALITY PROTEIN: GPI mannosyltransferase 4 [Felis catus]	XP_023116048.1	GI:1304926123
XLOC_059404	DI	DP	0	1.8384	Inf	0.0049878	gap junction gamma-2 protein isoform X1 [Felis catus]	XP_006927524.3	GI:1304877305
XLOC_070744	DI	DP	0	1.82372	Inf	0.0049878	LOW QUALITY PROTEIN: sprouty-related, EVH1 domain-containing protein 3 [Felis catus]	XP_023100694.1	GI:1304950833
XLOC_041047	DI	DP	0	1.82096	Inf	0.0049878	claudin-19 [Felis catus]	XP_003990009.1	GI:410966994
XLOC_080871	DI	DC	0	1.80917	Inf	0.0049878	zinc finger protein 157 isoform X1 [Felis catus]	XP_011289961.1	GI:755812545
XLOC_074904	DI	DC	0	1.71364	Inf	0.0049878	alpha-1,3-mannosyl-glycoprotein 4-beta-N-acetylglucosaminyltransferase-like protein MGAT4E isoform X1 [Felis catus]	XP_019677562.2	GI:1304959037
XLOC_039820	DI	DC	0	1.71263	Inf	0.0049878	complement C1q subcomponent subunit C [Felis catus]	XP_019691924.2	GI:1304918266
XLOC_068895	DI	DP	0	1.70018	Inf	0.0049878	LOW QUALITY PROTEIN: SH3 and multiple ankyrin repeat domains protein 1 [Felis catus]	XP_023100705.1	GI:1304950866
XLOC_018206	DC	DP	0	1.70007	Inf	0.0049878	LOW QUALITY PROTEIN: RAD51-associated protein 2 [Felis catus]	XP_023107853.1	GI:1304894936
XLOC_018206	DI	DP	0	1.70007	Inf	0.0049878	LOW QUALITY PROTEIN: RAD51-associated protein 2 [Felis catus]	XP_023107853.1	GI:1304894936
XLOC_037312	DI	DC	0	1.69665	Inf	0.0049878	cationic amino acid transporter 3 [Felis catus]	XP_004000646.1	GI:410988762
XLOC_047425	DI	DC	0	1.68989	Inf	0.0049878	chloride intracellular channel protein 6 [Felis catus]	XP_023094535.1	GI:1304929136
XLOC_046779	DC	DP	0	1.68233	Inf	0.0049878	melanoma-associated antigen B17-like, partial [Felis catus]	XP_023104723.1	GI:1304964957



XLOC_079437	DI	DP	0	1.6596	Inf	0.0049878	stAR-related lipid transfer protein 8 isoform X3 [Felis catus]	XP_004000627.1	GI:410988723
XLOC_000897	DI	DP	0	1.65905	Inf	0.0049878	LOW QUALITY PROTEIN: ADP-ribosylation factor-like protein 11 [Felis catus]	XP_003980437.2	GI:1304876317
XLOC_019864	DC	DP	0	1.64334	Inf	0.0049878	rho GTPase-activating protein 4 isoform X2 [Felis catus]	XP_023104641.1	GI:1304964585
XLOC_019864	DI	DP	0	1.64334	Inf	0.0049878	rho GTPase-activating protein 4 isoform X2 [Felis catus]	XP_023104641.1	GI:1304964585
XLOC_059148	DI	DC	0	1.63929	Inf	0.0049878	osteoclast-associated immunoglobulin-like receptor isoform X3 [Felis catus]	XP_023101503.1	GI:1304953881
XLOC_052979	DI	DP	0	1.61544	Inf	0.0049878	Ca(2+)-independent N-acyltransferase [Felis catus]	XP_006937500.1	GI:587003279
XLOC_041708	DC	DP	0	1.60627	Inf	0.0049878	thiamine transporter 2 [Felis catus]	NP_001265749.1	GI:523704408
XLOC_041708	DI	DP	0	1.60627	Inf	0.0049878	thiamine transporter 2 [Felis catus]	NP_001265749.1	GI:523704408
XLOC_041181	DI	DC	0	1.59034	Inf	0.0049878	ELKS/Rab6-interacting/CAST family member 1 isoform X8 [Felis catus]	XP_023112382.1	GI:1304912354
XLOC_051994	DI	DC	0	1.57629	Inf	0.0049878	pannexin-3 [Felis catus]	XP_011284721.1	GI:755767655
XLOC_000670	DI	DC	0	1.566	Inf	0.0049878	arylsulfatase I [Felis catus]	XP_003981535.2	GI:1304879933
XLOC_010866	DI	DP	0	1.56453	Inf	0.0049878	E3 ubiquitin-protein ligase HECW1 isoform X1 [Felis catus]	XP_006929154.2	GI:755701011
XLOC_019149	DI	DC	0	1.55847	Inf	0.0049878	LOW QUALITY PROTEIN: neurotensin receptor type 2 [Felis catus]	XP_019683678.1	GI:1126416326
XLOC_076061	DI	DC	0	1.54812	Inf	0.0049878	LIM/homeobox protein Lhx9 isoform X5 [Felis catus]	XP_023103420.1	GI:1304960035
XLOC_024767	DI	DC	0	1.53025	Inf	0.0049878	peptidase inhibitor 16 [Felis catus]	XP_006931722.1	GI:586986384
XLOC_008660	DI	DC	0	1.52735	Inf	0.0049878	phosphoglycerate mutase 2 [Felis catus]	XP_003982625.1	GI:410951890
XLOC_047584	DI	DC	0	1.50894	Inf	0.0049878	LOW QUALITY PROTEIN: GPI mannosyltransferase 4 [Felis catus]	XP_023116048.1	GI:1304926123
XLOC_047706	DI	DP	5.81381	0.9943	-2.54773	0.0325694	rho guanine nucleotide exchange factor 26 isoform X1 [Felis catus]	XP_023116224.1	GI:1304926903
XLOC_041731	DI	DC	6.63133	0.7971	-3.05646	0.019239	ephexin-1 [Felis catus]	XP_023115581.1	GI:1304924448

XLOC_077223	DI	DC	4.54825	0.78682	-2.53121	0.0237354	syntabulin isoform X2 [Felis catus]	XP_019678599.1	GI:1126492051
XLOC_077224	DI	DC	4.6089	0.60732	-2.92389	0.0145862	potassium voltage-gated channel subfamily V member 1 [Felis catus]	XP_004000117.1	GI:410987664
XLOC_074911	DI	DC	4.14886	0.51857	-3.00009	0.0049878	fibromodulin [Felis catus]	XP_006942940.1	GI:587018481
XLOC_025527	DI	DC	1.98551	0.247	-3.00691	0.0325694	cannabinoid receptor 1 isoform X1 [Felis catus]	XP_011280748.1	GI:755730165
XLOC_001184	DC	DP	1.9653	0	-Inf	0.0049878	anion exchange protein 4 isoform X5 [Felis catus]	XP_023111595.1	GI:1304878132
XLOC_024767	DC	DP	1.53025	0	-Inf	0.0049878	peptidase inhibitor 16 [Felis catus]	XP_006931722.1	GI:586986384
XLOC_025590	DI	DC	3.95833	0	-Inf	0.0049878	D-aspartate oxidase isoform X3 [Felis catus]	XP_019686631.2	GI:1304903208
XLOC_025590	DI	DP	3.95833	0	-Inf	0.0049878	D-aspartate oxidase isoform X3 [Felis catus]	XP_019686631.2	GI:1304903208
XLOC_030174	DI	DP	1.86315	0	-Inf	0.0049878	alpha-1,6-mannosylglycoprotein 6-beta-N-acetylglucosaminyltransferase A isoform X2 [Felis catus]	XP_023115040.1	GI:1304922274
XLOC_030331	DC	DP	1.83778	0	-Inf	0.0049878	LOW QUALITY PROTEIN: NACHT, LRR and PYD domains-containing protein 8 [Felis catus]	XP_023101633.1	GI:1304954345
XLOC_035918	DI	DC	1.79315	0	-Inf	0.0049878	patatin-like phospholipase domain-containing protein 5 isoform X2 [Felis catus]	XP_011282650.1	GI:755751505
XLOC_038003	DI	DP	2.04795	0	-Inf	0.0049878	EF-hand calcium-binding domain-containing protein 6 isoform X2 [Felis catus]	XP_023113343.1	GI:1304915941
XLOC_038003	DC	DP	2.03723	0	-Inf	0.0049878	EF-hand calcium-binding domain-containing protein 6 isoform X2 [Felis catus]	XP_023113343.1	GI:1304915941
XLOC_052878	DI	DP	2.99779	0	-Inf	0.0049878	homeobox protein aristaless-like 4 [Felis catus]	XP_003993239.2	GI:1304933116
XLOC_059643	DC	DP	2.05302	0	-Inf	0.0049878	myosin regulatory light chain 2, ventricular/cardiac muscle isoform [Felis catus]	XP_003994712.1	GI:410976614
XLOC_068883	DC	DP	2.18601	0	-Inf	0.0049878	kallikrein-12 [Felis catus]	XP_019674179.1	GI:1126478524
XLOC_074445	DC	DP	4.93425	0	-Inf	0.0049878	LIM/homeobox protein Lhx9 isoform X5 [Felis catus]	XP_023103420.1	GI:1304960035

XLOC_074561	DC	DP	2.22151	0	-Inf	0.0049878	TNF receptor-associated factor 5 isoform X1 [Felis catus]	XP_003999373.1	GI:410986146
XLOC_074757	DI	DP	1.52559	0	-Inf	0.0049878	myocilin precursor [Felis catus]	NP_001265779.1	GI:523704466
XLOC_076061	DC	DP	1.54812	0	-Inf	0.0049878	LIM/homeobox protein Lhx9 isoform X5 [Felis catus]	XP_023103420.1	GI:1304960035

**Supplementary Table 5. Differentially expressed genes present in one tooth class with FPKM less than 1.5 and absent in another tooth class.**

Gene ID	Sample 1	Sample 2	Value 1	Value 2	log <sub>2</sub> fold change	q value	Protein name blastx hit	Cat NCBI accession	Cat GI
XLOC_019561	DI	DC	1.45024	0	-Inf	0.0049878	neuronal acetylcholine receptor subunit alpha-9 [Felis catus]	XP_023108953.1	GI:1304899299
XLOC_019561	DI	DP	1.45024	0	-Inf	0.0049878	neuronal acetylcholine receptor subunit alpha-9 [Felis catus]	XP_023108953.1	GI:1304899299
XLOC_008398	DI	DC	1.41301	0	-Inf	0.0049878	uncharacterized protein KIAA1683 homolog isoform X1 [Felis catus]	XP_011289052.3	GI:1304883223
XLOC_006487	DC	DP	1.3797	0	-Inf	0.0049878	ribosomal protein S4, partial [Felis catus]	BAA21077.1	GI:4432938
XLOC_007800	DI	DC	1.35107	0	-Inf	0.0049878	coiled-coil domain-containing protein 146 [Felis catus]	XP_003982742.2	GI:755701412
XLOC_001393	DI	DC	1.31834	0	-Inf	0.0049878	gamma-aminobutyric acid receptor subunit pi isoform X6 [Felis catus]	XP_019694615.1	GI:1126401407
XLOC_001393	DI	DP	1.31834	0	-Inf	0.0049878	gamma-aminobutyric acid receptor subunit pi isoform X6 [Felis catus]	XP_019694615.1	GI:1126401407
XLOC_042850	DC	DP	1.31406	0	-Inf	0.0049878	suppressor of tumorigenicity 7 protein-like isoform X2 [Felis catus]	XP_023114752.1	GI:1304921159
XLOC_072423	DI	DC	1.31358	0	-Inf	0.0049878	tektin-4 [Felis catus]	XP_003999006.1	GI:410985391
XLOC_072423	DI	DP	1.31358	0	-Inf	0.0049878	tektin-4 [Felis catus]	XP_003999006.1	GI:410985391
XLOC_069912	DI	DC	1.26798	0	-Inf	0.0049878	LOW QUALITY PROTEIN: BTB/POZ domain-containing protein KCTD19 [Felis catus]	XP_023101865.1	GI:1304955035
XLOC_069912	DI	DP	1.26798	0	-Inf	0.0049878	LOW QUALITY PROTEIN: BTB/POZ domain-containing protein KCTD19 [Felis catus]	XP_023101865.1	GI:1304955035
XLOC_076962	DC	DP	1.21073	0	-Inf	0.0049878	protein NOV homolog [Felis catus]	XP_004000129.1	GI:410987692
XLOC_014490	DI	DC	1.15141	0	-Inf	0.0049878	proenkephalin-B [Felis catus]	XP_003983803.1	GI:410954299
XLOC_014490	DI	DP	1.15141	0	-Inf	0.0049878	proenkephalin-B [Felis catus]	XP_003983803.1	GI:410954299
XLOC_075427	DI	DC	1.11332	0	-Inf	0.0049878	LOW QUALITY PROTEIN: phospholipase DDHD1 [Felis catus]	XP_023111466.1	GI:1304908700

XLOC_075427	DI	DP	1.11332	0	-Inf	0.0049878	LOW QUALITY PROTEIN: phospholipase DDHD1 [Felis catus]	XP_023111466.1	GI:1304908700
XLOC_081626	DC	DP	1.0875	0	-Inf	0.0049878	type-2 angiotensin II receptor [Felis catus]	XP_019679764.1	GI:1126495504
XLOC_008258	DI	DP	1.0622	0	-Inf	0.0049878	LOW QUALITY PROTEIN: mucin-16 [Felis catus]	XP_023100591.1	GI:1304882210
XLOC_029647	DI	DC	0	1.499	Inf	0.0237354	GRAM domain-containing protein 2A isoform X1 [Felis catus]	XP_006932473.1	GI:586988595
XLOC_013604	DI	DP	0	1.4875	Inf	0.0049878	tyrosine-protein kinase Srms [Felis catus]	XP_019683567.2	GI:1304890471
XLOC_007009	DC	DP	0	1.4423	Inf	0.0049878	ankyrin repeat domain-containing protein 33B [Felis catus]	XP_011285591.2	GI:1304880457
XLOC_007009	DI	DP	0	1.4423	Inf	0.0049878	ankyrin repeat domain-containing protein 33B [Felis catus]	XP_011285591.2	GI:1304880457
XLOC_075084	DI	DP	0	1.4299	Inf	0.0049878	potassium/sodium hyperpolarization-activated cyclic nucleotide-gated channel 1 [Felis catus]	XP_011285149.2	GI:1304880070
XLOC_046182	DI	DP	0	1.4154	Inf	0.0049878	LOW QUALITY PROTEIN: ras-associated and pleckstrin homology domains-containing protein 1 [Felis catus]	XP_023115400.1	GI:1304923607
XLOC_032085	DC	DP	0	1.4062	Inf	0.0049878	inactive caspase-12 isoform X4 [Felis catus]	XP_019666718.1	GI:1126455378
XLOC_032085	DI	DP	0	1.4062	Inf	0.0049878	inactive caspase-12 isoform X4 [Felis catus]	XP_019666718.1	GI:1126455378
XLOC_013994	DI	DC	0	1.391	Inf	0.0049878	V-type proton ATPase subunit B, kidney isoform [Felis catus]	XP_003984152.2	GI:1304893550
XLOC_008321	DI	DC	0	1.3896	Inf	0.0049878	LOW QUALITY PROTEIN: Krueppel-like factor 2 [Felis catus]	XP_023102535.1	GI:1304882955
XLOC_006487	DI	DC	0	1.3797	Inf	0.0049878	ribosomal protein S4, partial [Felis catus]	BAA21077.1	GI:4432938
XLOC_041202	DI	DP	0	1.3722	Inf	0.0049878	collagen alpha-1(XXIV) chain isoform X1 [Felis catus]	XP_019692917.1	GI:1126444797
XLOC_068944	DI	DC	0	1.3614	Inf	0.0049878	netrin-5 [Felis catus]	XP_023100932.1	GI:1304951718
XLOC_004013	DI	DC	0	1.3608	Inf	0.0049878	uncharacterized protein LOC102900045 [Felis catus]	XP_023111616.1	GI:1304878137
XLOC_079438	DI	DC	0	1.3501	Inf	0.0049878	stAR-related lipid transfer protein 8 isoform X3 [Felis catus]	XP_004000627.1	GI:410988723

XLOC_034297	DI	DP	0	1.3453	Inf	0.0049878	double-strand-break repair protein rad21 homolog [Felis catus]	XP_004000123.3	GI:1304964121
XLOC_040026	DI	DP	0	1.3294	Inf	0.0049878	tetraspanin-1 [Felis catus]	XP_019692480.1	GI:1126443552
XLOC_047174	DI	DC	0	1.3281	Inf	0.0049878	MDS1 and EVI1 complex locus protein EVI1 isoform X6 [Felis catus]	XP_023116185.1	GI:1304926685
XLOC_000992	DI	DC	0	1.3141	Inf	0.0049878	fibroblast growth factor 14 isoform X2 [Felis catus]	XP_023108747.1	GI:1304877032
XLOC_042850	DI	DC	0	1.3141	Inf	0.0049878	suppressor of tumorigenicity 7 protein-like isoform X2 [Felis catus]	XP_023114752.1	GI:1304921159
XLOC_000541	DI	DC	0	1.3114	Inf	0.0049878	G-protein coupled receptor 98 isoform X5 [Felis catus]	XP_023114121.1	GI:1304878987
XLOC_079411	DI	DC	0	1.2907	Inf	0.0049878	LOW QUALITY PROTEIN: uncharacterized protein CXorf67 homolog [Felis catus]	XP_023104872.1	GI:1304965434
XLOC_056425	DI	DC	0	1.287	Inf	0.0049878	FTS and Hook-interacting protein isoform X2 [Felis catus]	XP_006937105.1	GI:587002141
XLOC_039821	DI	DC	0	1.2822	Inf	0.0049878	complement C1q subcomponent subunit B [Felis catus]	XP_003989691.2	GI:1304918268
XLOC_070131	DC	DP	0	1.2694	Inf	0.0049878	multimerin-2 [Felis catus]	XP_023096397.1	GI:1304936309
XLOC_070131	DI	DP	0	1.2694	Inf	0.0049878	multimerin-2 [Felis catus]	XP_023096397.1	GI:1304936309
XLOC_018729	DI	DC	0	1.2664	Inf	0.0049878	mitochondrial brown fat uncoupling protein 1 [Felis catus]	XP_003985034.1	GI:410956817
XLOC_003187	DC	DP	0	1.2598	Inf	0.0049878	coiled-coil domain-containing protein 39 [Felis catus]	XP_004001225.1	GI:410989970
XLOC_003187	DI	DP	0	1.2598	Inf	0.0049878	coiled-coil domain-containing protein 39 [Felis catus]	XP_004001225.1	GI:410989970
XLOC_072044	DI	DC	0	1.2509	Inf	0.0049878	CENPB DNA-binding domain-containing protein 1 [Felis catus]	XP_003998428.1	GI:410984221
XLOC_074212	DI	DP	0	1.2469	Inf	0.0049878	insulin-like growth factor-binding protein complex acid labile subunit isoform X2 [Felis catus]	XP_023102173.1	GI:1304956065
XLOC_024342	DI	DP	0	1.2345	Inf	0.0049878	D(1B) dopamine receptor [Felis catus]	XP_003985568.4	GI:1304899744
XLOC_012918	DI	DC	0	1.2186	Inf	0.0049878	LOW QUALITY PROTEIN: sp110 nuclear body protein [Felis catus]	XP_011283934.3	GI:1304924307



XLOC_041697	DI	DC	0	1.2178	Inf	0.0049878	protein FAM124B [Felis catus]	XP_003991263.1	GI:410969561
XLOC_020587	DI	DC	0	1.2156	Inf	0.0049878	dolichyl-diphosphooligosaccharide-- protein glycosyltransferase subunit STT3B [Felis catus]	XP_023116416.1	GI:1304927704
XLOC_037312	DI	DP	0	1.2148	Inf	0.0049878	cationic amino acid transporter 3 [Felis catus]	XP_004000646.1	GI:410988762
XLOC_029746	DI	DP	0	1.2148	Inf	0.0049878	dmX-like protein 2 isoform X2 [Felis catus]	XP_019687979.1	GI:1126429886
XLOC_082075	DI	DC	0	1.2128	Inf	0.0049878	proline-rich protein 36 isoform X1 [Felis catus]	XP_023100409.1	GI:1304882138
XLOC_076962	DI	DC	0	1.2107	Inf	0.0049878	protein NOV homolog [Felis catus]	XP_004000129.1	GI:410987692
XLOC_074585	DI	DC	0	1.2086	Inf	0.0049878	V-set and immunoglobulin domain- containing protein 8 isoform X2 [Felis catus]	XP_006943110.1	GI:587018980
XLOC_007675	DI	DC	0	1.2057	Inf	0.0049878	histamine H1 receptor isoform X1 [Felis catus]	XP_023105790.1	GI:1304884892
XLOC_040390	DI	DC	0	1.1694	Inf	0.0049878	E3 ubiquitin-protein ligase TRIM7 isoform X1 [Felis catus]	XP_003980686.1	GI:410947913
XLOC_035433	DI	DC	0	1.1614	Inf	0.0049878	microfibrillar-associated protein 5 isoform X2 [Felis catus]	XP_006933549.1	GI:586991814
XLOC_079438	DI	DP	0	1.1588	Inf	0.0049878	stAR-related lipid transfer protein 8 isoform X3 [Felis catus]	XP_004000627.1	GI:410988723
XLOC_000770	DI	DP	0	1.1538	Inf	0.0049878	LOW QUALITY PROTEIN: dynein heavy chain 5, axonemal [Felis catus]	XP_023095239.1	GI:1304880445
XLOC_053165	DC	DP	0	1.1375	Inf	0.0049878	protocadherin-20 [Felis catus]	XP_003980488.2	GI:755688442
XLOC_041029	DC	DP	0	1.136	Inf	0.0049878	cytosolic 5'-nucleotidase 1A [Felis catus]	XP_003989938.1	GI:410966846
XLOC_063720	DI	DC	0	1.1318	Inf	0.0049878	LOW QUALITY PROTEIN: death- associated protein kinase 1 [Felis catus]	XP_023098003.1	GI:1304942190
XLOC_081831	DI	DP	0	1.1241	Inf	0.0049878	HAUS augmin-like complex subunit 4 isoform X2 [Felis catus]	XP_019688361.1	GI:1126430958
XLOC_017743	DI	DP	0	1.1195	Inf	0.0049878	tetratricopeptide repeat protein 39B-like [Felis catus]	XP_011279461.1	GI:755710804
XLOC_025447	DI	DC	0	1.1116	Inf	0.0049878	adhesion G protein-coupled receptor F5 isoform X2 [Felis catus]	XP_006931850.2	GI:1304902359

XLOC_001381	DI	DP	0	1.1052	Inf	0.0049878	hemicentin-1 isoform X6 [Felis catus]	XP_019677283.1	GI:1126487972
XLOC_066187	DI	DC	0	1.1018	Inf	0.0049878	intersectin-1 isoform X5 [Felis catus]	XP_019694973.1	GI:1126450977
XLOC_016331	DC	DP	0	1.0978	Inf	0.0049878	somatostatin receptor type 4 [Felis catus]	XP_003983887.3	GI:755709023
XLOC_016331	DI	DP	0	1.0978	Inf	0.0049878	somatostatin receptor type 4 [Felis catus]	XP_003983887.3	GI:755709023
XLOC_014129	DC	DP	0	1.0933	Inf	0.0049878	3-oxo-5-alpha-steroid 4-dehydrogenase 2 [Felis catus]	XP_006930441.1	GI:586982522
XLOC_081626	DI	DC	0	1.0875	Inf	0.0049878	type-2 angiotensin II receptor [Felis catus]	XP_019679764.1	GI:1126495504
XLOC_052053	DI	DP	0	1.0614	Inf	0.0049878	V-set and transmembrane domain-containing protein 5 [Felis catus]	XP_023095101.1	GI:1304931399
XLOC_049250	DC	DP	0	1.0547	Inf	0.0049878	olfactory receptor 2M5-like [Felis catus]	XP_011281449.2	GI:1126396310
XLOC_049250	DI	DP	0	1.0547	Inf	0.0049878	olfactory receptor 2M5-like [Felis catus]	XP_011281449.2	GI:1126396310
XLOC_001290	DI	DC	0	1.0505	Inf	0.0049878	ankyrin repeat domain-containing protein 34B [Felis catus]	XP_003981159.1	GI:410948888
XLOC_039944	DI	DC	0	1.0431	Inf	0.0049878	adhesion G protein-coupled receptor L2 isoform X16 [Felis catus]	XP_023114620.1	GI:1304920466
XLOC_035544	DI	DP	0	1.0406	Inf	0.0049878	rap guanine nucleotide exchange factor 3 isoform X1 [Felis catus]	XP_003988644.1	GI:410964201
XLOC_003268	DC	DP	0	1.0382	Inf	0.0049878	uncharacterized protein LOC105260444 [Felis catus]	XP_023095181.1	GI:1304875494
XLOC_003268	DI	DP	0	1.0382	Inf	0.0049878	uncharacterized protein LOC105260444 [Felis catus]	XP_023095181.1	GI:1304875494
XLOC_008574	DI	DC	0	1.0286	Inf	0.0049878	clathrin heavy chain linker domain-containing protein 1 isoform X5 [Felis catus]	XP_019682787.1	GI:1126413624
XLOC_042009	DI	DP	0	1.0184	Inf	0.0049878	uncharacterized protein LOC102901615 isoform X2 [Felis catus]	XP_023107649.1	GI:1304894059
XLOC_075084	DI	DC	0	1.0136	Inf	0.0049878	potassium/sodium hyperpolarization-activated cyclic nucleotide-gated channel 1 [Felis catus]	XP_011285149.2	GI:1304880070

**Supplementary Table 6. Relative volumetric measurements of the dental epithelium for each tooth at the early bell stage.** Measurements are based on a 3-D reconstruction from a  $\mu$ CT scan and were taken in VG StudioMax v3.3.4. Tooth positions that correspond to the teeth that were RNA-sequenced are in bold. Note that fixation and contrast-enhancing agents are known to induce shrinkage in the tissue. The measurements for each tooth were obtained from reconstructed  $\mu$ CT data from a single cat embryo (see Figure 1B, C, D-F) from the right and left sides.

<b>Dentition</b>	<b>Right/Left</b>	<b>Tooth</b>	<b>Volume (<math>\mu\text{m}^3</math>)</b>
Upper	Left	First incisor	5,423,720.93
Upper	Left	Second incisor	6,278,222.89
<b>Upper</b>	<b>Left</b>	<b>Third incisor</b>	<b>9,095,191.96</b>
<b>Upper</b>	<b>Left</b>	<b>Canine</b>	<b>28,227,092.70</b>
<b>Upper</b>	<b>Left</b>	<b>Third premolar</b>	<b>48,742,834.48</b>
Upper	Left	Fourth premolar	22,582,519.80
Upper	Right	First incisor	4,229,050.60
Upper	Right	Second incisor	4,479,171.71
<b>Upper</b>	<b>Right</b>	<b>Third incisor</b>	<b>7,518,879.60</b>
<b>Upper</b>	<b>Right</b>	<b>Canine</b>	<b>26,773,735.88</b>
<b>Upper</b>	<b>Right</b>	<b>Third premolar</b>	<b>46,030,990.78</b>
Upper	Right	Fourth premolar	23,488,787.93
Lower	Left	First incisor	1,819,271.94
Lower	Left	Second incisor	5,576,059.22
Lower	Left	Third incisor	4,416,788.46
Lower	Left	Canine	19,201,211.63
Lower	Left	Third premolar	41,234,564.04
Lower	Left	Fourth premolar	56,093,011.05
Lower	Right	First incisor	2,065,777.08
Lower	Right	Second incisor	5,763,940.05
Lower	Right	Third incisor	4,308,698.70
Lower	Right	Canine	19,401,211.29
Lower	Right	Third premolar	44,696,468.86
Lower	Right	Fourth premolar	56,774,430.00

**Supplementary Table 7. Primary and secondary antibodies used in immunofluorescence.**

Antibody Type	Antibody Name and Abbreviation	Manufacturer	Catalogue Number	Dilution
Primary	Anti-collagen 1 (COL1)	Santa Cruz	SC 8783	1:50
Primary	Anti-keratin16 (KRT16)	Sigma Aldrich	SAB 4501660	1:50
Primary	Anti-tenascin (TENC)	Santa Cruz	SC 20932	1:50
Primary	Anti-tenascin (TENC)	US Biological Life Sciences	T2550-23	1:100
Primary	Anti-wnt inhibitory factor 1 (WIF1)	Genetex	GTX 16429	1:100
Primary	Anti-follistatin (FST)	Thermo Fisher Scientific	PA5-114319	1:100
Secondary	Donkey anti-goat IgG (H+L) AF 488	Invitrogen	A11055	1:200
Secondary	Goat anti-rabbit IgG (H+L) AF 546	Invitrogen	A11035	1:200
Secondary	Goat anti-rabbit IgG (H+L) AF 647	Invitrogen	A32733	1:200

**Supplementary Table 8. Primers used for genotyping cat tissue.** Primers specific to UTX and UTY were used to determine the sex of each cat embryo used in the study via PCR using 35 cycles with an annealing temperature of 56°C.

Primer Name	Primer Sequence (5'-3')	Amplicon length
UTX Forward	CTA-AGT-CAC-CAG-GTT-TAC-TAA-GTT-C	298
UTX Reverse	ATG-GGG-CTC-TGA-GAT-TCT-TCC	
UTY Forward	TGG-CTG-TGC-TGG-TGT-CAA-AAG	378
UTY Reverse	ACA-GAG-CTC-TGT-GAG-TTC-TCT-AGC	

**Supplementary Table 9. Jensen-Shannon distances between incisor, canine, and premolar based on FPKM values.** Distances are given for the dataset with a fold change cut-off of  $\geq 1.5$  and FPKM  $\geq 1$  (N=111 genes). Distances were calculated in CummeRbund from a matrix of FPKM values using the makeprobs and JSdist functions (Goff et al., 2013).

		Incisor	Canine
<b>Fold change <math>\geq 1.5</math> and FPKM <math>\geq 1</math></b>	Canine	0.4856923	0
	Premolar	0.5609820	0.2569888